MORPHOLOGY OF V1 NEURONS PROJECTING TO V2 IN MACAQUE: CELL TYPES AND CIRCUITS REVEALED BY PROJECTION TARGET

by

Jeff T. Yarch

A dissertation submitted to the faculty of
The University of Utah
in partial fulfillment of the requirements for the degree of

Doctor of Philosophy

Interdepartmental Program in Neuroscience

The University of Utah

May 2017

The University of Utah Graduate School

STATEMENT OF DISSERTATION APPROVAL

The dissertation of **Jeff T. Yarch**

has been approved by the following supervisory committee members:

Alessandra Angelucci	, Chair	**12/19/2016** Date Approved
Robert Marc	, Member	**12/19/2016** Date Approved
Sarah Creem-Regehr	, Member	**12/19/2016** Date Approved
Tolga Tasdizen	, Member	**12/19/2016** Date Approved
K.C. Brennan	, Member	**12/19/2016** Date Approved

and by **Richard Dorsky** , Chair/Dean of

the Department/College/School of **Interdepartmental Program in Neuroscience**

and by David B. Kieda, Dean of The Graduate School.

ABSTRACT

In order to understand how our brains produce our visual experience of the world, a mechanistic understanding of the circuitry of the visual system is necessary. Neural circuits in the brain extract a 3D image of the world by executing computations on 2D information gathered by the eye. Area V1 in visual cortex receives information from the eye and re-distributes it into the dorsal and ventral pathways of the visual system. Somehow, the dorsal pathway enables us to perceive motion and locate objects in space, while the ventral pathway enables us to perceive and recognize what the object is. Developing a comprehensive circuit diagram of V1 would be a significant step towards understanding how information from the eye is re-combined and routed into the dorsal and ventral streams. In this study, we investigated the neurons that project from layer 4B (L4B) in V1 to the adjacent visual area V2. We specifically examined neurons in L4B that provide information to the thick (dorsal pathway) and thin (ventral pathway) stripes within V2. We also investigated the local (intra-V1) axonal branching patterns of L4B neurons projecting to thick stripes in order to understand where they are distributing information to within V1. We first find evidence that there is a greater contribution of motion information (magnocellular) from L4B than previously

reported to both thin and thick stripes. Further, we find that the information relayed to these V2 stripes comes from a variety of cell sizes, which differs from previous descriptions and suggests further specialization in the connectivity between these two areas. Finally, we find evidence for different circuits within V1 for the L4B neurons projecting to V2 thick stripes. We show that the pattern of information distribution within V1 is not homogenous, as has been previously described. We also show that L4B neurons provide information to functional areas (interblobs) that were previously considered devoid of L4B input. Overall, our findings reveal different morphological cell types and circuits in L4B of V1, which we attribute to the identification of these neurons' projection targets outside of V1, which was lacking in previous studies.

TABLE OF CONTENTS

LIST OF FIGURES

ACKNOWLEDGMENTS

I would like to thank the faculty of the California State University, Chico, particularly the Psychology department, for putting me in a position to succeed in graduate school. Special thanks to: Terry Miller-Herringer, Larry Herringer, Linda Kline, Joyce Norman, Penelope Kuhn, Ted Singelis, Dan Worthen, Brian Oppy, Jane Rysberg, Jill Emanuel, Barbara Heidinger, Larry Kirk, Martin van den Berg, Eddie Vela, and Celeste Jones. Thank you to Gary Bunn for being an exemplar of perfection. Thank you to Kristen Keefe, Rich Dorsky, and especially Mary Lucero for giving me the opportunity to pursue my Ph.D. and for leading an exceptional Neuroscience Program. Thank you to Tracy Marble for running an exceptional Neuroscience Program. Thank you to my mother for being an exemplar of work ethic. Thank you to my father for pursuing opportunity. Thank you to Jen Ichica, Fred Federer, and Sam Merlin for guidance, training, and experimental assistance. Thank you to Kesi Sainsbury for technical work and training. Thank you to Maryam Bijanzadeh for her enduring comradery and spirit. Thank you to Lauri Nurminen for his enthusiasm and passion for science. Thank you to the large animal facility team for their professionalism. A special thank you to Marcus Chen, Christina Cotrell, Mike Fiedel, and

especially Anny Pham and Hannah Larsen for all of their hard work. Finally, thank you to Alessandra Angelucci for accepting me into her laboratory and providing me the opportunity to earn my Ph.D.

CHAPTER 1

INTRODUCTION

Our sensory experience of the world is dominated by our vision. What appears to be a seamless, uninterrupted visual scene is actually a reconstruction of a 3D world from bits of 2D information captured by our eyes and sent to our brains (Figure 1.1). A primary goal of visual neuroscience is to figure out how our brains rebuild the visual scene.

The heavily studied field of visual neuroscience has established a number of principles for how our visual system is organized. First, it is understood that visual information is processed in parallel pathways. Distinct pathways carry different kinds of information, and thus, different elements of the visual scene are processed in different areas of the brain. Parallel processing streams begin in the eye and continue to and throughout the brain. Two primary streams of visual information have been discovered in the cortex: the dorsal and ventral visual pathways (Figure 1.1). The dorsal pathway primarily deals with information that helps us to locate objects in 3D space, while the ventral visual pathway allows us to identify different kinds of objects. For example, tracking a moving object, and perhaps

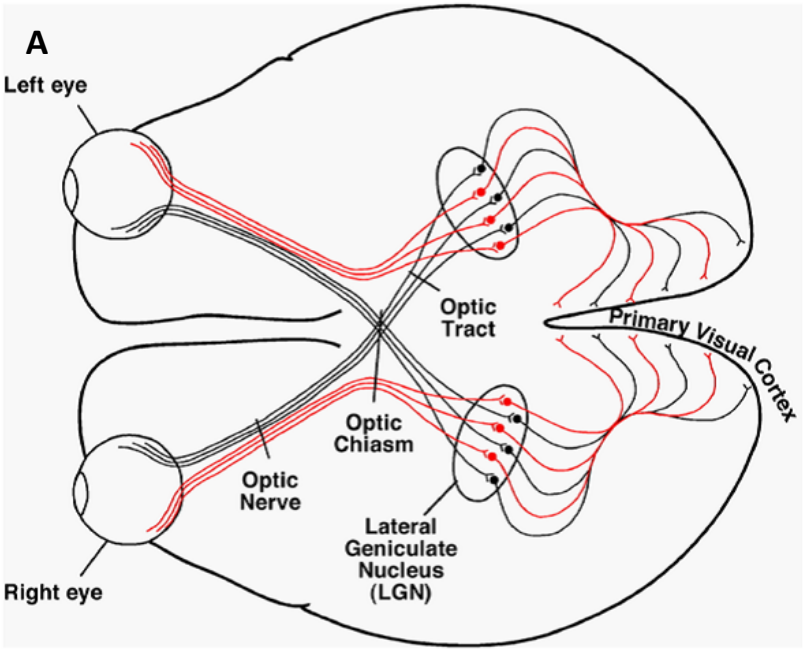

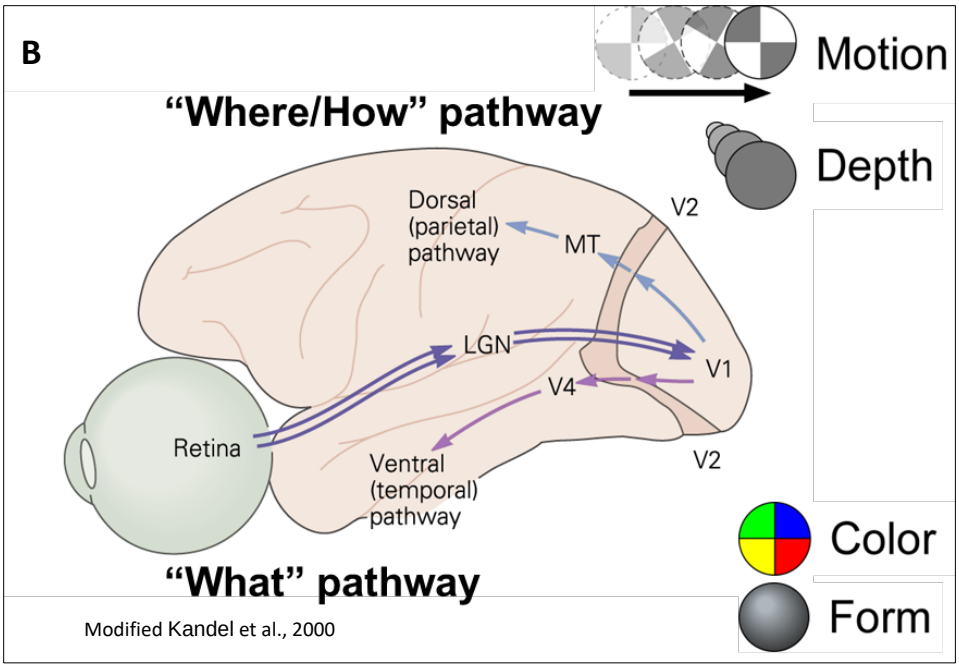

Figure 1.1: Central visual pathways. **A**, Information from the eye is relayed to the LGN. From the LGN, information is relayed to the primary visual cortex (V1) **B**, Beginning in the retina, information is relayed to the brain via multiple parallel pathways. From V1 the dorsal and ventral visual pathways begin to emerge. The dorsal visual pathway is involved with the perception of motion and depth. The ventral visual pathway is involved with the identification of objects in the visual scene.

understanding how to act upon it, would primarily be a function of the dorsal pathway; understanding what the object is and does, and that it is distinct from other objects, would primarily be a function of the ventral visual pathway (Ungerleider and Mishkin, 1982; DeYoe and Van Essen, 1988; Desimone and Ungerleider, 1989; Merigan and Maunsell, 1993; Ungerleider and Haxby, 1994). A second important principal of our visual system is that it works hierarchically, meaning that our vision is 'built up' from small, discrete elements into whole objects and scenes (Figure 1.2). Neurons located in the lower parts of the hierarchy respond to basic elements of the visual scene, such as whether or not a small spot of light is present or absent within the neurons monitoring area, referred to as the neurons receptive field (RF) (Figure 1.2). Neurons in higher stages of the hierarchy begin to respond to more complex objects, such as bars of light oriented at specific angles within their receptive field, referred to as orientation tuning. At the highest levels of the hierarchy, neurons respond to entire complex objects, such as human faces. In addition to hierarchical processing, feedback processing, which is the transfer of information from higher centers back to lower centers, is also a critical component to the workings of the visual system. Feedback processing is outside the scope of this manuscript and will not be discussed further here. Understanding how the visual system rebuilds the visual scene using parallel and hierarchical processes is a primary objective of visual neuroscience, and it has proved to be an extraordinarily difficult, yet

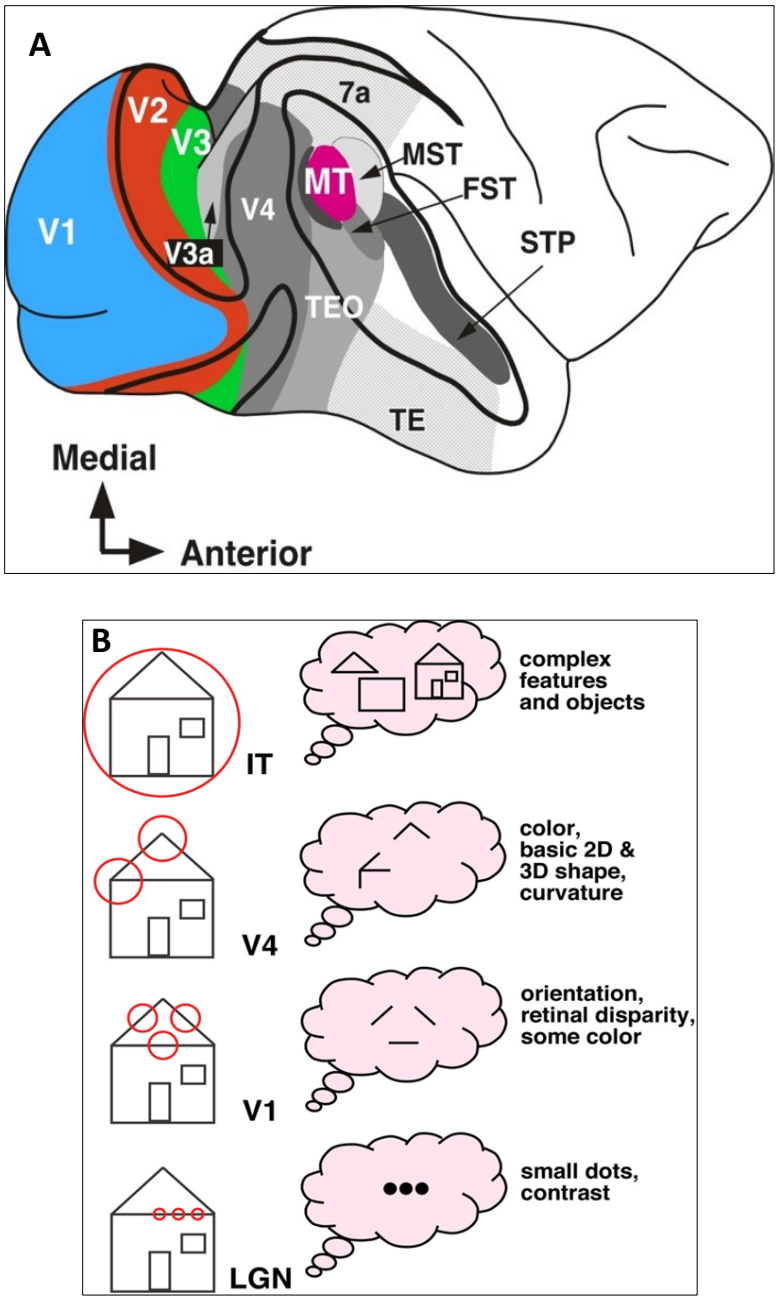

Figure 1.2: Cortical areas involved in hierarchical processing within the visual system. **A**, Moving from posterior cortex (V1) roughly anteriorly (e.g., toward V4), visual information is passed across modules (V2,V3) in a hierarchical fashion. **B**, Receptive Field (RF) properties of neurons in the hierarchy. Moving "up" through the hierarchy, neurons respond to more complex stimuli (e.g., 'spots' of light in V1, oriented lines in V2, and conjoined lines in V4). Somehow, neurons in areas such as area IT respond to specific objects.

tractable, problem to tackle. A third feature of the visual system is the instantiation of parallel and hierarchical processing via layered structures found consistently within the eye, thalamus, and cerebral cortex. Laminar structures provide a substrate for parallel and hierarchical processing. For example, different pathways of information can remain segregated by being exclusively confined to specific layers (Figure 1.3). In turn, the sequential passing of information from one layer to another provides the opportunity for that information to be modified or elaborated upon in each subsequent layer (Figure 1.3). Additionally, and a fourth visual system principle, is the discovery of distinct areas of cortex, or modules, each of which contain their own map of the entire visual field (Figure 1.4). Each of these visual modules is distinct in their anatomical location and physiological functions. A modular organization of the visual system allows for the passing of information processed from internal laminar circuits in one module to be worked on by other modules. Visual information can thus be expanded upon by modules along a hierarchy, each with their own unique purpose. Interactions among modules somehow result in the construction of our visual perception.

Finally, it has recently become clear that the basic units of the visual system, neurons, are unique in and of themselves and in their connectivity. There is a deep history of anatomical and physiological research throughout all of neuroscience, but uniting these two approaches to understanding brain

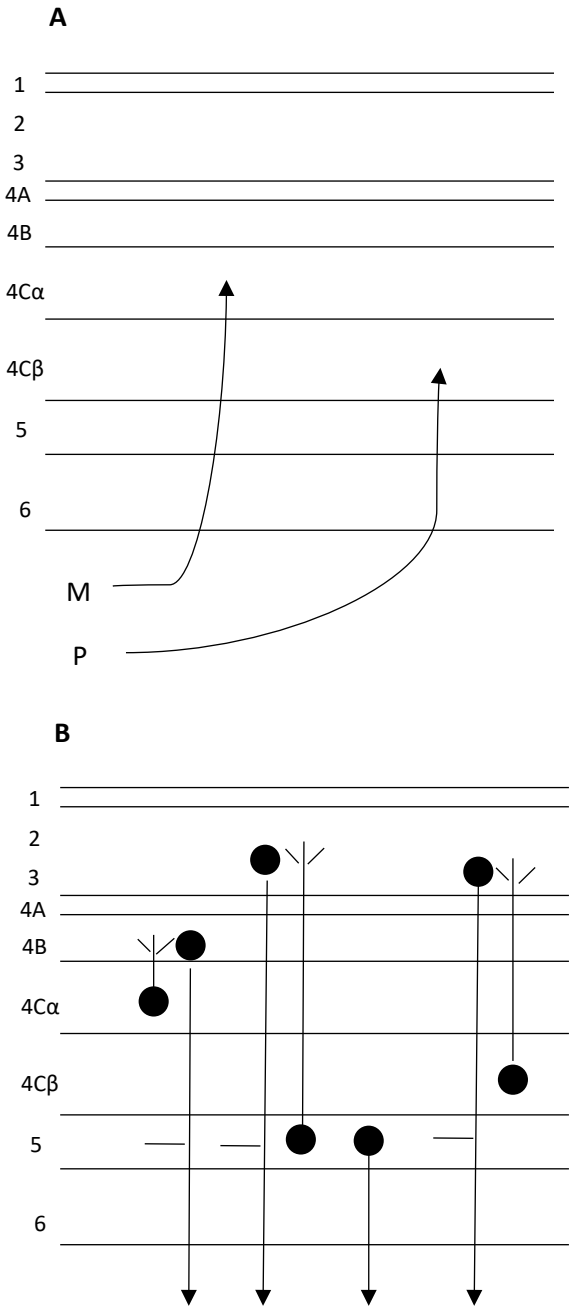

Figure 1.3: Segregation of parallel pathways via layers. A, Input from the LGN remains segregated upon arrival in V1. M axons terminate in L4Cα, P axons terminate in L4Cβ. **B,** Passing of information across V1 layers. Both local and projection neurons in V1 are able to pass information to different and specific layers. L4Cα neurons can relay information to L4B. L4Cβ neurons can relay information to L2/3. Adapted from Kandel et al., 2000.

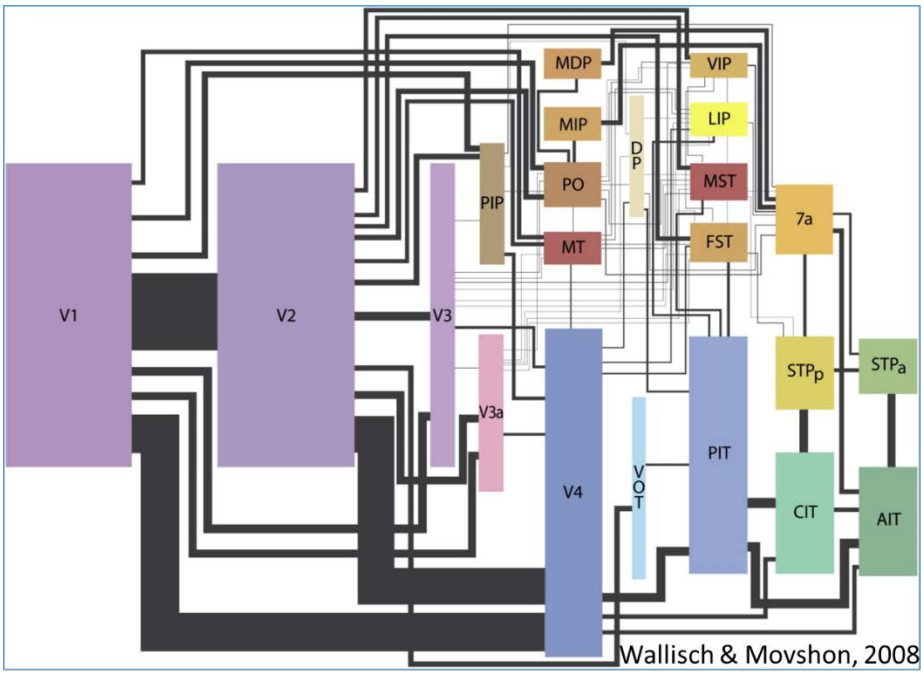

Figure 1.4: Cortical modules within the visual system. Information is passed from module to module generally in a hierarchical fashion. Interconnectivity amongst modules somehow results in visual perception. See Figure 1.2A for the cortical location of some visual modules within the brain

function at the single cell level has been a more recent endeavor. For example, in the retina, numerous cells had been identified that have different morphological features (e.g., dendrites, axonal branching patterns), and more recently have been shown to have corresponding molecular and electrophysiological signatures. In turn, these different neurons have different connectivity patterns, thus forming unique circuits. Retinal amacrine cells help illustrate this structure-function relationship, as well as the existence of specialized circuitry. A2 amacrine cells have dendrites that spread over a small area, 20-60um in diameter, and they have been categorized as narrow-field cells, meaning they monitor relatively small areas of visual space. Their dendrites are primarily confined to retinal sublamina-A. A2 cells have been shown to signal with the inhibitory neurotransmitter, glycine. These neurons are active when there is no light found in the center of their RFs, and they pass this information to RGCs in sublamina-A, which also signal when no light is detected. In contrast, starburst amacrine cells have dendrites that cover a larger amount of space, approximately 300um-500um in diameter, and are categorized as medium-field cells. The dendrites of subclass-b starburst cells are located in sublamina-B of the retina. Interestingly, starburst amacrine cells signal with both acetycholine (Ach) and gamma-Aminobutyric acid (GABA) neurotransmitters. These neurons are active when light is detected in the center of their receptive fields, and they can pass information to directionally selective RGCs in sublamina-B

(reviewed in Marc 2008, 2011). These are just two of many different types of amacrine cells in the retina, and they clearly demonstrate an important concept in visual system organization: differently structured neurons have different physiological functions and are embedded in different circuits. Identifying, characterizing, and understanding specific cell types and their patterns of connectivity throughout the visual system is essential to understanding how our visual circuitry creates our visual experiences of the world.

This dissertation will focus on the identification and morphological characterization of specific populations of neurons in area V1 that project to specific functional domains in area V2. This work builds on our understanding of how specific populations of neurons can have different structures, and subsequently, different functions.

1.1 Overview of the Neuroanatomical Structures of the Primate Central Visual System

The following sections will describe basic anatomical structures within the visual system, and how visual information flows through these structures.

1.1.1 The Retina

The process of vision begins when light enters the eye. Light travels in the form of photons and is detected by photoreceptors (PR) that are embedded in the retina, the eye's light detection organ. Light information sensed by photoreceptors is passed and processed across multiple layers within the retina before being transmitted to the brain. Across the multiple layers of the retina, multiple circuits are embedded, each of which extracts and processes different information from the pattern of light striking the retina (see Field and Chichilinisky, 2007). The output of retinal processing to the brain is a function of retinal ganglion cells (RGCs). In mammalian retina, where more recent research and technological breakthroughs have been focused, there are at least 15 different types of RGCs, each with different functions (Masland, 2001; Rockhill et al., 2002). While there is likely similar diversity in primate retina (Hendry and Reid, 2000; Dacey, 2003), two primary RGCs have been identified and studied extensively in primate, parasol and midget RGCs. These two cell types were initially identified by their size; parasol RGCs have large dendritic fields, while midget RGCs' dendritic fields are much smaller, suggesting they monitor smaller areas of visual space (Polyak, 1941; Watanabe and Rodieck, 1989; Kaplan et al., 1990; Dacey and Petersen, 1992; Rodieck and Watanabe 1993) (Figure 1.5). The differential structure between these cells suggests that in turn they have different physiological functions. Indeed, a structure-function relationship

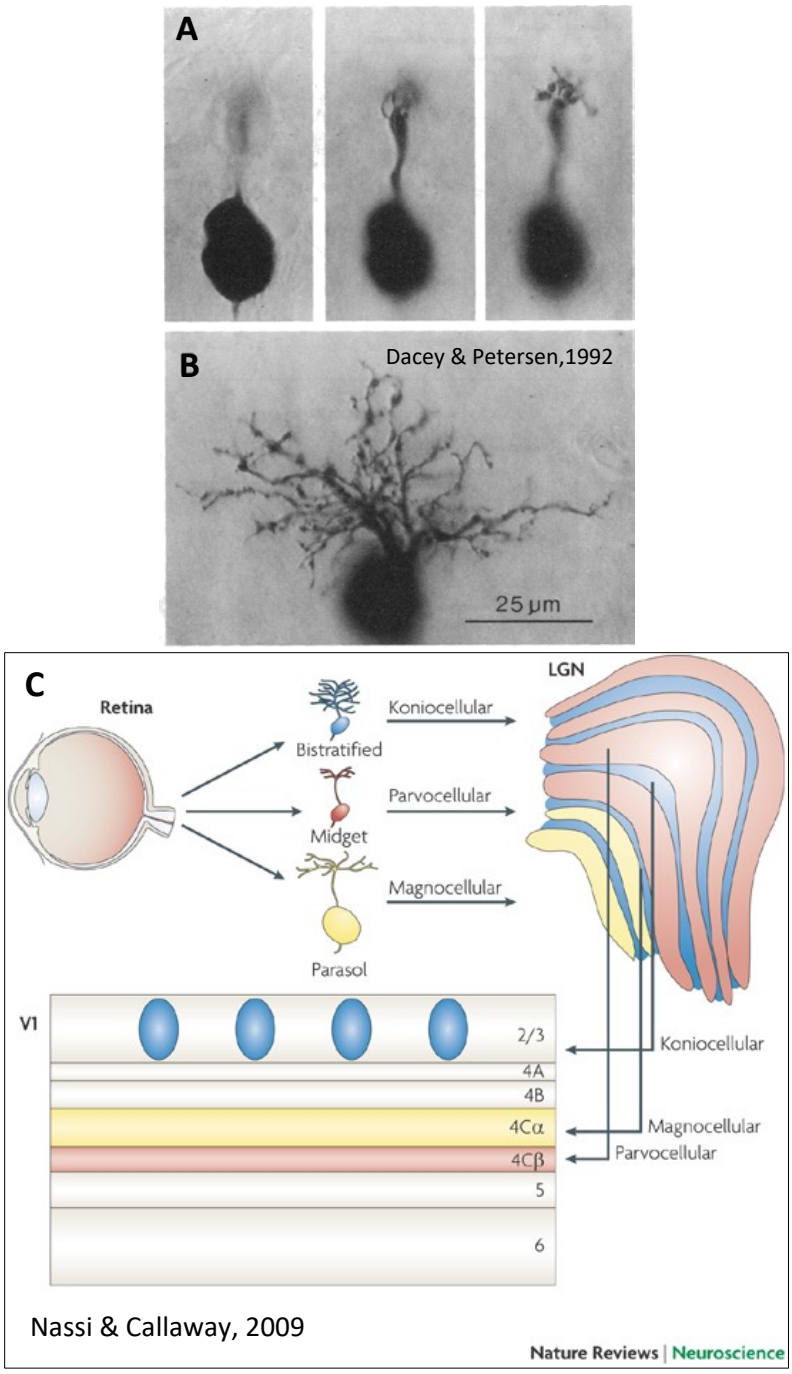

Figure 1.5: Midget (M) and Parasol (P) neurons. A, Midget RGGs have small dendritic fields. **B**, Parasol RGCs have large dendritic fields. **C,** Midget and Parasol axons (optic nerve) terminate in specific layers in the LGN. In turn, the M and P pathways from the LGN terminate in specific layers in V1 (M-to-L4Ca, P-to-L4Cb).

has been shown between these cells, as well as among the bipolar and amacrine cells, which primarily comprise the intervening layers between PRs and RGCs (reviewed in Marc, 2008). Physiological properties of midget and parasol cells are discussed further below.

1.1.2 Lateral Geniculate Nucleus of the Thalamus

The optic nerve connects the eye to the brain and is comprised of RGC axons that carry information from the retina to the lateral geniculate nucleus of the thalamus (LGN) (Figure 1.1). The LGN is also organized in a laminar structure, with parasol and midget RGC axons terminating within specific layers (Figure 1.5). The LGN transmits information to multiple cortical and subcortical areas, but its main target is the primary visual cortex, often referred to as V1, striate cortex, or Broadman's area 17 (Figure 1.5).

1.1.3 V1 and the Dorsal and Ventral Visual Processing Streams

V1 is located across the occipital cortex, covering the area from the most posterior part of the neocortex, the occipital pole, anteriorly up to the lunate sulcus. In V1, information from the LGN is received, organized, processed, and then distributed to other areas of the cortex. From V1, the dorsal and ventral visual processing streams begin to emerge (see Figure 1.1). Thus, understanding how V1 processes information from the LGN, and

then passes it onto other cortical modules within the dorsal and ventral pathways, is crucial to understanding how the visual system works (see Nassi and Callaway, 2009 for an excellent review).

1.2 Overview of the Physiological Functions Within the Primate Central Visual System

The following section will broadly discuss physiological functions associated with different structures (i.e., retina, LGN, V1) in the visual system.

1.2.1 General Physiological Functions in the Retina

The detection of light by photoreceptors in the retina changes the continuous flow of neurotransmitter release onto postsynaptic targets. RGCs eventually receive this input and transform it into discrete signals that are relayed to the LGN as action potentials. Parasol and midget RGCs have been shown to have distinct response properties. Parasol RGCs generate fast moving action potentials when there is achromatic, high contrast, moving patterns of light over larger areas of the visual field. Midget ganglion cells respond to different wavelengths of light (color) over smaller areas of the visual field with slower moving action potentials. Midget RGCs also respond best when there is a dense amount of information within their receptive fields, while parasol RGCs respond best when the information content is low

(Kaplan and Shapley, 1986; Shapley and Perry, 1986; Merrigan, 1989; Lee et al., 1990; Dacey et al., 2003). Thus, parasol cells are better suited to capture a broad sketch of an object moving against a background, while midget cells are better able to distinguish the fine details of the objects in the visual scene.

1.2.2 General Physiological Functions of LGN Neurons

The different response properties of midget RGCs are inherited by parvocellular (P) neurons in the LGN, while parasol RGCs relay information to magnocellular (M) LGN neurons. Multiple parasol RGCs can converge onto an M LGN neuron, enabling the M cell to monitor and integrate information over a larger area of the visual scene. The Midget-to-P pathway has less convergence, as 1:1 relationships between Midget and P cells are more common in order to maintain high spatial resolution (Michael, 1988; reviewed in Dacey, 2000). Both M and P neurons monitor small circumscribed areas, or spots, of visual space. P neurons communicate to V1 more slowly, have smaller RFs that are sensitive to color and densely packed information, and they are less interested in contrast/luminance or temporal frequency (De Valois et al., 1966; Dreher et al., 1976; De Valois et al., 1977; Kruger, 1977; Schiller and Malpeli, 1978; Shapley et al., 1981; Hicks et al., 1983; Derrington and Lennie, 1984; Xu et al., 2001). M neurons communicate to V1 more quickly, have larger RFs, are sensitive to achromatic contrast rather than color, and prefer faster moving stimuli with low information

content (De Valois et al., 1966; Hubel and Wiesel, 1966; Dreher et al., 1976; De Valois et al., 1977; Kruger, 1977; Schiller and Malpeli, 1978; Shapley et al., 1981; Hicks et al., 1983; Derrington and Lennie, 1984; Xu, 2001).

1.2.3 General Physiological Properties of V1 Neurons

Within V1, information from the LGN is initially segregated in specific layers, but is then eventually combined across layers, allowing neurons to respond to more complex stimuli. For example, V1 neurons can respond preferentially to rectangular bars of light positioned in specific directions, referred to as orientation tuning. Convergence of LGN spot-like RF information onto V1 cells is hypothesized to be the basis for the emergence of this orientation tuning property in V1 (Hubel and Wiesel, 1962). Somehow, V1 neurons can also become tuned to respond to additional stimulus features, which are discussed in further detail below.

Overall, within the central visual pathways, different anatomical structures are associated with different physiological functions, and this organizational feature is repeated along each step of the visual processing system.

1.3 Detailed Neuroanatomical Structure of V1

The circuitry embedded within and across V1 layers is highly complex. While much is known about how layers are generally organized and how they

interact with one another, much is still to be determined regarding the organization and interaction among specific cell types distributed across these layers.

1.3.1 V1 Layers

Within V1, there are six primary layers (1-6), most of which contain sublayers. Layer 4C (L4C) is the primary recipient of LGN input. Layers 4A and 6 also receive direct LGN input, but will not be discussed further here. L4Cα predominantly receives M input from the LGN, while L4Cß receives dominant P input (Hubel and Wiesel, 1972, Hendrickson et al., 1978; Blasdel and Lund, 1983; Chatterjee and Callaway, 2003) (see Figures 1.3, 1.5). Thus, from RGCs, to LGN, to L4C in V1, two primary streams of information (M and P) remain relatively segregated. However, outside of L4C, other V1 layers provide the opportunity for combining information from the M and P streams.

In general, M stream information is relayed from L4Cα to L4B, while P stream information is relayed from L4Cß to L2/3 (Lund, 1973; Fitzpatrick et al., 1985; Yoshioko et al., 1994; Callaway and Wiser, 1996; Yabutta and Callaway, 1998). Neurons in L4B can send local projections up to L2/3 and down to L5. L2/3 neurons can send projections to L4B and L5. Neurons in L5 can send axons to both L2/3 and L4B (Lund and Boothe, 1975; Blasdel et al., 1985; Lund and Yoshioka, 1991; LaChica et al., 1992; Callaway and

Wiser, 1996). Thus, for neurons in V1 layers outside of L4C, there is opportunity for cells to mix M and P information across layers. Understanding which cells in which layers mix, or do not mix, M and P information, and deciphering how these neurons are connected, is a part of the visual system wiring diagram that is needed in order to understand how circuits are formed, and subsequently, approach solving their computations (see Yabutta and Callaway, 2001; Nassi et al., 2006; Nassi and Callaway, 2007).

1.3.2 V1 Cytochrome Oxidase (CO) Domains

In addition to laminar specificity within V1, there are also specialized compartments that span across layers. Neurons with similar functions (e.g., ocular dominance, orientation selectivity) can be found clustered together into columns. From L2 down to L6, within a circumscribed area of the cortex, neurons that respond to specific visual stimuli tend to sit atop one another, forming vertically oriented functional columns (Hubel and Wiesel, 1974; Levay et al., 1975; Hubel et al., 1977; Blasdel and Salama, 1986). Superimposed onto these columns are other domains of clustered organization, namely the cytochrome oxidase compartments.

An interesting architectural feature of V1, particularly apparent in L3, is the emergence of dark patchy domains when tissue is stained for the mitochondrial enzyme cytochrome oxidase (CO). The dark regions of CO

staining are referred to as blobs, while the pale regions between blobs are referred to as interblobs (Horton and Hubel, 1981) (Figure 1.6). There is evidence that neurons in blobs and interblobs may have different physiological response properties, which is discussed further below.

1.3.3 Projections Outside of V1 (Extrastriate Cortex)

With the exception of L4C and layer 1, there are cells in all V1 layers that project outside of V1 (see Sincich and Horton, 2002; Federer et al., 2009). Neurons in L2/3 and L4B project primarily to either V2, V3, or MT (Tigges et al., 1981; Burkhalter et al., 1986; Livingstone and Hubel, 1987; Shipp and Zeki, 1989; Sincich and Horton 2002; Federer et al., 2009). There is also evidence that some cells project to multiple areas, although these cells appear to be rare (Sincich and Horton, 2003; Federer et al., 2009). Both L5 and L6 neurons send projections to subcortical targets; L5 neurons project to the superior colliculus, pulvinar, or pons, and L6 neurons project to the LGN and claustrum (Lund and Boothe, 1975; Fries and Distel, 1983; Fries, 1984; Lund, 1988; Lia and Olavarria, 1996) (Figure 1.6). Interestingly, neurons in blob domains send projections to different functional areas in V2 compared to cells in interlob domains. Thus, it is clear that there are different CO domains in V1, and their segregated output to V2 further strengthens the idea that these two compartments are performing different functions.

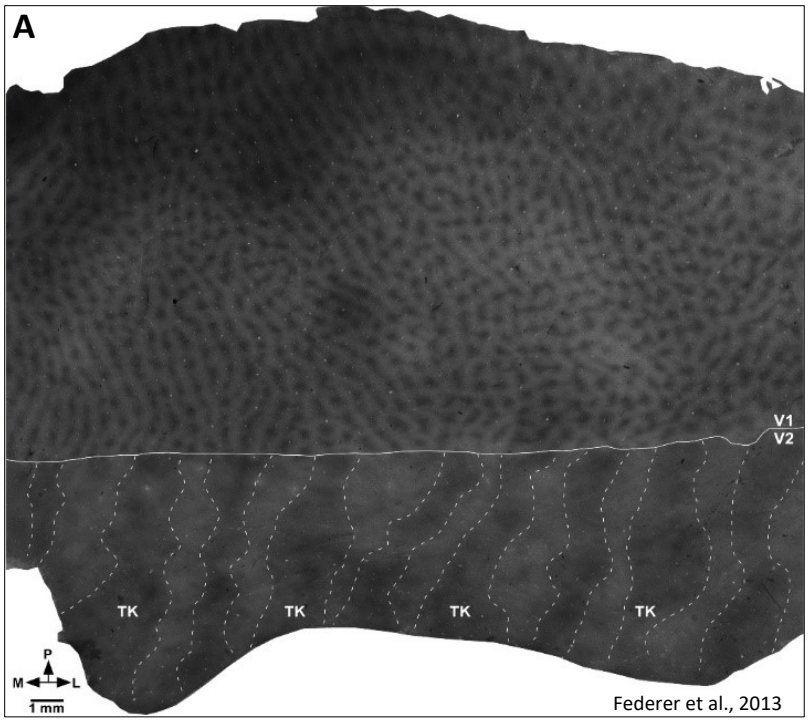

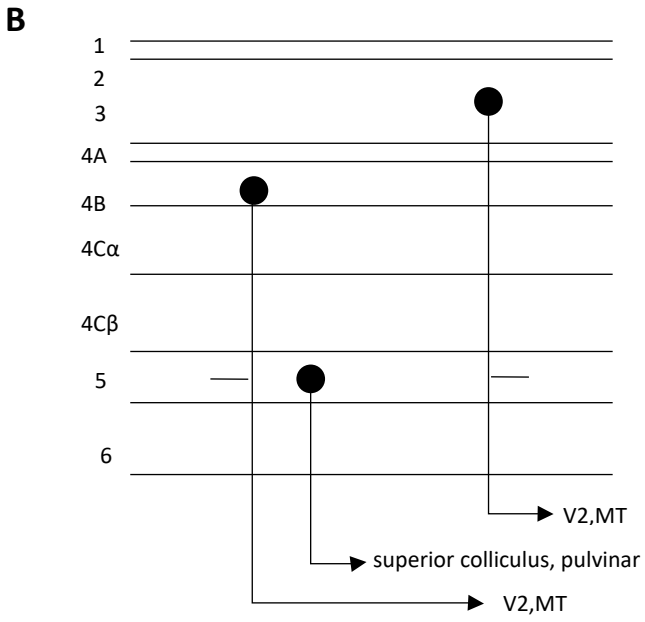

Figure 1.6: CO compartments and layers in V1 and V2. A, In the top portion of the picture, dark spots are blobs and pale areas are interblobs in V1. In the bottom portion, the V2 stripes are shown (thick, pale, thin, pale) **B,** Projection targets of neurons across V1 layers. Layers 4B and 2/3 project to extrastriate regions (e.g., V2, MT). Layer 5 projects subcortically (e.g., superior colliculus). Adapted from Kandel et al.,2000.

1.4 Detailed Neurophysiological Functions of V1

The anatomical layout of V1, including layers and CO compartments, was previously described. Now, the physiological functions associated with these different structural features will be discussed.

1.4.1 Physiological Properties of V1 Layers

As mentioned above, axons from the M layers of LGN primarily terminate in L4Cα, while P layer axons terminate primarily in L4Cß. In turn, L4Cα neurons respond to M-like stimuli, and L4Cß neurons respond to P-like stimuli (Blasdel and Fitzpatrick, 1984). However, outside of L4C, the M and P pathway segregation is much less clear and there is considerable opportunity for elaboration upon, and mixing of, this information. Generally, across layers outside of L4C, one of the most notable functional properties that emerges in V1 is orientation tuning. Orientation tuning, touched on previously, refers to a neuron's preference for bars of light oriented in specific directions. For example, some cells may respond preferentially to bars of light oriented at 90° with increased action potentials (spiking), while other V1 neurons would not increase spiking to a 90° stimuli, but would to a 180° stimuli. Orientation tuned neurons exist throughout all V1 layers, especially L2/3. In addition to orientation tuning, some neurons in L2/3 of V1 have been shown to be tuned for wavelength sensitivity (a substrate for color vision) (Livingstone and Hubel, 1984; Ts'o and Gilbert, 1988; Edwards et al.,

1995; Leventhal et al., 1995; Yoshioka and Dow, 1996). However, the functional organization of color tuned neurons in V1 remains unclear (e.g., Okeefe et al., 1998). Neurons in L4B have been shown to be orientation tuned, but are also sensitive to direction of motion, and possibly disparity (a substrate for depth perception) (Dow, 1974; Poggio and Fischer, 1977; Livingstone and Hubel, 1984; Blasdel and Fitzpatrick, 1984; Ohzawa and Freeman, 1986; Livingstone and Hubel, 1987). L4B neurons do not seem to be tuned for color selectivity (Livingstone and Hubel, 1988) and the overall functional organization of cells in this layer has yet to be systematically mapped.

1.4.2 V1 CO Compartment Physiological Properties

Neurons located in the CO dark blob patches in V1, which are most visible in L3, were initially shown to respond preferentially to different wavelengths of light, i.e., color selectivity/tuning (Livingstone and Hubel, 1984). Neurons located in the CO bereft interblob domains were originally shown to be primarily orientation tuned (Livingstone and Hubel, 1987). This dichotomy of function fit neatly into the architectural blob/interblob dichotomy, and appeared to explain the functional organization of color and orientation selectivity in V1 (Livingstone and Hubel, 1988), but it has since been shown that neurons in either blobs or interblobs can be tuned to either wavelength or orientation (Edwards et al., 1995; Leventhal et al., 1995;

O'Keefe et al., 1998; also see Cassagrande and Xu, 2004). However, there still seems to be a bias for color selective neurons to be associated with blobs (Lu et al., 2008). It remains difficult to cleanly characterize the physiological functions of blob and interblob domains. However, as will be elaborated upon below, data have consistently shown that the output of blobs and interblobs is dedicated to different functional areas of V2, suggesting that blobs and interblobs have different physiological functions that have yet to be clearly elucidated.

1.5 Neuroanatomical and Neurophysiological Organization of V2

The majority of output from area V1 is directed to V2. V1 output to V2 primarily comes from L4B and L2/3. V2 output appears to be neatly segregated into the dorsal and ventral pathways.

1.5.1 V2 Layers

Area V2 is the cortical area immediately anterior to, and abutting with V1 (see Figures 1.1, 1.2, 1.6.). There is an exposed portion of V2 along the dorsal lip of the lunate sulcus, where it abuts with V1. However, the bulk of area V2 is buried within the lunate sulcus. The location of V2 has made it relatively difficult to comprehensively study, but the exposed region outside of the sulcus provides simple access and has been the target of many V2 studies. This area of V2, which is investigated in this dissertation,

represents ~2-5° eccentricity (i.e., degrees away from the fovea in visual space), and is mostly covering the lower hemifield of visual space (Roe and Tso, 1995). Like V1, V2 has a laminar structure; however, the layers are more simplified than in V1. In V2, input is primarily received in lower layer 3 and 4, with layers 2/3 projecting to other extrastriate areas, and layer 5 and 6 projecting subcortically (Shipp and Zeki, 1984; DeYoe and Van Essen, 1985; Levitt et al., 1995; Anderson and Martin, 2009).

1.5.2 V2 CO Domains: Thick, Thin, Pale Stripes

Similar to V1, there are areas in V2 that stain darkly due to their CO rich composition. The dark stained areas are interrupted by not dark areas, creating a 'stripe-cycle' across V2. By eye, there appears to be two types of dark CO stripes in V2, those that are wide (thick stripes), and those that are relatively more narrow (thin stripes). Intervening between the dark stripes are the areas that do not stain strongly for CO, these domains are referred to as pale stripes. Across V2, there is a repeating pattern of thick (TK), pale (PL), thin (TN), and pale stripes (Tootell et al., 1983; Horton, 1984) (Figure 1.6). These four repeating stripes constitute a single stripe cycle, and each cycle covers approximately 4 mm of cortex. Multiple studies have shown that V1 blobs send information to V2 thin stripes, while V1 interblobs send information to V2 thick and pale stripes (Livingstone and Hubel, 1984; Sincich and Horton, 2002; Sincich and Horton, 2005; Federer et al., 2009;

Sincich and Horton, 2010; Federer et al., 2011) (Figure 1.7).

1.5.3 V2 Physiological Functions

Physiologically, the dark CO stripes (TK, TN) have been shown to differ from each other, and from the pale stripes. Thin stripes have been shown to have a large proportion of color selective neurons while thick stripes are more involved with orientation, direction of motion, and disparity tuning (DeYoe and Van Essen, 1985; Peterhan and von der Heydt, 1993; Levitt et al., 1994; Munk et al., 1995; Roe and Ts'o, 1995; Gegenferter et al., 1996; Shipp and Zeki, 2002; Lu et al., 2008). Pale stripes have been shown to respond to orientation and direction of motion, but generally less to disparity (DeYoe and Van Essen, 1985; Peterhans and von der Heydt, 1993; Roe and Tso, 1995). It is important to highlight the different physiological functions associated with the different CO compartments in both V1 and V2 because it demonstrates that these structural differences are not arbitrary; there is evidence showing that the differential structures are associated with differential functions. While the physiological functions associate with blobs and interblobs, thick, thin, and pale stripes are not clear cut, and our current interpretations will likely be amended, this is more likely due to our lack of understanding rather than a lack of functional heterogeneity across areas.

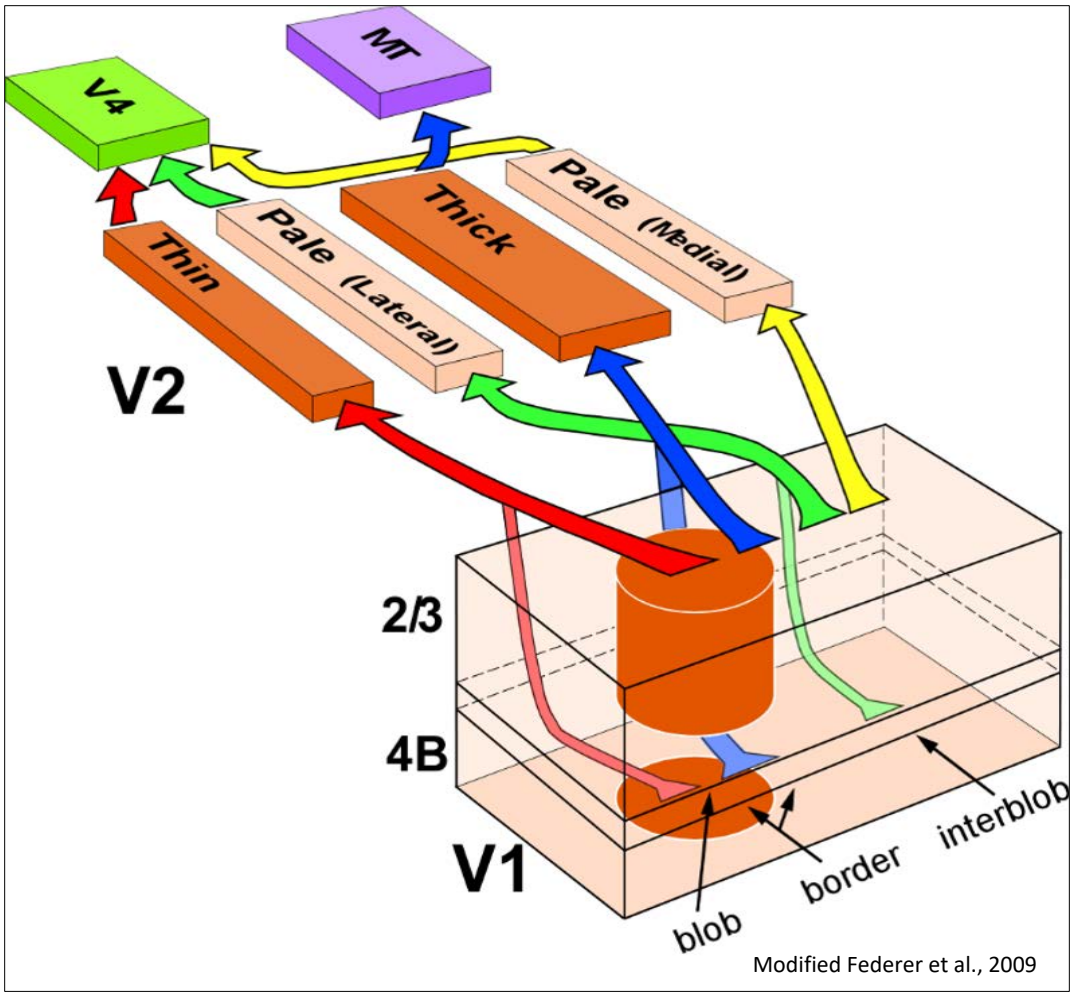

Figure 1.7: Pathways from V1 CO compartments to V2 CO compartments. Blobs in L2/3 of V1, and in the column below in L4B, project to V2 thin stripes. Neurons in interblobs in L2/3 and below in L4B project to thick and pale stripes, but there appears to be a bias for thick stripe projecting neurons to be located at the blob border. Thick stripes project to MT (dorsal pathway), thin stripes project to V4 (ventral pathway).

1.5.4 V2 Projections to Dorsal and Ventral Streams

V2 thick stripes have been shown to project exclusively to the medial temporal area (MT), while thin and pale stripes have been shown to project exclusively to V4 (DeYoe and Van Essen, 1985; Shipp and Zeki, 1985) (Figure 1.7). This is important for two reasons: 1) it shows that there is segregation of output from V2 CO domains to other extrastriate visual areas, strongly suggesting different functions for the different stripes, 2a) Area MT is a primary component of the dorsal visual pathway, a stream of information heavily involved in the perception of motion and location of objects in space, 2b) Area V4 is a primary component of the ventral visual pathway; this stream is heavily involved with the construction, identification, and perception of whole objects (Ungerleider and Mishkin, 1982; Mishkin et al., 1983).

1.6 The Role of V1, L4B Neurons in the Visual System

L4B in V1 is unique, because unlike other layers outside of L4C, it is primarily driven by one type of input – M-type from L4Cα (Callaway and Wiser, 1996; Yabutta and Callaway, 2001). Unlike L4C neurons, L4B neurons project out of V1 and directly to other extrastriate regions, including strong projections to MT and V2 TK stripes (Livingstone and Hubel, 1987; Sincich and Horton, 2002; Sincich and Horton, 2003; Federer et al., 2009). Interestingly, L4B is comprised of two morphologically distinct cell types that

project out of V1, spiny stellates and pyramids (Shipp and Zeki, 1989; Sincich and Horton, 2003; Nassi and Callaway, 2007).

1.6.1 L4B Cell Types and Their Morphological Characteristics

Layer 4B in V1 is located in an interesting position within the visual system. L4B receives almost exclusive M channel input from Layer 4Cα (Yabutta and Callaway, 2001). Because of this homogenous input, neurons in L4B can be thought of as being 'M-type' neurons, and their response properties represent some kind of a transformative step of M-pathway information. However, this simple characterization is complicated by the fact that there are at least two grossly distinct types of neurons in L4B that send output to area MT and V2. Spiny stellate neurons have the majority of their dendrites confined to L4B, and are thus representative M-type cells characterized above. Pyramidal cells, however, have an apical dendrite that extends out of L4B and up, well into L2 and perhaps L1 (Lund, 1973; Lund and Boothe, 1975). Thus, pyramidal cells have the capacity to integrate an array of unknown information from all layers above L4B, making their functional output likely more complex and more difficult to understand than neighboring spiny stellate cells. However, it has been shown that L4B pyramids respond to activation of L4Cα and L4Cß, making them at a minimum M+P-type neurons (Yabuta and Callaway, 2001). Interestingly, all L4B cells, whether stellate or pyramid, appear to have similar axonal

characteristics, and thus may be contributing to the same interlaminar circuits within V1. L4B neurons have been shown to predominantly send axons to L2/3, L4B, and L5 in V1, and primarily avoid L1, L4A, L4C, and L6 (Callaway and Wiser, 1996; but see Lund, 1973). Additionally, axons projecting into L2/3 exclusively target CO blobs, while the axons in L4B and L5 are non-specific relative to CO columns (Callaway and Wiser, 1996).

1.6.2 L4B Physiological Properties

While general tuning properties of L4B neurons have been established (orientation, motion, disparity), detailed characteristics on a cell by cell basis have not, and remain an interesting area for future study. However, because of the clear differences in dendritic structure of spiny stellates and pyramidal cells, it can be inferred that the two cells represent at least two unique pathways out of L4B: the pyramidal pathway is likely a mix of at least M+P information, while the stellate pathway is likely comprised of a relatively simple elaboration on 'pure' M-pathway information from L4Ca (Yabuta et al., 2001).

1.6.3 L4B Output to Extrastriate Areas

L4B neurons are known to contribute information directly to areas V3, MT, and V2 (Burkhalter et al., 1986; Livingstone and Hubel, 1987; Shipp and Zeki 1989; Sincich and Horton, 2002; Sincich and Horton, 2003; Federer et

al., 2009). L4B Projections are particularly strong to MT and the thick stripes in V2, both of which are involved in the dorsal visual pathway. However, it has been consistently shown that L4B also contributes input to thin stripes and at least one of the two pale stripes in V2, regions that are both involved in the ventral visual pathway (Sincich and Horton, 2005; Federer et al., 2009; Sincich and Horton, 2010). The fact that there are at least two obvious output channels formed by L4B stellates and pyramids begs the question of how much information from each of these channels is contributed to each projection target. Since each projection target has grossly different physiological response properties, it is plausible that these different properties are influenced by different inputs from L4B.

1.6.4 Questions Regarding L4B Neurons

The architecture of areas V1 and V2, as reviewed above, raises a simple question: Do V2 thick stripes, which are primarily orientation, motion, and disparity tuned, receive different input from L4B than V2 thin stripes, which are biased toward being chromatically tuned? Additionally, the canonical axonal branching motif in V1 for L4B neurons (axons target blobs in L2/3, L4B and L5) described above is derived from data that do not indicate the projection target of the cells described. Furthermore, there are no data investigating the construction of local circuits in V1 as a function of a cell's output target. Do neurons projecting to different functional targets

participate in different local circuits within V1?

1.7 Summary to the Introduction

By understanding L4B neurons in greater depth, we can begin to understand the kinds of information being transmitted from V1 to other extrastriate areas. The dorsal visual pathway is generally thought to be dominated by M-like information, as fast axonal conduction velocity, large receptive fields, and sensitivity to low contrast and high temporal frequencies are all conducive to detecting and locating moving objects. Thus, it may be expected that thick stripes, which project to area MT in the dorsal pathway, primarily receive M-dominated stellate information from L4B. The ventral visual pathway is generally thought to be dominated by P-type information. Preference for dense information in small receptive fields, as well as chromatic sensitivity and a lack of interest in temporal information, are response properties conducive to extracting the details and coherence of different objects in the visual scene. Thus, it may be expected that thin stripes, which project to V4 and the ventral pathway, primarily receive M+P pyramidal cell information from L4B. However, it is clear that there is some input from both M and P streams to both dorsal and ventral pathways (Nassi et al., 2006). Lesions of either the M or P layers in the LGN result in deficits in both dorsal and ventral pathways (Merigan et al.,1991a; Merigan et al., 1991b). Understanding L4B input to thick and thin stripes will further our

understanding of the sources of M and P input that are routed into dorsal and ventral pathways. Finally, the local circuits within area V1 affect the output of V1 neurons. Local circuits in V1 are constructed from the axons of V1 neurons spanning across layers. No information is available for the local circuits of L4B neurons as they relate to the different output targets (e.g., V2, V3, MT). Thus, it is an open question whether a previously identified single axonal motif is sufficient to explain the local V1 circuitry of all L4B neurons, or if this circuitry could differ as a function of clearly distinct and unique projection targets. A single stereotyped intra-V1 circuit for L4B cells would suggest a more homogenous computation is relayed to each projection target, perhaps making the comprehension of the L4B computation more tractable. Different intra-V1 circuits as a function of the different targets of L4B cells would suggest heterogeneous local computations, and would require identification of the projection target in order to comprehend the computation being performed. Answering the above questions will result in knowledge that will help to transform simple visual system wiring diagrams into more informative circuit diagrams, which are essential to understanding how human brains instantiate visual perception.

In this dissertation, I describe the morphological characteristics of L4B neurons that project specifically to V2 thick and thin CO stripes. In Chapter 2, we show that different proportions of stellates and pyramids contribute information to thick vs. thin stripes, and that these proportions differ from

previously described proportions going to V2 generally. We also present evidence for different classes of L4B neurons categorized by their size, with different sizes of cells projecting to thick and thin stripes, and between thick and thin stripes. In Chapter 3, we investigate the V1 layers targeted by L4B neurons that project to thick stripes and show that there are neurons that do not recapitulate the canonical L2/3, L4B, L5 circuit motif. In Chapter 4, we look at the location of V1 axons relative to CO blob/interblob compartments for this thick stripe projecting population of L4B cells. We find that the axons of all sampled neurons, across all layers, avoid CO blobs in L2/3, and the CO column below, which is in stark contrast to canonical L4B circuitry. Chapter 5 will summarize the results of this dissertation and briefly discuss overall implications and future directions.

1.8 References

Anderson JC, Martin KA (2009) The synaptic connections between cortical areas V1 and V2 in macaque monkey. J Neurosci 29:11283-11293.

Blasdel GG, Lund JS (1983) Termination of afferent axons in macaque striate cortex. J Neurosci 3:1389-1413.

Blasdel GG, Fitzpatrick D (1984) Physiological organization of layer 4 in macaque striate cortex. J Neurosci 4:880-895.

Blasdel GG, Lund JS, Fitzpatrick D (1985) Intrinsic connections of macaque striate cortex: axonal projections of cells outside lamina 4C. J Neurosci 5:3350-3369.

Blasdel GG, Salama G (1986) Voltage-sensitive dyes reveal a modular organization in monkey striate cortex. Nature 321:579-585.

Burkhalter A, Felleman DJ, Newsome WT, Van Essen DC (1986) Anatomical and physiological asymmetries related to visual areas V3 and VP in macaque extrastriate cortex. Vision Res 26:63-80.

Callaway EM, Wiser AK (1996) Contributions of individual layer 2–5 spiny neurons to local circuits in macaque primary visual cortex. Vis Neurosci 13:907-922.

Casagrande V, Xu X (2004) Parallel visual pathways: a comparative perspective. In: The Visual Neurosciences (Chalupa LM, Werner JS, eds), pp 494-506. Cambridge, MA: MIT

Chatterjee S, Callaway EM (2003) Parallel colour-opponent pathways to primary visual cortex. Nature 426:668-671.

Dacey DM, Petersen MR (1992) Dendritic field size and morphology of midget and parasol ganglion cells of the human retina. Proc Natl Acad Sci USA 89:9666–9670.

Dacey DM (2000) Parallel pathways for spectral coding in primate retina. Annu Rev Neurosci 23:743–775.

Dacey DM, Peterson BB, Robinson FR, Gamlin PD (2003) Fireworks in the primate retina: in vitro photodynamics reveals diverse LGN-projecting ganglion cell types. Neuron, 37:15-27.

De Valois RL, Abramov I, Jacobs GH (1966) Analysis of response patterns of LGN cells. J Opt Soc Am 56:966-977.

De Valois RL, Snodderly DM, Yund EW, Hepler NK (1977) Responses of macaque lateral geniculate cells to luminance and color figures. Sens Processes 1:244-259.

Derrington AM, Lennie P (1984) Spatial and temporal contrast sensitivities of neurones in lateral geniculate nucleus of macaque. J Physiol 357:219-240.

Desimone R, Ungerleider LG (1989) Neural mechanisms of visual processing in monkeys. Handbook of Neuropsycho 2:267-299.

DeYoe EA, Van Essen DC (1985) Segregation of efferent connections and receptive field properties in visual area V2 of the macaque. Nature 317:58-61.

DeYoe EA, Van Essen DC (1988) Concurrent processing streams in monkey visual cortex. Trends Neurosci 11:219-226.

Dow BM (1974) Functional classes of cells and their laminar distribution in monkey visual cortex. J. Neurophysiol 37:927-946.

Dreher B, Fukada Y, Rodieck RW (1976) Identification, classification and anatomical segregation of cells with X-like and Y-like properties in the lateral geniculate nucleus of old-world primates. J Physiol 258:433-452.

Edwards DP, Purpura KP, Kaplan E (1995) Contrast sensitivity and spatial frequency response of primate cortical neurons in and around the cytochrome oxidase blobs. Vision Res. 35:1501-1523.

Federer F, Ichida JM, Jeffs J, Schiessl I, McLoughlin N, Angelucci A (2009) Four projection streams from primate V1 to the cytochrome oxidase stripes of V2. J Neurosci 29:15455-15471.

Federer F, Williams D, Ichida JM, Merlin S, Angelucci A (2013) Two projection streams from macaque V1 to the pale cytochrome oxidase stripes of V2. J Neurosci 33:11530-11539.

Field GD, Chichilnisky EJ (2007) Information processing in the primate retina: circuitry and coding. Annu Rev Neurosci 30:1-30.

Fitzpatrick D, Lund JS, Blasdel GG (1985) Intrinsic connections of macaque striate cortex: afferent and efferent connections of lamina 4C. J Neurosci 5:3329-3349.

Fries W, Distel H (1983) Large layer VI neurons of monkey striate cortex (Meynert cells) project to the superior colliculus. Proc Roy Soc Lond: Bio Sci 219:53-59.

Fries W (1984) Cortical projections to the superior colliculus in the macaque monkey: a retrograde study using horseradish peroxidase. J Comp Neurol 230:55-76.

Gegenfurtner KR, Kiper DC, Fenstemaker SB (1996) Processing of color, form, and motion in macaque area V2. Vis Neurosci 13:161-172.

Hendrickson AE, Wilson JR, Ogren MP (1978) The neuroanatomical organization of pathways between the dorsal lateral geniculate nucleus and visual cortex in Old World and New World primates. J Comp Neurol 182:123-136.

Hendry SH, Reid RC (2000) The koniocellular pathway in primate vision. Annu Rev Neurosci 23:127-153.

Hicks TP, Lee BB, Vidyasagar TR (1983) The responses of cells in macaque lateral geniculate nucleus to sinusoidal gratings. J Physiol 337:183-200.

Horton JC, Hubel DH (1981) Regular patchy distribution of cytochrome oxidase staining in primary visual cortex of macaque monkey. Nature 292:762-764.

Hubel DH, Wiesel TN (1962) Receptive fields, binocular interaction and functional architecture in the cat's visual cortex. J Physiol 160:106-154.

Hubel DH, Wiesel TN (1966) Effects of varying stimulus size and color on single lateral geniculate cells in Rhesus monkeys. Proc Natl Acad Sci USA, 55:1345-1346.

Hubel DH, Wiesel TN (1972) Laminar and columnar distribution of geniculo-cortical fibers in the macaque monkey. J Comp Neurol 146:421-450.

Hubel DH, Wiesel TN (1974) Sequence regularity and geometry of orientation columns in the monkey striate cortex. J Comp Neurol 158:267-293.

Hubel DH, Wiesel TN, Stryker MP (1977) Orientation columns in macaque monkey visual cortex demonstrated by the 2-deoxyglucose autoradiographic technique. Nature 269:328-330.

Kandel ER, Schwartz JH, Jessell TM (2000) Principles of Neural Science. New York, NY: McGraw-Hill.

Kaplan E, Shapley RM (1986) The primate retina contains two types of ganglion cells, with high and low contrast sensitivity. Proc Natl Acad Sci USA 83:2755–2757.

Kaplan E, Lee BB, Shapley RM (1990) New views of primate retinal function. Prog Retinal Res 9:273-336.

Kruger J (1977) Stimulus dependent colour specificity of monkey lateral geniculate neurones. Exp Brain Res 30:297-311.

Lachica EA, Beck PD, Casagrande VA (1992) Parallel pathways in macaque monkey striate cortex: anatomically defined columns in layer III. Proc Natl Acad Sci USA 89:3566-3570.

Lee BB, Pokorny J, Martin PR, Valbergt A, Smith VC (1990) Luminance and chromatic modulation sensitivity of macaque ganglion cells and human observers. JOSA A 7:2223-2236.

LeVay S, Hubel DH, Wiesel TN (1975) The pattern of ocular dominance columns in macaque visual cortex revealed by a reduced silver stain. J Comp Neurol 159:559-575.

Leventhal AG, Thompson KG, Liu D, Zhou Y, Ault SJ (1995) Concomitant sensitivity to orientation, direction, and color of cells in layers 2, 3, and 4 of monkey striate cortex. J Neurosci 15:1808-1818.

Levitt JB, Kiper DC, Movshon JA (1994) Receptive fields and functional architecture of macaque V2. J Neurophysiol 71:2517-2542.

Levitt JB, Yoshioka T, Lund JS (1995) Connections between the pulvinar complex and cytochrome oxidase-defined compartments in visual area V2 of macaque monkey. Exp Brain Res 104:419-430.

Lia B, Olavarria JF (1996) The distribution of corticotectal projection neurons correlates with the interblob compartment in macaque striate cortex. Vis Neurosci 13:461-466.

Livingstone MS, Hubel DH (1984) Anatomy and physiology of a color system in the primate visual cortex. J Neurosci 4:309-356.

Livingstone MS, Hubel DH (1987) Connections between layer 4B of area 17 and the thick cytochrome oxidase stripes of area 18 in the squirrel monkey. J Neurosci 7:3371-3377.

Livingstone MS, Hubel DH (1987) Psychophysical evidence for separate channels for the perception of form, color, movement, and depth. J Neurosci, 7:3416-3468.

Livingstone M, Hubel D (1988) Segregation of form, color, movement, and depth: anatomy, physiology, and perception. Science 240:740-749.

Lu HD, Roe AW (2008) Functional organization of color domains in V1 and V2 of macaque monkey revealed by optical imaging. Cerebral Cortex 18:516-533.

Lund JS (1973) Organization of neurons in the visual cortex, area 17, of the monkey (Macaca mulatta). J Comp Neurol 147:455-495.

Lund JS, Boothe RG (1975) Interlaminar connections and pyramidal neuron organisation in the visual cortex, area 17, of the macaque monkey. J Comp Neurol 159:305-334.

Lund JS (1988) Anatomical organization of macaque monkey striate visual cortex. Annu Rev Neurosci 11:253-288.

Lund JS, Yoshioka T (1991) Local circuit neurons of macaque monkey striate cortex: III. neurons of laminae 4B, 4A, and 3B. J Comp Neurol 311:234-258.

Marc RE (2008) Functional neuroanatomy of the retina. In: Albert and Jakobiec's principles and practice of ophthalmology, 3rd edition (Albert D, Miller J, Azar D, Blodi B, eds), pp 1565-1592. New York, NY: Elsevier.

Marc RE (2011) Synaptic organization of the retina. In: Adler's physiology of the eye, 11th edition (Levin L, Nilsson S, Ver Hoeve J, Wu S, Kaufman P, Alm A, eds), pp 443-458. New York, NY: Elsevier.

Masland RH (2001) The fundamental plan of the retina. Nat Neurosci 4:877-886.

Merigan WH (1989) Chromatic and achromatic vision of macaques: role of the P pathway. J Neurosci 9:776–783.

Merigan WH, Byrne CE, Maunsell JH (1991) Does primate motion perception depend on the magnocellular pathway? J Neurosci 11:3422-3429.

Merigan WH, Katz LM, Maunsell JH (1991) The effects of parvocellular lateral geniculate lesions on the acuity and contrast sensitivity of macaque monkeys. J Neurosci 11:994-1001.

Merigan WH, Maunsell JH (1993) How parallel are the primate visual pathways? Annu Rev Neurosci 16:369-402.

Michael CR (1988) Retinal afferent arborization patterns, dendritic field orientations, and the segregation of function in the lateral geniculate nucleus of the monkey. Proc Natl Acad Sci USA 85:4914-4918.

Mishkin M, Ungerleider LG, Macko KA (1983) Object vision and spatial vision: two cortical pathways. Trends Neurosci 6:414-417.

Munk MH, Nowak LG, Girard P, Chounlamountri N, Bullier J (1995) Visual latencies in cytochrome oxidase bands of macaque area V2. Proc Natl Acad Sci USA 92:988-992.

Nassi JJ, Callaway EM (2007) Specialized circuits from primary visual cortex to V2 and area MT. Neuron 55:799-808.

Nassi JJ, Callaway EM (2009) Parallel processing strategies of the primate visual system. Nat Rev Neurosci 10:360-372.

Nassi JJ, Lyon DC, Callaway EM (2006) The parvocellular LGN provides a robust disynaptic input to the visual motion area MT. Neuron 50:319-327.

O'Keefe LP, Levitt JB, Kiper DC, Shapley RM, Movshon JA (1998) Functional organization of owl monkey lateral geniculate nucleus and visual cortex. J Neurophysiol 80:594-609.

Ohzawa I, Freeman RD (1986) The binocular organization of simple cells in the cat's visual cortex. J Neurophysiol 56:221-242.

Peterhans E, Heydt R (1993) Functional organization of area V2 in the alert macaque. Eur J Neurosci 5:509-524.

Poggio GF, Fischer B (1977) Binocular interaction and depth sensitivity in striate and prestriate cortex of behaving rhesus monkey. J Neurophysiol 40:1392-1405.

Polyak SL (1941) The retina: the anatomy and the histology of the retina in man, ape, and monkey, including the consideration of visual functions, the history of physiological optics, and the histological laboratory technique. Chicago, IL: University of Chicago Press.

Rockhill RL, Daly FJ, MacNeil MA, Brown SP, Masland RH (2002) The diversity of ganglion cells in a mammalian retina. J Neurosci 22:3831-3843.

Rodieck R, Watanabe M (1993) Survey of the morphology of macaque retinal ganglion cells that project to the pretectum, superior colliculus, and parvicellular laminae of the lateral geniculate nucleus. J Comp Neurol 338:289-303.

Roe AW, Ts'o DY (1995) Visual topography in primate V2: multiple representation across functional stripes. J Neurosci 15:3689-3715.

Shapley R, Kaplan E, Soodak R (1981) Spatial summation and contrast sensitivity of X and Y cells in the lateral geniculate nucleus of the macaque. Nature 292:543-545.

Schiller PH, Malpeli JG (1978) Functional specificity of lateral geniculate nucleus laminae of the rhesus monkey. J Neurophysiol 41:788-797.

Shapley R, Perry VH (1986) Cat and monkey retinal ganglion cells and their visual functional roles. Trends Neurosci 9:229–235.

Shipp S, Zeki S (1984) Segregation of pathways leading from area V2 to areas V4 and V5 of macaque monkey visual cortex. Nature 315:322-325.

Shipp S, Zeki S (1989) The organization of connections between areas V5 and V1 in macaque monkey visual cortex. Eur J Neurosci 1:309-332.

Shipp S, Zeki S (2002) The functional organization of area V2, I: specialization across stripes and layers. Vis Neurosci 19:187-210.

Sincich LC, Horton JC (2002) Divided by cytochrome oxidase: a map of the projections from V1 to V2 in macaques. Science 295:1734-1737.

Sincich LC, Horton JC (2003) Independent projection streams from macaque striate cortex to the second visual area and middle temporal area. J Neurosci 23:5684-5692.

Sincich LC, Horton JC (2005) Input to V2 thin stripes arises from V1 cytochrome oxidase patches. J Neurosci 25:10087-10093.

Sincich LC, Jocson CM, Horton JC (2010) V1 interpatch projections to V2 thick stripes and pale stripes. J Neurosci 30:6963-6974.

Tigges J, Tigges M, Anschel S, Cross NA, Letbetter WD, McBride RL (1981) Areal and laminar distribution of neurons interconnecting the central visual cortical areas 17, 18, 19, and MT in squirrel monkey (Saimiri). J Comp Neurol 202:539-560.

Tootell RB, Silverman MS, De Valois RL, Jacobs GH (1983) Functional organization of the second cortical visual area in primates. Science 220:737-739.

Ts'o DY, Gilbert CD (1988) The organization of chromatic and spatial interactions in the primate striate cortex. J Neurosci 8:1712-1727.

Ungerleider LG, Haxby JV (1994) 'What' and 'where' in the human brain. Curr Opin Neurobiol 4:157-165.

Ungerleider LG, Miskin ME (1982) Two visual pathways in DJ Ingle, MA Goodale & RJW Mansfield. Analys Vis Behav, 1:549-586.

Wallisch P, Movshon JA (2008) Structure and function come unglued in the visual cortex. Neuron 60:195-7.

Watanabe M, Rodieck RW (1989) Parasol and midget ganglion cells of the primate retina. J Comp Neurol 289:434-454.

Wiser AK, Callaway EM (1996) Contributions of individual layer 6 pyramidal neurons to local circuitry in macaque primary visual cortex. J Neurosci 16:2724-2739.

Xu X, Ichida JM, Allison JD, Boyd JD, Bonds AB, Casagrande VA (2001) A comparison of koniocellular, magnocellular and parvocellular receptive field properties in the lateral geniculate nucleus of the owl monkey (Aotus trivirgatus). J Physiol 531:203-218.

Yabuta NH, Callaway EM (1998) Functional streams and local connections of layer 4C neurons in primary visual cortex of the macaque monkey. J Neurosci 18:9489-9499.

Yabuta NH, Sawatari A, Callaway EM (2001) Two functional channels from primary visual cortex to dorsal visual cortical areas. Science 292:297-300.

Yoshioka T, Dow BM (1996) Color, orientation and cytochrome oxidase reactivity in areas V1, V2 and V4 of macaque monkey visual cortex. Behav Brain Res 76:71-88.

Yoshioka T, Levitt JB, Lund JS (1994) Independence and merger of thalamocortical channels within macaque monkey primary visual cortex: anatomy of interlaminar projections. Vis Neurosci 11:467-489.

CHAPTER 2

DIFFERENT PROPORTIONS AND MORPHOLOGICAL PROPERTIES OF V1, L4B SPINY STELLATE AND PYRMIDAL NEURONS PROJECTING TO V2 THICK AND THIN STRIPES

2.1 Introduction

There are two different cell types in L4B of V1 that can be characterized simply by their gross morphological features. Spiny stellate neurons have dendrites which are predominately confined to L4B. The basal dendrites of pyramidal neurons are similarly organized, but these cells also have an apical dendrite that extends up towards L1 (Lund, 1973). Thus, spiny stellate neurons primarily receive M-type information in L4B from L4Cα neurons, while pyramidal cells integrate an additional undetermined type, or types, of information from the layers above L4B (L4A-L1). It has been shown that L4B pyramids can be driven by both L4Cα and L4Cβ, making them at least M+P integrating cells (Yabuta and Callaway, 2001). The existence of these two different cell types is very interesting in the context of understanding visual system circuitry because L4B neurons

provide input to multiple areas, including V2 and MT (Livingstone and Hubel, 1987; Shipp and Zeki, 1989; Sincich and Horton 2002; Sincich and Horton 2003; Sincich and Horton 2005; Federer et al., 2009; Nassi and Callaway, 2009; Sincich and Horton, 2010; Federer et al., 2013). More specifically, within V2, L4B provides input to thick and thin stripes, both of which have distinct physiological properties, as well as distinct output targets, (thick stripes project to MT [dorsal pathway], thin stripes project to V4 [ventral pathway]) (DeYoe and Van Essen, 1985; Shipp and Zeki, 1985; Sincich and Horton, 2002; Federer et al., 2009). These organizational properties present a simple and intriguing question: What kind of input do thick and thin V2 stripes receive from L4B of V1? Do thick stripes receive dominant stellate, M-type input, as may be imagined due to their involvement in the dorsal visual pathway? Do thin stripes receive a more mixed signal, possibly M+P-type from pyramids, due to their projections to V4 and involvement in the ventral visual pathway? Or, do both stripes receive similar L4B input, suggesting that L4B output is mostly homogenous to all projection targets? Perhaps each output target receives a different combination of input, which may help explain their differential functions? To answer these questions, L4B cells projecting to thin and thick stripes have to be located, and then fully reconstructed in order to verify their identity. In practice, this has historically been a challenging, almost impossible, task.

In order to locate neurons that project from one area of the brain to

another, classical retrograde tracers such as BDA, WGA, or fluorescent Alexas can be used. Studies using these techniques can show, at a population level, where the somas of neurons are generally located in one area of the brain when an injection is placed in a different area (e.g, Sincich and Horton, 2002; Federer et al., 2009). However, these classical retrograde tracers cannot fully fill cells so that their morphology can be visualized and completely reconstructed. Techniques such as Golgi staining and intracellular as well as juxtacellular biocitin labelling do fully fill cells, and allow for complete reconstruction (e.g., Lund, 1973; Callaway and Wiser, 1996). However, following the axons of these cells to their projection targets, while theoretically possible, would require a high degree of labor, and would subsequently result in a very low yield, and thus this has never been achieved for V1-V2 connections.

Recent technological advances in the fields of virology, genetics, and molecular biology have produced a tool which resolves these problems. The rabies virus selectively infects axon bouton terminals, and then travels retrogradely to the cell body of a neuron, where it replicates at an exponential rate. The rabies virus genome is now well understood, and its simple genetic code, which contains instructions for five protein structures, can be manipulated (Albertini et al., 2011). The G-protein of the rabies virus, which covers its protein capsule, allows the virus to enter into neurons. Wickersham et al. (2000) have manipulated rabies viral particles so that

their genomes lack the G-protein, yet their structures do not. In each rabies particle's genome, the G-protein sequence has been replaced by a sequence for green fluorescent protein (GFP). Thus, the rabies virus can infect the terminal boutons of a neuron, travel retrogradely to the cell body, replicate GFP exponentially, and is then unable to infect other cells (e.g., Nassi and Callaway, 2007). This tool enables experiments which aim to locate neurons that project to certain areas, and characterize the morphology of these neurons after they have been located. Nassi and Callaway (2007) used this tool to ask which L4B cells projected to area MT and area V2. This study found that, of the neurons labelled from injections of rabies-GFP into MT, ~80% were spiny stellates and ~20% were pyramids. When injections were placed randomly into V2, of the cells found in L4B, ~20% were spiny stellates, while ~80% were pyramids (Figure 2.1). This ground breaking study showed that MT and V2 receive differential, but not exclusive, input from L4B stellates and pyramids. However, an important limitation to this study is that the stripes in V2, in which the blind injections landed, were not identified. Thus, it remains unknown if the contribution of L4B stellate and pyramid input to each V2 stripe reflects the general 80% pyramid, 20% stellate, proportions. Because each stripe has different functions, and because output targets of each stripe can differ, it is plausible that the input to each stripe may deviate from that of V2 overall. If all stripes do receive 80% pyramid input and 20% stellate input, this strongly suggests a more

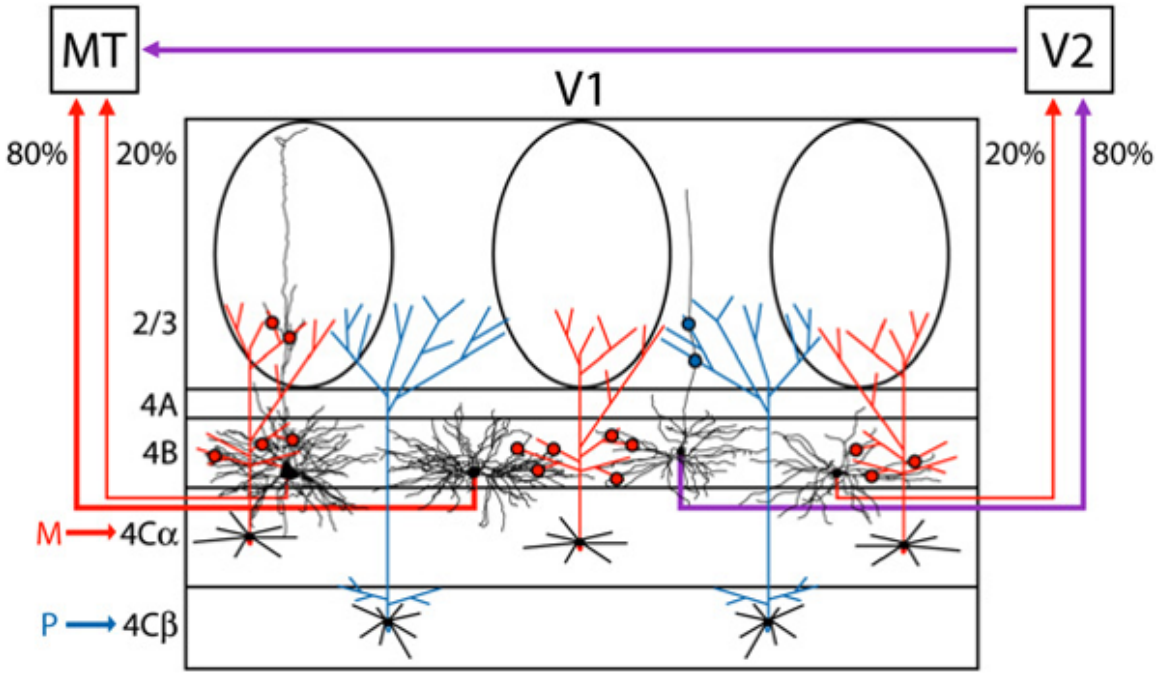

Figure 2.1: L4B spiny stellates and pyramids to MT and V2. Model from Nassi and Callaway (2009) depicting the proportion of spiny stellate and pyramidal neurons in L4B of V1 projecting to both MT and V2. It is important to note that the V2 stripes (thick, thin, pale) that received rabies-GFP injections were not identified in this study. Also note that the neurons depicted projecting to are MT are much larger than those projecting to V2.

homogeneous circuit between L4B and V2 overall, and that other factors (e.g., V1 soma location relative to CO, V2 intrinsic circuitry, V2 feedback circuits) are more involved in the emergence of the different functions associated with each V2 stripe. Unexpectedly, the Nassi and Callaway study also revealed an additional differentiating factor between the pathway between L4B and MT and L4B and V2; all neurons projecting to MT were almost two times larger than those projecting to V2. There is some tepid support for this finding from one other study (Sincich and Horton, 2003), which will be addressed in the discussion at the end of this chapter. While interesting, the implication of this gross morphological size difference remains unclear. In addition, noting the small sample size and lack of stripe identification in the Nassi and Callaway study, it remains to be determined if this morphological dichotomy holds across all V2 stripes. Are there only two sizes of neurons in L4B? Do large stellates and pyramids project exclusively to MT? Are the neurons projecting to each V2 stripe homogeneous in size? If there is a clean dichotomy of L4B cells projecting to MT and V2, then this discovery creates a simple criteria to separate L4B neurons by: large stellates and the small number of large pyramids project to MT, while smaller pyramids and the small amount of smaller stellates project to all V2 stripes. This dichotomy would make it easier to study the different circuits between L4B and MT and L4B and V2, and thus make understanding their computations more approachable, as the constituent components are easily identifiable.

In this study, we have utilized the rabies-GFP tool in order to locate and characterize the neurons in L4B of V1 that project to thick and thin stripes in V2. We find that the ~80% small pyramids, 20% small stellates, description of neurons projecting from L4B to V2 overall, does not sufficiently described the circuits to V2 thick and thin stripes. Here we present data showing that there is an ~55%-45% proportion of stellates and pyramids projecting to thick stripes, respectively, and a slightly different trend, ~60% pyramid, ~40% stellate proportion to thin stripes. Moreover, we find a wide range of neuron sizes projecting to both thick and thin stripes that may be grouped into different categories. Finally, we find evidence for large neurons, of very similar size to those going to MT in the Nassi and Callaway (2007) study, projecting to thick stripes, but not to thin stripes. Thus, large neurons in L4B do not exclusively project to area MT, but it is still likely that they are a strong differentiating factor for describing the circuit from L4B to MT vs. L4B to V2.

2.2 Materials and Methods

In order to reveal neurons in L4B of V1 that project to thick and thin stripes in area V2, we used visual stimuli to drive, and intrinsic signal optical imaging (OI) to locate, the different V2 stripe domains in-vivo. We then placed injections of a modified version of the retrogradely traveling rabies virus (rabies-GFP) into thick or thin stripes. Labeled cells in L4B of V1 were

subsequently identified and reconstructed across serial tissue sections in order to examine their morphological characteristics.

2.2.1 Animals

Five adult male macaque monkeys were used in this study. All experimental procedures were in accordance with protocols approved by the University of Utah Institutional Animal Care and Use Committee. Each animal received at least one injection of rabies-EGFP (SADΔG-EGFP) in a single hemisphere of the brain (Nassi and Callaway, 2007; Wickersham et al., 2007; Briggs et al., 2016). Injections were targeted at the exposed portion of V2, on the posterior portion of the dorsal lip of the lunate sulcus (e.g, Federer et al., 2013). Injections were delivered via glass micropipettes (~35-45 μm tip diameter) and picospritzer applied pressure. In case MK327, injections of CTGg, CTB555, and CTB647 were placed in V2 approximately 3mm from the rabies injection, and an additional injection of rabies was placed contralaterally in V2. For case MK339, two injections of rabies-EGFP were placed approximately 5mm apart; 3 injections of CTB55 were also made. One EGFP injection in MK339 was located in a pale-medial stripe and was excluded from this study. For case MK340, 1 injection of rabies-EGFP and one injection of rabies-Mcherry were targeted to two different thick stripes separated by a thin and pale stripe. The M-cherry injection in MK340 was found to be located in a pale-lateral stripe and was excluded from this study.

In cases MK339 and MK340, the contralateral hemisphere was used for other experiments that did not involve tracer injections. Thus, MK327, MK339, and MK340 each yielded one injection into a thick stripe. In case MK368, three injections of rabies-EGFP were place approximately 5 mm apart, two injections were in thin stripes, and one injection was ambiguous and was discarded. In MK370, two injections of rabies-EGFP were placed 5 mm apart, and both landed in thin stripes. Thus, MK368 and MK370 each yielded two injections into two thin stripes.

2.2.1.1 Surgical and Tracer Injection Procedures

Surgical procedures were performed as in Federer et al. (2009, 2012). Animals were pre-anesthetized with ketamine (25 mg/kg, i.m.), intubated, and artificially ventilated while in a stereotax. Isoflurane (0 - 2.5%) was used to maintain anesthesia while a craniotomy and durotomy were performed posterior to lunate sulcus in order to reveal areas V1 and V2. For optical imaging, anesthesia was maintained with sufentanil citrate (5-10 ug/kg/h) and animals were paralyzed with vercromium bromide (0.3 mg/kg/h). One of the primary goals for these experiments was to obtain sparse labelling of cells in V1 in order to facilitate complete reconstruction of all neuronal processes. Thus, our rabies injections were very small with volumes ranging from 375 nl to 500 nl; injections were placed 600 um – 1 mm from the cortical surface. Animals were kept under anesthesia for the entirety of the experiment and

euthanized with sodium pentobarbital (150 mg/kg; i.v.) 3 - 5 days after injection. Cases MK339, MK340, and MK370 were perfused with saline for 2-3 min, followed by 4% paraformaldehyde in 0.1 M phosphate buffer for 5 min. For case MK327 and MK368, the animal was perfused with 0.5% paraformaldehyde for 15 min.

2.2.2 Optical Imaging

The implantation of the optical imaging chamber, acquisition of imaging maps, and analysis of acquired images was performed as in Federer et al. (2009). Visual stimuli consisted of full-field, high contrast (100%) achromatic drifting square-wave gratings of eight different orientations and 1.0 cycles/° spatial frequency, moving back and forth at 1 or 2°/s in directions perpendicular to the grating orientation. After imaging maps indicating V2 stripe response properties were acquired (12-24 h), injections of the rabies-EGFP or M-Cherry were made. Thick stripes were identified as the areas with the strongest orientation responses. Weaker responses adjacent to the thick stripes were indicative of pale stripes, and a lack of responses was indicative of thin stripes. Full-field flashing color stimulus (red-green, blue-yellow, black-white) were also used to confirm thin stripe locations. A full cycle of stripes is estimated to be about 4-5 mm (Roe and Ts'o, 1995), this scale was also used to assist in identification of stripe cycles. Injections sites were subsequently verified with histology (see below).

2.2.3 Histology

For cases MK339, MK340, and MK370, V1 was dissected away from V2 by cutting along the V1-V2 border. The V1 block was postfixed in 0.5% PFA for 1-2 h, sunk in 30% sucrose for cryoprotection, and frozen-sectioned from pia to white matter along the V1-V2 border axis at 40 μm. The V2 blocks were unfolded and cut parallel to the cortical surface in 40 μm sections in order to visualize injection sites and CO stripes. For case MK327 and MK368, the cortex was flattened gently above the imaged region. V1 and V2 were separated from the rest of the brain by cutting through the bottom of the lunate sulcus. The V1/V2 block was postfixed in 4% PFA between glass slides for 1-2 h, sunk in 30% sucrose for cryoprotection, and frozen-sectioned tangentially at 40 μm.

For case MK327, every third section was reacted free floating for CO. For MK339, every second section was reacted for CO. For MK368 and MK370, all sections were reacted for CO. For MK340, after the tissue was reacted for DAB to reveal GFP labeled cells (see below), we used Fluorescent nissl stain to identify the cortical layers. Mounted sections were bathed in 200 ul of 100 fold diluted Neuro Trace for 60 min and digital images were captured using fluorescence and bright field microscopy. For the V2 block of MK339, MK340, and MK370, every section was reacted free floating for CO, and digitized images of CO stripes were taken prior to permanent mounting of the tissue. For all cases, every section was immunostained for GFP using

the anti-GFP rabbit polyclonal antibody, the biotinylated goat anti-rabbit secondary antibody, and an ABC avidin-peroxidase kit revealed with a diaminobenzidine (DAB) reaction enhanced with nickel and cobalt to create a black reaction product (similar to Nassi and Callaway, 2007). Injections sites were identified by the labelling of a small field of glial cells located around the pipette track. To localize injections, an aggregate of all injection sites was created in Photoshop (Adobe Systems Inc.) and aligned using radial blood vessels to a composite image of CO stripes (as in Federer et al., 2009, 2012; Figure 2.2).

2.2.4 Data Analysis

2.2.4.1 Identification, Selection, and Reconstruction of L4B Cells

For cases MK327 and MK368, which were cut in the tangential plane, CO staining revealed stereotypical L2/3 blobs, L4A honeycomb, followed by CO pale L4B and CO dark L4C. CO stained sections were aligned to adjacent sections to reveal the location of L4B cells if necessary. For MK327, in one section, where L4B cell location was unambiguous, we fully reconstructed all cells ($n = 11$). While this was likely not exhaustive of all L4B cells in the sample, there were few potential L4B cells beyond those reconstructed. For MK368, for each injection ($n = 2$), all L4B cells were categorized as stellate or pyramids ($n = 73$). The dendrites of all cells able to be reconstructed in one section for each injection site were fully reconstructed, and then additional

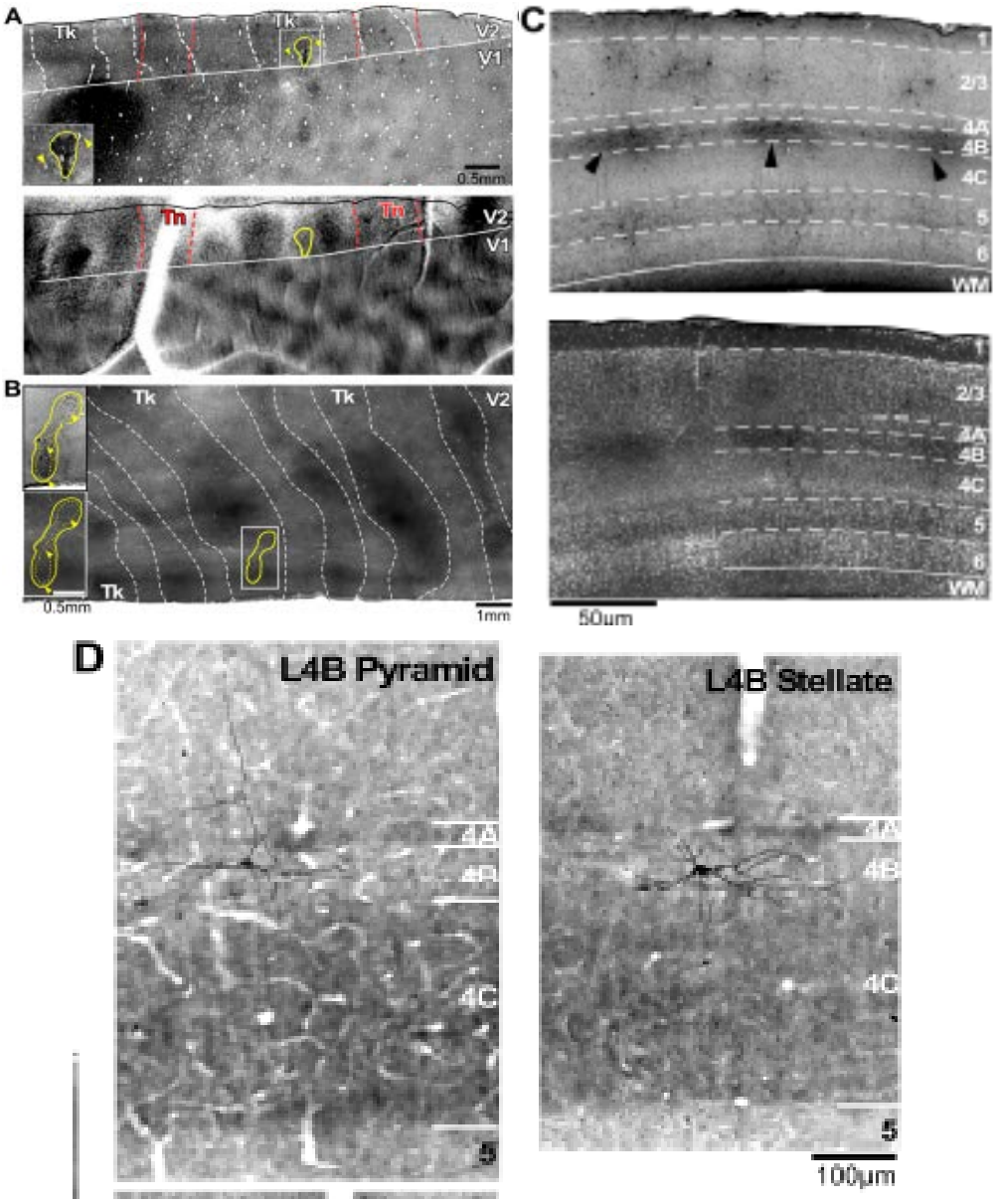

Figure 2.2: Injection sites and resulting label. **A, Top**: Image of rabies-GFP injection site into a V2 thick stripe. **Bottom:** In-vivo optical imaging map showing orientation responses in a putative thick stripe domain. **B,** Additional case showing rabies-GFP injection into a thick stripe. **C, Top:** Label field from rabies-GFP injection shown with CO stained tissue which reveals V1 layers. **Bottom:** Label field shown with fluorescent nissl staining to reveal V1 layers. **D, Left:** Example L4B pyramidal cell. **Right:** Example L4B stellate cell.

L4B neurons across other sections were randomly selected and reconstructed for a total of ten neurons for injection one, and four neurons for injection two.

Cases MK339 and MK370 were cut in the para-sagittal plane and identification of L4B cells was straightforward; the dark thin strip of CO representing L4A was clear, as was dark stained L4C, and cells in the intervening pale L4B were selected for reconstruction (Figure 2.2). For MK339, the dendrites of all L4Bcells ($n = 10$) were attempted to be reconstructed; however, due to intermittent dark CO staining in this case, only seven cells could confidently be considered sufficiently reconstructed. For MK370, all cells' dendrites were reconstructed ($n = 3$).

For case MK340, identical fluorescent and brightfield images were imported into Neurolucida software (MicroBrightField, Williston, VT), layers were identified and drawn using the fluorescent image, then overlaid onto the DAB reacted tissue revealing the location of L4B cells (Figure 2.2). For this case, there was dense labeling toward the anterior portion of the label field, making it impossible to reconstruct axons. Thus, the reconstructed somas ($n = 31$) and dendrites ($n = 19$) were from cells located in the more posterior, sparsely labeled portion of the label field.

All cells were digitally reconstructed using Neurolucida software on a Zeiss Axioskop 2 microscope with 40x and 63x objectives under brightfield illumination using a Qimaging color CCD camera. The axon of each neuron was initially identified as a small caliber, spine de-void, process exiting the

bottom of the cell (Figure 2.2). All remaining processes emanating from the cell were considered dendrites and were clearly identifiable by the high density of spines studding thick caliber processes. In order to reconstruct cells across multiple serial sections, the section outline and radial blood vessels were used for coarse alignment across sections. For fine scale alignment, local blood vessels and multiple exit points of processes exiting one section of tissue were marked, and subsequently aligned to their corresponding continuations in the next section. This process of using global and very local fiducial points made highly accurate and complete reconstruction of dendrites possible. In addition to dendrite reconstruction, spines were plotted for neurons in case MK327. Spines were identified as punctation relieved from, yet attached to, the dendrite.

2.2.4.2 Clustering and Statistical Analyses

Hierarchical clustering analysis was used to classify neurons based on soma perimeter and the total amount of dendritic length. Soma perimeter and soma area were found to be highly correlated, which is a potential violation of the independence assumption of the cluster analysis. We thus chose to use soma perimeter as the metric for soma size as we feel it is a more accurate measure due to possible inconsistencies in recording depth in the Z-plane. The hierarchical clustering analysis plots the position of each cell in N-dimensional space based on the number of metrics used to describe the

cell, which in this study is soma size and dendritic length. The distance between cells in this space was calculated using squared Euclidian distance and linkages between cells were created using Wards method, similar to Briggs et al. (2016). All analyses were performed in SPSS. Significance testing was performed using one-way ANOVA or Kruskal-Walis with post-hoc Bonferroni tests, and all tests were conducted after different classes of cells were identified by the cluster analysis.

2.3 Results

2.3.1 Cell Types to Thick and Thin Stripes

After injection of rabies-GFP into three thick stripes (n = 3 animals, 3 hemispheres, and 3 injections) and four thin stripes (n = 2 animals, 2 hemispheres, and 4 injections), the identity of L4B cells in V1 was established (Figure 2.2). Table 2.1 shows the number of spiny stellates and pyramidal cells in L4B after each injection. Overall, we find that ~55% of the cells labeled after thick stripe injections were spiny stellate, and ~45% were pyramids. For thin stripes, ~40% of labeled L4B cells were stellates, while ~60% were pyramids.

The difference between the proportions of stellates and pyramids projecting to thick stripes vs. thin stripes was not quite statistically significantly different (p = 0.08, Fisher's exact test). However, our total sample of cells is different from that sampled from V2 randomly ($p < 0.001$),

Table 2.1: Proportion of spiny stellate and pyramidal cells projecting to various targets. Case by case results are shown for injections into thick and thin V2 stripes in this study, and results from the Nassi and Callaway (2007) study were multiple injections were randomly placed into V2. Note the difference in overall proportion of stellates between thin and thin stripes from this study, and either stripe in this study and V2 overall from the Nassi and Callaway study.

Thick Stripe	#Stellate	#Pyramid	Total	Proportion Stellate	Avg. Proportion Stellate
MK327	8	7	15	53%	
MK339	6	4	10	60%	
MK341	17	14	31	55%	
Combined	31	25	56	55%	56%
Thin Stripe					
MK368-M	21	26	47	45%	
MK368-W	8	18	26	31%	
MK371-M	1	1	2	50%	
MK371-W	0	1	1	0%	
Combined	30	46	76	40%	32%
V2 Cases (Nassi, 2007)					
JNM8	3	17	20	15%	
JNM12	20	92	112	18%	
Combined	23	109	132	17%	16%

and from MT ($p < 0.001$) (comparison to Nassi and Callaway, 2007 data) (Figure 2.3). Additionally, the proportions of L4B cells projecting to thin stripes are significantly different from those projecting to V2 randomly ($p < 0.001$) and MT ($p < 0.001$), and thick stripe proportions are also different from V2 randomly ($p < 0.001$) and MT ($p = 0.04$). Thus, our data show that an ~80% stellate, ~20% pyramid input proportion is not sufficient to explain the amount of stellate and pyramid input from L4B to thick or thin stripes. Our data suggest that thick stripes receive ~55% of their input from stellates and 45% from pyramids, while thin stripes receive ~40% of their input from stellates, and ~60% from pyramids. The proportions of stellates and pyramids going to thick and thin stripes found in this study are also significantly different from those previously shown going to MT. This result supports the Nassi and Callaway data showing that area MT receives are greater proportion of spiny stellate input compared to V2.

2.3.2 Pyramid and Stellate Size: Soma Size of Neurons Projecting to Thick and Thin Stripes

In order to characterize spiny stellate and pyramidal cells by their morphological characteristics, we first fully reconstructed the somas of neurons projecting to thick ($n = 56$) and thin ($n = 76$) stripes. Soma perimeter and area were both recorded, and were strongly correlated, $r = 0.917$, $p < 0.001$). Soma area is calculated by integrating the depth of tissue traveled

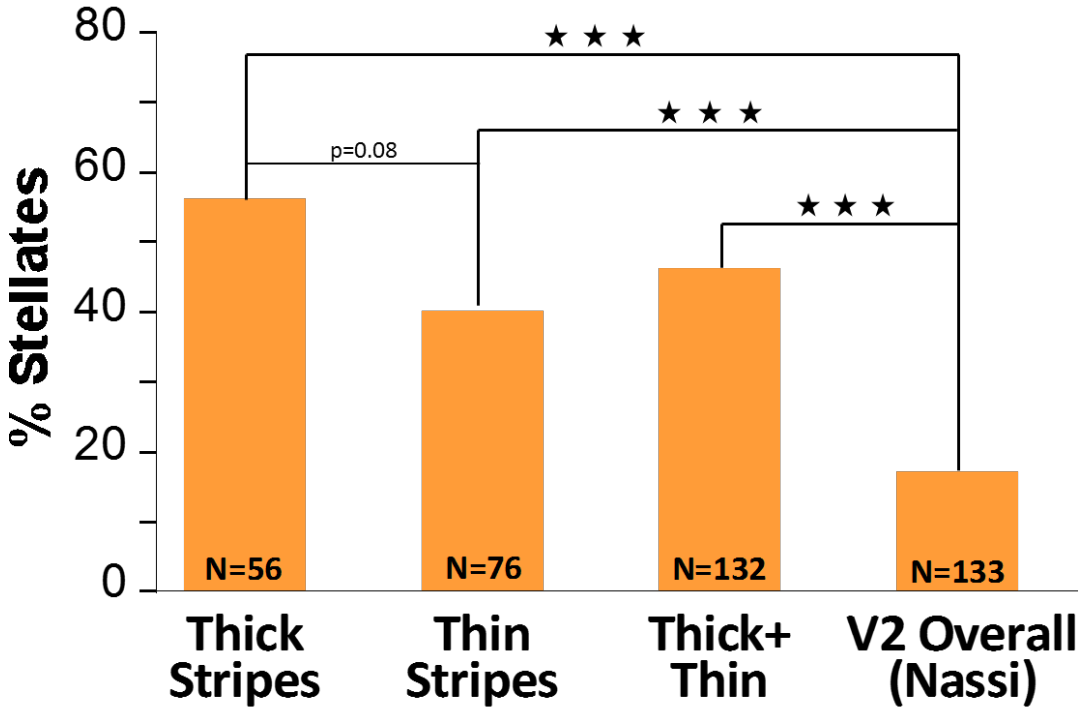

Figure 2.3: Comparisons of the proportions of spiny stellate cells projecting to different targets. The proportion of stellates projecting to thick stripes, thin stripes, or thick and thin stripes combined is significantly greater than the sample drawn by Nassi and Callaway from V2 overall, and significantly less than the sample drawn from MT. Fisher's exact test used for analysis. Stars represent $p < 0.05$.

(Z-axis) when tracing a soma's perimeter in a single serial section of tissue.

2.3.2.1 Soma Perimeter and Area of Pyramids and Stellates Projecting to Thick and Thin Stipes

We first asked if there were any differences in the size of neurons projecting to thick vs. thin stripes (mean and SEM values in microns are reported first for soma perimeter, and then for soma area). For pyramidal cells, we found that pyramids projecting to thick stripes (n = 25, 40.2, 1.56; 100.7, 6.43) were significantly smaller than pyramids projecting to thin stripes (n = 46, 45.3, 0.85; 136.2, 4.85), t = 3.18, p = 0.002; t = 4.38, p < 0.001 (Figure 2.4). For spiny stellate cells, we found that stellates projecting to thick stripes (n = 31, 43.2, 1.68; 115.9, 8.47) were significantly smaller than stellates projecting to thin stripes (n = 30, 49.0, 1.42; 156.0, 8.56), t = 2.66, p = 0.01, t = 3.33, p = 0.002 (Figure 2.4). These data suggest that there are at least two different sizes of pyramidal and stellate cells projecting to V2; smaller pyramids and stellates project to thick stripes, while larger pyramids and stellates project to thin stripes. These data also suggest that the smaller pyramids and stellates projecting to thick stripes may monitor smaller areas of visual space than the pyramids and stellates projecting to thin stripes. Concordance between soma size data and dendritic length data would substantiate this finding.

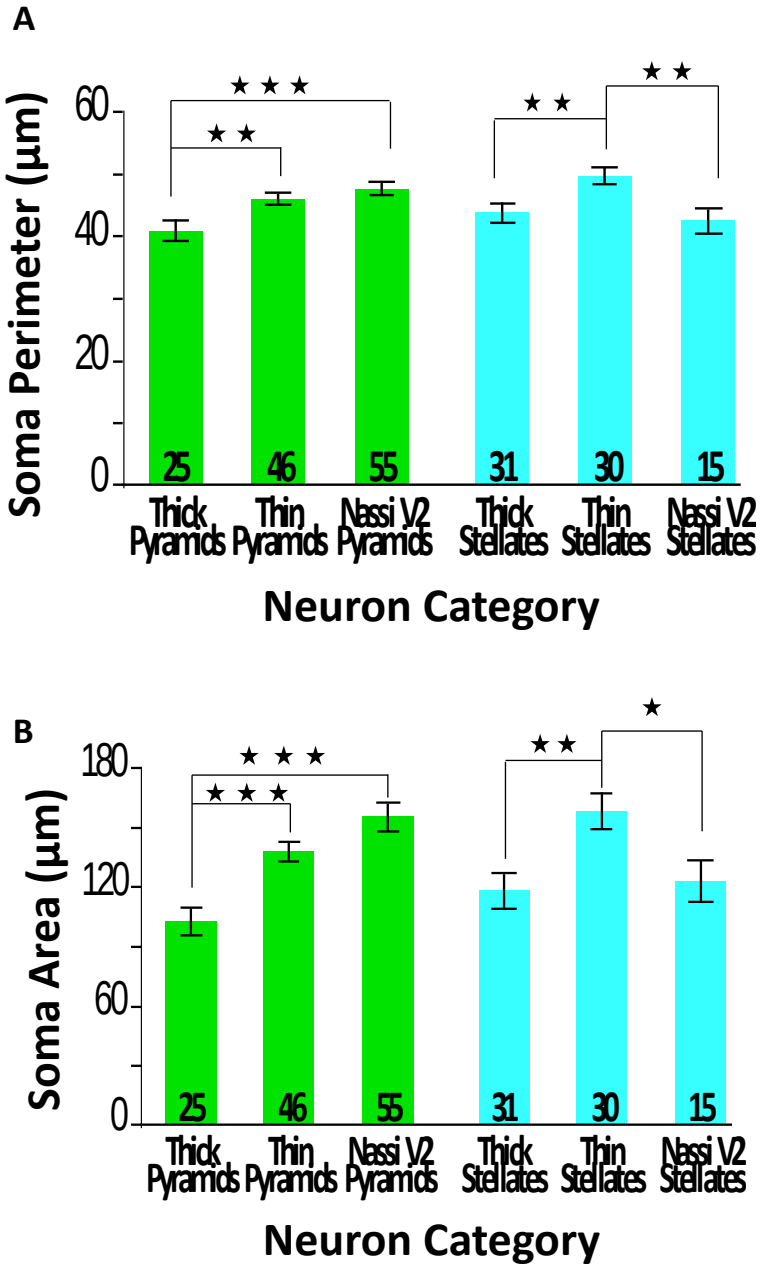

Figure 2.4: Soma size of stellates and pyramids projecting to thick and thin stripes. **A,** Soma perimeter for stellates and pyramids projecting to thick stripes is smaller than those cells projecting to thin stripes or V2 overall (Nassi and Callaway, 2007 data). **B,** Soma area for stellates and pyramids projecting to thick stripes is smaller than those cells projecting to thin stripes or V2 overall. T-test analysis. Stars are $p < 0.05$

2.3.2.2 Overall Soma Size of Pyramids vs. Stellates

We next looked at our entire sample of stellate and pyramidal cells in order to compare them with previous data showing the sizes of cells in L4B when injections were randomly placed in V2. We first asked if there were any overall differences between the sizes of pyramids vs. stellates in our samples. We found that pyramidal cells (n = 71, 43.5, 0.83; 123.7, 4.34) from our samples were not quite significantly smaller than spiny stellates (n = 61 46.0, 1.16; 135.7, 6.51), t = 1.82, p = 0.07; t = 1.53, p = 0.13. The trend in our findings, however, are in contrast to the trend in the Nassi and Callaway study that shows pyramids (n = 55, 46.8, 1.09; 153.2, 6.98) tend to be larger than stellates (n = 15, 41.8, 2.05; 121.2, 10.0). We thus became interesting in comparing each of our individual groups of sampled neurons to those randomly sampled by Nassi and Callaway (2007).

2.3.2.3 Soma Size of Pyramids and Stellates Projecting to Thick and Thin Stripes Compared to Pyramids and Stellates Projecting to V2 Overall

We found that our pyramidal cells projecting to thick stripes (n = 25, 40.2, 1.56; 100.7, 6.44) were much smaller than the pyramids reported by Nassi and Callaway (n = 55, 46.8, 1.09; 153.2, 6.98), t = 3.40, p = 0.001; t = 4.67, p < 0.0001 (Figure 2.3). We found that our pyramids projecting thin stripes (n = 46, 45.3, 0.85; 136.2, 4.85) were closer in size to the data reported

by Nassi and Callaway and were not significantly different from each other, $t = 1.05$, $p = 0.30$, $t = 1.93$, $p = 0.057$. This suggests that the pyramids observed by Nassi and Callaway were from thin stripe injections. We found that our stellates projecting to thin stripes ($n = 30$, 49.0, 1.42; 156.0, 8.56), were much larger than the stellates reported by Nassi and Callaway ($n = 15$, 41.8, 2.05; 121.2, 10.0), $t = 2.90$, $p = 0.006$, $t = 2.47$, $p = 0.018$ (Figure 2.4). Stellates projecting to thick stripes ($n = 31$, 43.2, 1.68; 115.9, 8.47) were much closer in size to those reported by Nassi and Callaway and were not significantly different, $t = 0.50$, $p = 0.62$; $t = 0.38$, $p = 0.71$ (Figure 2.4). This suggests that the stellates observed by Nassi and Callaway were from thick stripes. We next turned to full reconstructions of dendrites to ask if differences found within our soma data, and between our data and that from Nassi and Callaway, were substantiated.

2.3.3 Pyramid and Stellate Size: Dendritic Length of Neurons Projecting to Thick and Thin Stripes

We analyzed the dendritic length, an indication of neuron size, of L4B stellates and pyramids to see if the results supported differences we found between neurons using soma data. For pyramidal neurons, we were most interested in the amount of dendrite dedicated to L4B, which is a proxy for M-type input. Since the type of information being received by an apical dendrite is indeterminate, and may differ depending on the soma location

relative to CO compartments, here, we only look at the length of basal dendrites of pyramidal cells.

2.3.3.1. Dendritic Length of Stellates and Pyramids Projecting to Thick and Thin Stipes

First, we looked at the dendritic length of pyramids projecting to thick stripes (n = 21, 2797 μm, 219.2 μm) vs. those projecting to thin stripes (n = 6, 3515 μm, 326.4 μm) and found that they were not statistically different from each other, t = 1.60 p = 0.12. We note that this may be due to the smaller number of pyramids going to thin stripes that we were able to be reconstruct, as pyramids projecting to thin stripes were larger than those projecting to thick stripes when looking at soma perimeter or area. Next we looked at the dendritic length of stellates projecting to thick stripes (n = 21, 4010 μm, 395.0 μm) vs. stellates projecting to thin stripes (n = 11, 4023 μm, 267.0 μm) and found no significant differences between the two, t = 0.28, p = 0.98. Previously, our soma analysis showed that stellates projecting to thin stripes were larger than those projecting to thick stripes. Overall, analysis of the dendritic length of these cells does not seem to show any difference in the average size of these neurons, which is in contrast to our findings when looking at soma size.

2.3.3.2 Overall Dendritic Length of Stellates and Pyramids

We next looked to see if the dendritic length of all of our pyramidal cells differed from our spiny stellates. Overall dendritic length differences between pyramids and stellates may suggest that one cell type generally integrates less M-type information over a smaller area of the visual filed than the other cell type. Our soma data suggested that, overall, there was a strong trend for pyramidal cells to be smaller than stellates, and this trend was in the opposite direction as that reported by Nassi and Callaway. Our dendritic length data shows that all of our pyramids (n = 27, 2957 μm, 191.7 μm) were significantly smaller than all of our stellates (n = 32, 4014 μm, 271.9 μm), t = 3.07, p = 0.002. This statistically significant result compliments the trend in our soma data, and contradicts the size trend previously reported by Nassi and Callaway.

Overall, our pyramids (mean, 2957 μm) were also significantly smaller than those observed by Nassi and Callaway (mean, 4371 μm), t = 2.89, p = 0.007. Again, this difference in dendritic length is supportive of our soma data. Overall, the difference in total dendritic length for our stellates (mean, 4014 μm) was not significantly larger than that reported by Nassi and Callaway's (mean, 2869 μm), t = 1.27, p = 0.21 (Figure 2.5). This is in disagreement with results from our soma data, which showed that our stellates were larger than those in the Nassi and Callaway study. But note, however, that the dendrites of only three stellates were reconstructed in the Nassi and Callaway study, thus making null results from this test of

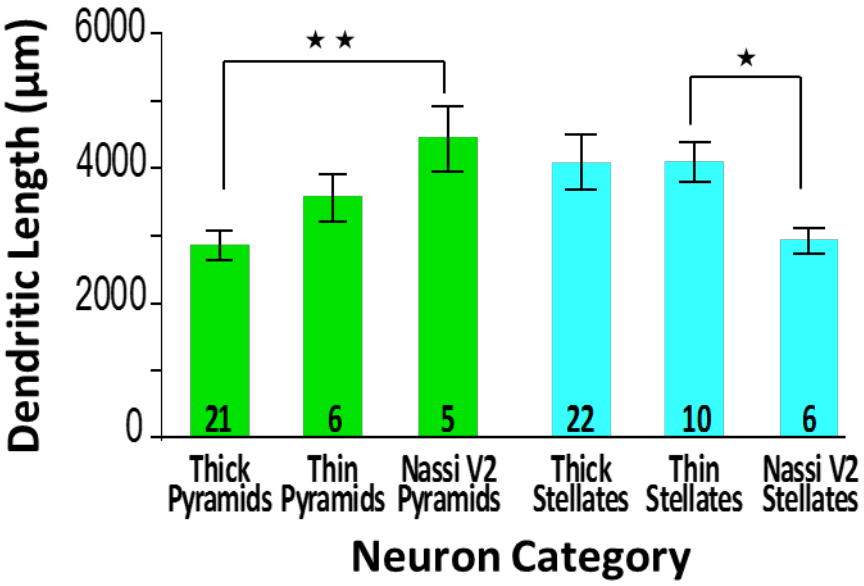

Figure 2.5: Dendritic length of stellates and pyramids projecting to different target areas. Pyramids projecting to thick stripes are not different from those going to thin stripes, but are significantly smaller than the sample drawn from the Nassi and Callaway (2007). Stellates projecting to thin stripes are not significantly different from those projecting to thick stripes, but are significantly larger than those sampled by Nassi and Callaway.

significance tenuous, as we may have committed a Type II error due to their small sample size.

2.3.3.3 Dendritic Length of Stellates and Pyramids Projecting to Thick and Thin Stripes Compared to Stellates and Pyramids Projecting to V2 Overall

We next looked to compare our individual groups of neurons to previously reported data to determine if the size of neurons projecting from L4B to V2 overall accurately described the size of L4B neurons projecting specifically to thick and thin V2 stripes. We found that our pyramids projecting to thick stripes (n = 21, 2797 μm, 219.2 μm) were significantly smaller than the pyramids sampled by Nassi and Callaway, (mean, 4371 μm), t = 3.12, p = 0.005. Our pyramids projecting to thin stripes (n = 6, 3515 μm, 326.5 μm) were not significantly different than pyramids sampled by Nassi and Callaway, t = 1.53, p = 0.16. Both of these findings are supportive of our soma data (Figure 2.5). Collectively, these results suggest that the pyramidal cells sampled in the Nassi and Callaway study were more likely to be from thin stripe injections. These results also suggest that there are at least two different sizes of pyramidal neurons projecting to V2, and yet another size projecting to MT.

The stellates projecting to thick stripes in our sample (n = 21, 4010 μm, 394.9 μm) did not differ from those sample by Nassi and Callaway (n = 3,

2869 μm, 191.7 μm), t =1.46, p = 0.17, but stellates projecting to thin stripes (n = 11, 4023 μm, 267.3 μm) were significantly larger, t = 2.16, p = 0.052 (Figure 2.5). This finding supported the results from comparisons between samples using data for soma size. Similar to results from pyramidal cell comparisons, collectively, our morphological data describing spiny stellates suggest there are at least two different sizes of stellates projecting to V2, and three sizes when including MT as a projection target.

It is interesting to note that although the means for the dendritic length of stellates projecting to thick and thin stripes were nearly identical, the variance within the samples (i.e., SEM) differed. Thus, we found that stellates projecting to thin stripes (smaller variance) were statistically different from those in the Nassi and Callaway study, but stellates projecting to thick stripes (larger variance) were not found to be different. This difference in variance between groups of neurons led us to investigate our samples further, which led us to the observation that there is a much greater range of data in our thick stripe sample than in our thin stripe sample. This observation prompted us to investigate additional analytic techniques that would enable us to look at our data from a different perspective.

2.3.4 Summary of Neuron Size Data (Somas, Dendrites)

Overall, using data for cell size (soma perimeter, soma area, dendritic length) we find evidence for at least two different sizes of pyramids and

stellates projecting to V2. Our soma size data indicate that pyramidal and stellate neurons projecting to thin stripes are both larger than those projecting to thick stripes. However, this finding is not supported by the dendritic length data, which show no differences between these neurons. It is important to note that we have smaller samples of cells for dendritic length than for soma size due to the laborious processes of reconstructing entire dendritic arbors over multiple serial sections. However, when we compare soma size or dendritic length to the sample of neurons drawn in the Nassi and Callaway study, we again find evidence for two different sizes of neurons projecting to V2. These strong, yet inconsistent, findings prompted us to investigate our raw dendritic length data more thoroughly. Observation of the raw data showed that there is a large range of dendritic length for neurons projecting to thin stripes (2613 μm – 4723 μm), and a very large range for neurons projecting to thick stripes (1019 μm – 7521 μm). The heterogeneity in the dendritic length data, the significant differences in soma size data, and differences found between our samples and those from Nassi and Callaway, prompted us to analyze our samples of pyramids and stellates in an unbiased manner in order to determine if there are indeed different sizes of neurons projecting to V2. We chose to use hierarchical clustering analysis to further investigate the size of pyramidal and spiny stellate neurons projecting to V2 thick and thin stripes. This is a well-established technique for unbiasedly investigating how data might be grouped together

(Briggs et al., 2016).

2.3.5 Cluster Analysis of Stellates and Pyramids Projecting to Thick and Thin Stripes

In order to quantitatively and unbiasedly categorize neurons by size, we used hierarchical clustering analysis with Ward's method and squared Euclidian distance. Soma perimeter and dendritic length parameters were used to describe each cell; soma area was removed for the analysis as it was correlated with soma area (see Methods).

For spiny stellate cells, the cluster analysis identified four different sizes of neurons: smaller stellates (n = 2, mean, 1032 μm, SEM, 12.4 μm), medium stellates (n = 15, mean, 3109 μm, SEM, 128.0 μm), larger stellates (n = 13, mean, 4977 μm, SEM, 138.8 μm), and giant stellates (n = 2, mean, 7309 μm, SEM, 211.7 μm) (Figures 2.6, 2.7). For pyramidal cells, this analysis identified three different sizes of neurons: smaller pyramids (n = 4, mean, 1465 μm, SEM, 122.4 μm), medium pyramids (n = 15, mean, 2704 μm, SEM, 92.7 μm), and larger pyramids (n = 8, mean, 4177 μm, SEM, 190.4 μm) (Figures 2.8, 2.9). The stellate and pyramid small neuron groups were not significantly different from each other, but both were significantly smaller than all other groups F = 83.5, $p < 0.001$ (Bonferonni correction). The stellate and pyramid medium neuron groups were not different from each other, but were different from all other groups ($p < .001$). Large stellates were larger

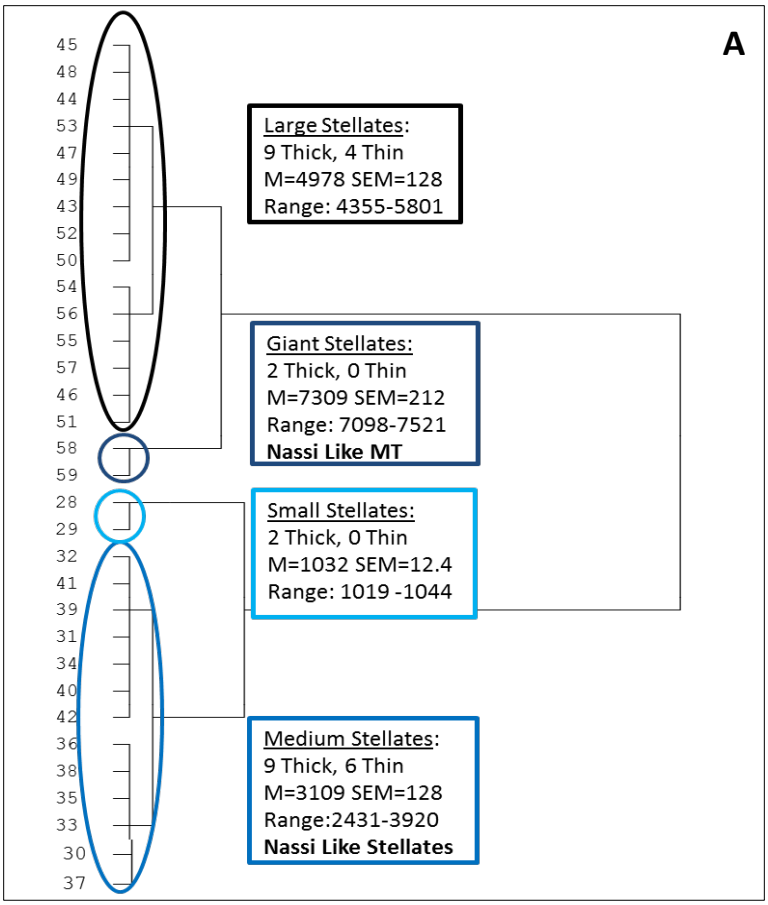

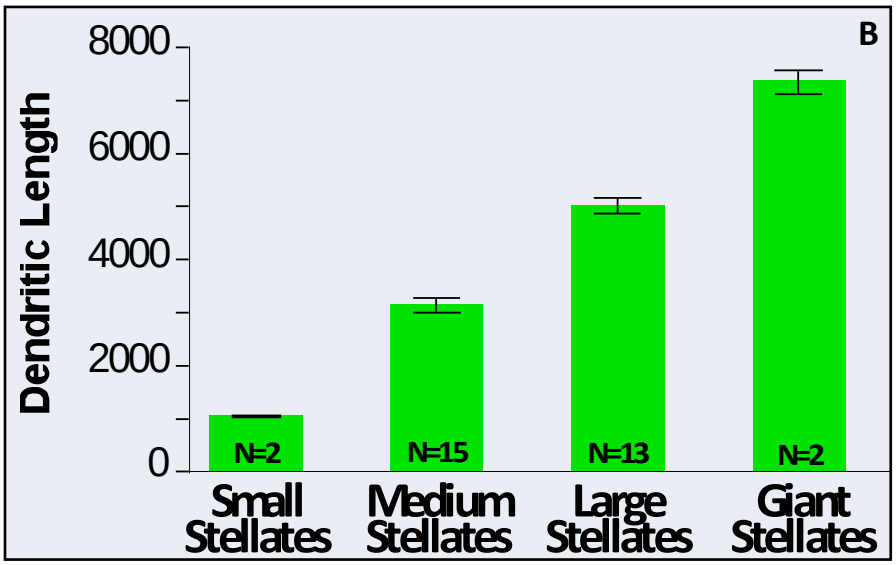

Figure 2.6: Groups of stellates. A, Cluster analysis results showing 4 different groups of stellates. **B,** Bar graph showing different sizes of neurons classified by dendritic length.

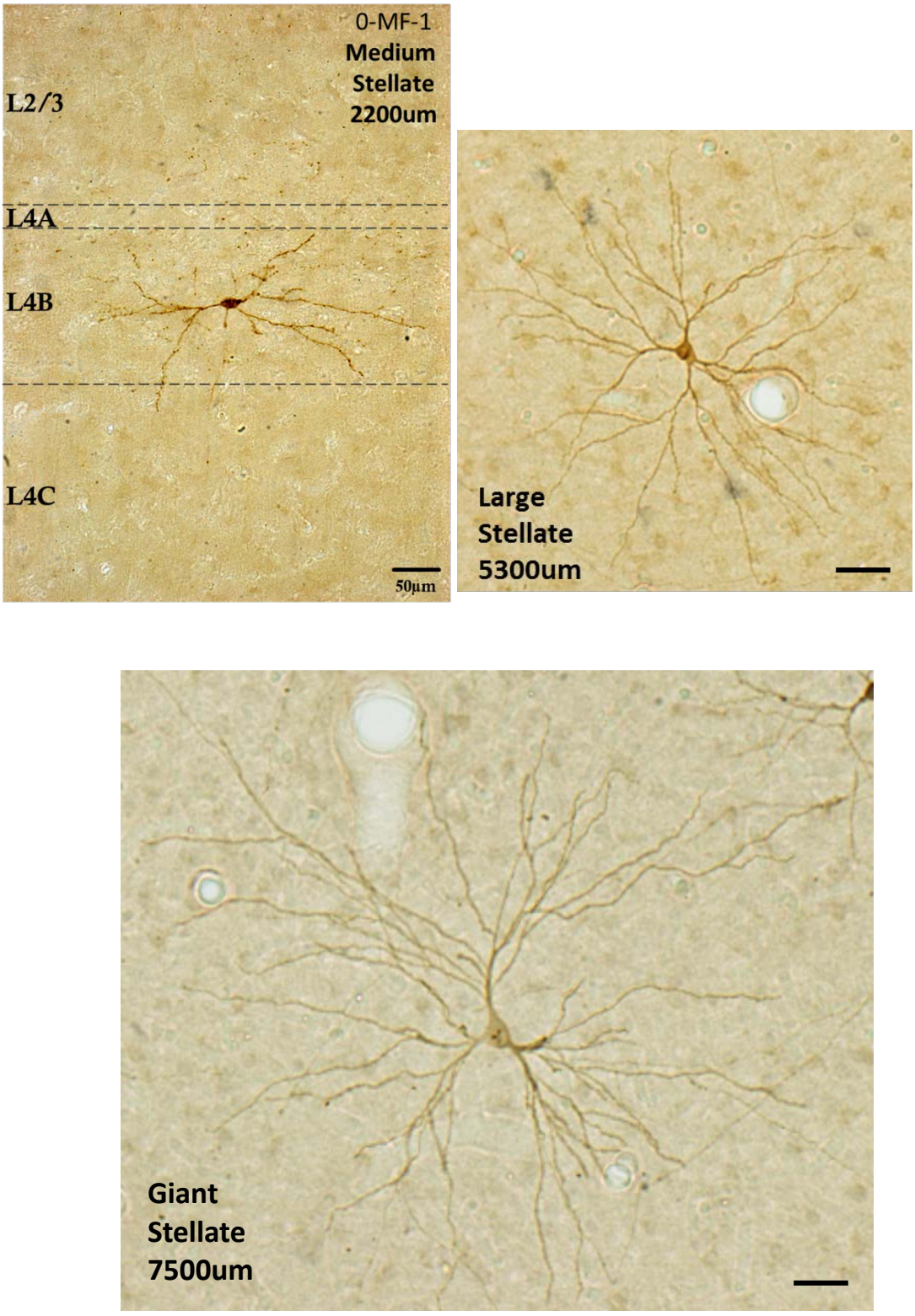

Figure 2.7: Images of different sizes of spiny stellate neurons projecting to thick and thin stripes in V2.

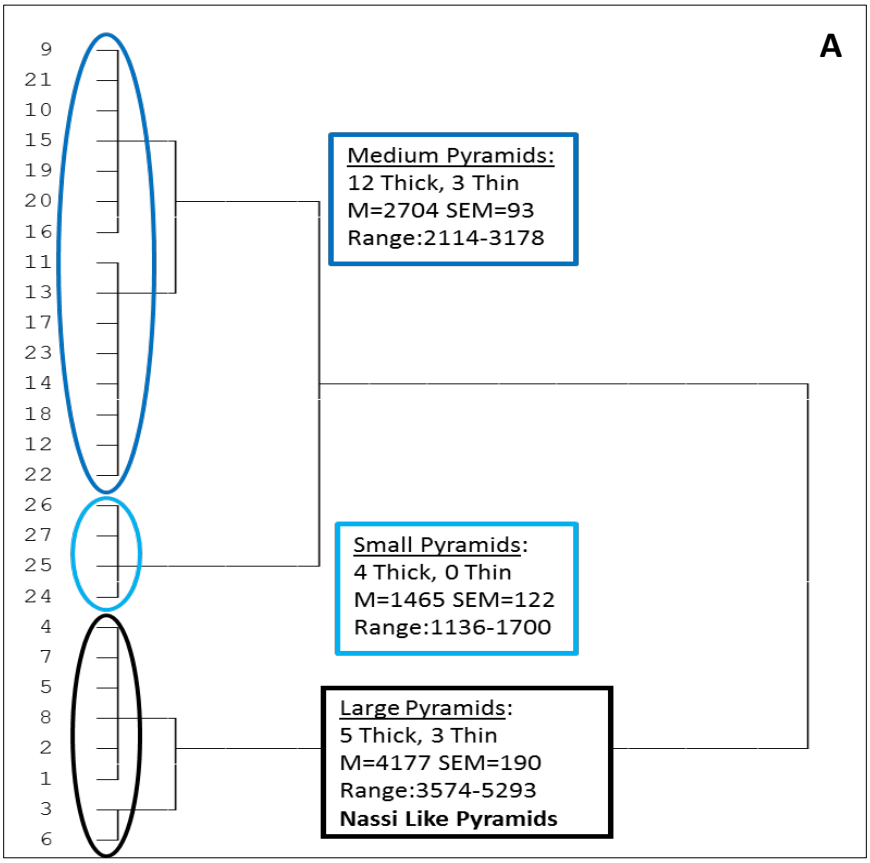

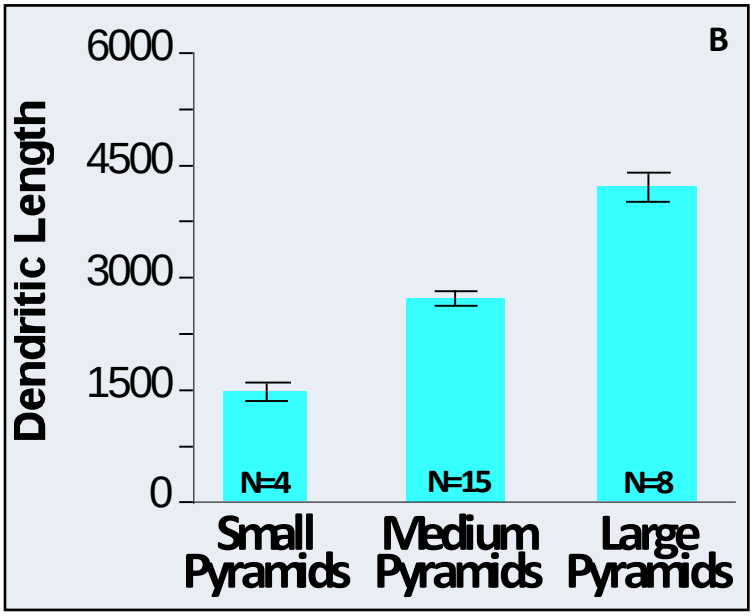

Figure 2.8: Groups of pyramids. A, Cluster analysis results showing 3 different group of pyramids. **B,** Bar graph showing different sizes of neurons classified by dendritic length.

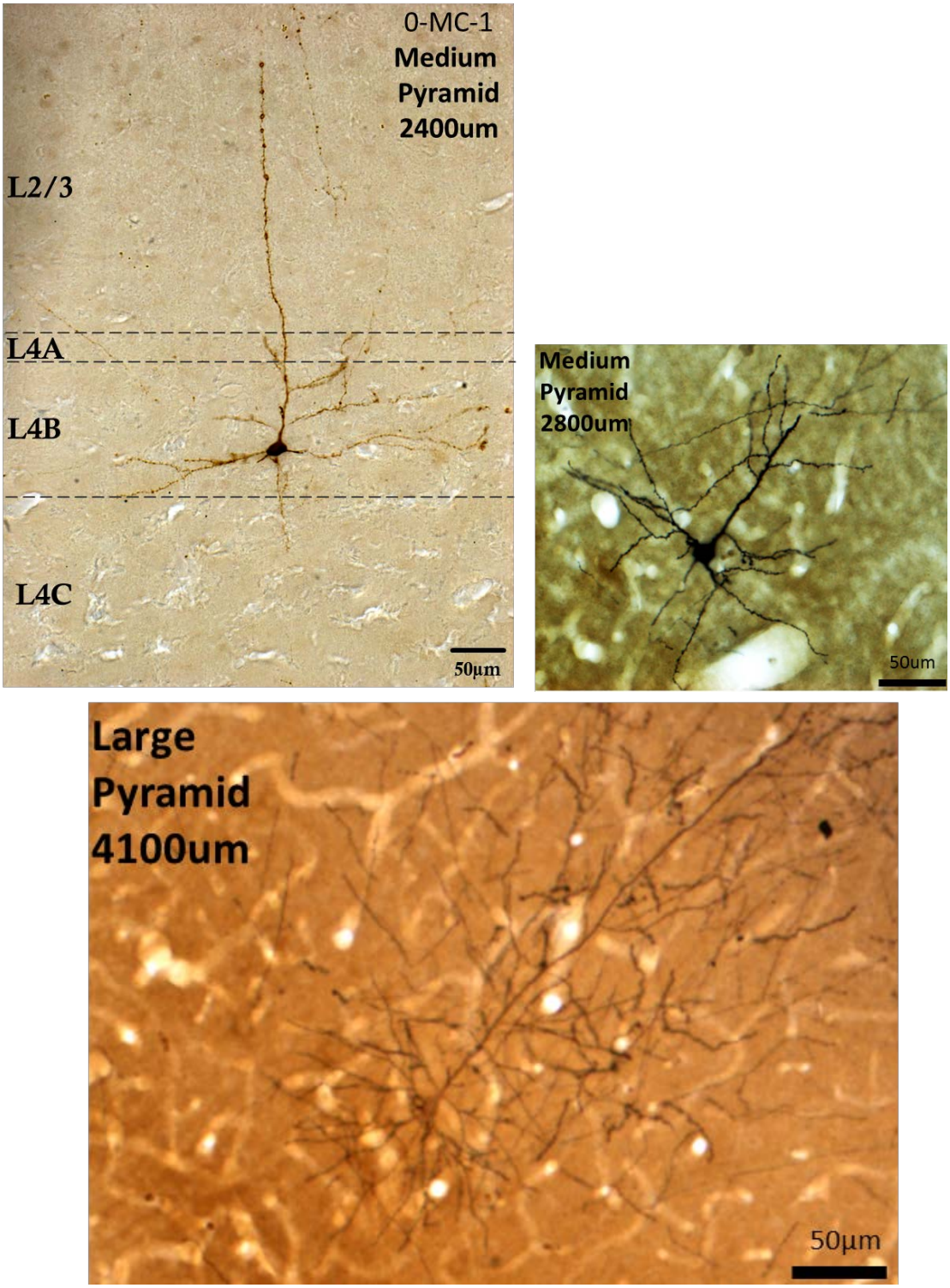

Figure 2.9: Images of different sizes of pyramidal neurons projecting to thick and thin stripes in V2.

than large pyramids ($p = 0.005$), and both groups were different from all other groups ($p < 0.001$). Giant stellates were significantly larger than all other groups ($p < 0.001$) (Figure 2.10). This quantitative categorization of neurons by soma size and dendritic length offers a framework which can account for the different sizes of cells found within our samples, and between our samples and those reported previously by Nassi and Callaway. These data suggest there are at least five sizes of cells projecting from V1, L4B to thick and thin stripes: small pyramids and stellates project to thick stripes; medium stellates and pyramids project to both thick and thin stripes; large pyramids project to thick and thin stripes; larger stellates project to thick and thin stripes; and giant stellates project only to thick stripes (Figure 2.10). Pyramidal neurons from the Nassi and Callaway data fall into the large pyramid group, while their stellates fall into the medium stellate group.

2.4 Discussion

Previous research investigated the types of cells (spiny stellate, pyramidal) in L4B of V1 that project to areas V2 and MT. The results from that study showed that area MT receives ~80% of its L4B input from stellates, and ~20% from pyramids, while area V2 receives ~20% of its L4B input from stellates, and ~80% from pyramids. It is well documented that area V2 is not homogeneous in structure (Tootell et al., 1983) nor function (Shipp and Zeki, 2002), and thus, in order to accurately understand the type

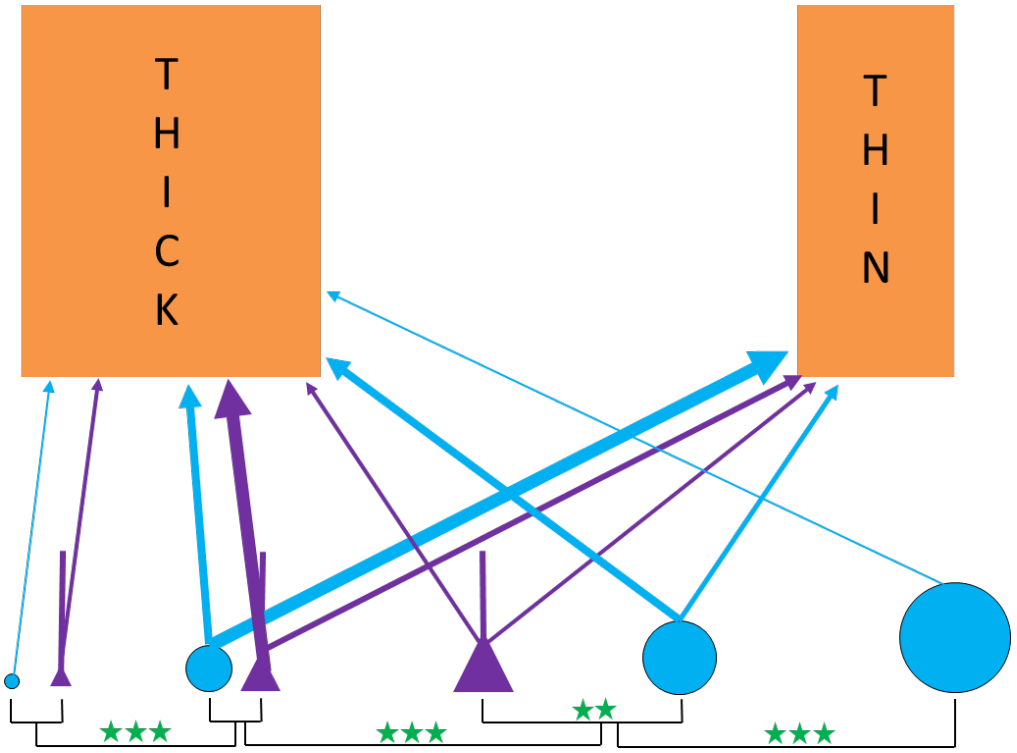

Figure 2.10: Summary of groups of stellates and pyramids.
Groups of different sizes of neurons and their projection targets. Two stars, $p < 0.01$, Three stars, $p < 0.001$. One way ANOVA.

of input from L4B of V1 to area V2, each V2 stripe type (thick, thin, pale) must be studied individually. In this study, we investigated the input from L4B of V1 to thick and thin V2 stripes. Our results suggest that thick stripes receive ~55% of their L4B input from stellates, and 45% from pyramids; thin stripes receive ~40% of their L4B input from stellates, and ~60% from pyramids. The proportion of stellate and pyramidal input to thick and thin stripes was not quite statistically different from one another, but proportions going to both stripe types were significantly different from those previously shown going to V2 overall. Our results strongly suggest that an ~80% pyramidal, ~20% stellate description of the input from L4B of V1 to V2 does not accurately describe the kind of input that goes from L4B to thick and thin stripes (Nassi and Callaway, 2007). This is important because our data suggest a much stronger stellate, and thus M-type, component of input to both thick and thin stripes. We did not comprehensively investigate the proportions of input to the pale stripes. Previous research (Federer et al., 2013) suggests that only one of the two pale stripes (pale-lateral) receives L4B input; pale-medial stripes do not receive L4B input (but see Sincich and Horton, 2010). It is not immediately clear why we found different results from the Nassi and Callaway study, which showed more significant pyramidal, and thus mixed M+P type, input going to V2 overall. One possible explanation is that the blind injections made in that study primarily landed in pale stripes. If this were the case, it suggests that pale stripe input from

L4B is dominated by pyramidal cells. Note that injections into pale-medial stripes should result in no L4B label, and thus the total number of effective injections would be reduced, and results would be more heavily biased toward whichever stripes were injected. However, the authors guessed that their blind injections may have primarily hit thick stripes. Our data would argue against this interpretation. Differences between the two studies may also be attributed to injection location within the stripe, and/or across layers within the stripe. Our injections were aimed between 1000 μm and 600 μm below the surface of the brain, targeting L4 in V2, which is the layer primarily receiving input from V1. The exact location of the injection core is difficult to pinpoint as the rabies virus does not leave definitive injection core markings. Glial cell staining is thought to represent the densest uptake zone of the rabies virus. Our observations were that our injections mostly spanned across all layers, with a couple possibly only extending into layer 5. It may be the case that our injection core was biased more towards the upper part of L4 and L3, and that the Nassi and Callaway injections cores were biased toward lower parts of L4 and L5. The inverse could also be true, and in either case, it could result in the infection of subsets of L4B neurons that have biased projections to the upper and lower parts of L4 in V2. Alternatively, it could also be the case that there are different functional sub-regions within thick and thin stripes that we hit with our small injections, thus resulting in a different sampling than the large nonspecific injections in

the Nassi and Callaway study. Similarly, our injections were targeted toward the most posterior portion of the lip of the lunate sulcus, nearest the V1-V2 border. It is unclear exactly where injections were placed in the Nassi and Callaway study regarding the posterior-anterior plane. It seems unlikely that variability in this plane of the injection site would result in meaningfully different samples, but remains a possibility. The simplest explanation for differences between studies, although wholly incomplete and unsatisfying, is that the rabies virus randomly infected different samples of neurons in both studies. One strength of the rabies virus tool is that it completely fills neurons with label, but a weakness of the tool is that it is not known to comprehensively infect all neurons in a given area. Thus, using the rabies virus to sample proportions of neurons projecting to a specific area is inherently error prone, but this limitation can be mitigated by sampling multiple times from the same area in a similar fashion. When combining all of our data from five animals (three injections into thick stripes, four injections into thin stripes), our total proportion of spiny stellate and pyramidal neurons is significantly different from that found by Nassi and Callaway. Because we have a greater sample of animals and a similar (somas), if not greater (dendrites), sample of neurons, I feel our data represent a more thorough and accurate sampling of the L4B neurons that project to V2. Finally, we note in our methods that for one case, MK340, we only classified the neurons in the posterior portion of the label field. This

portion of the label field was chosen because the anterior portion of the label field was too dense with label, and perhaps had inconsistent histological processing, for us to be confident in the classification of these neurons. In this anterior portion of the label field, it did appear that there may have been a relatively greater number of very small (much smaller than the smallest neurons we reconstructed) pyramidal neurons. Because these neurons, and importantly neighboring neurons that appeared to be stellates, could not be confidently categorized, they were excluded. This was also the only case in which we used fluorescent nissl staining in order to identify the different layers in V1. While we are very confident that the neurons we chose to categorize were clearly in L4B, these uncharacterized neurons tended to be toward the top of L4B, and could have been L4A neurons. The fluorescent nissl staining does not provide a clean and clear L4A boundary as can be seen when using CO, thus we could not conclusively determine the laminar position of these tiny cells. Of our five animals and seven injections, this was the only animal and injection that exhibited this density of label and seemingly incompletely filled tiny pyramidal neurons. We therefore believe this case was an outlier. Compared to the results from the Nassi and Callaway study, overall, each of our samples show a robust difference in stellate and pyramid proportion from that reported by those authors. The two cases in the Nassi and Callaway study showed 15% and 18% stellates projecting to V2; the smallest proportion of stellates we found in any single

case (thick or thin stripes) was 31%. Because of the robust presence of spiny stellate neurons in all of our samples, any potential error in any one case would have little impact on the overall results. It should also be noted that while Nassi and Callaway classified 132 neurons as either spiny stellates or pyramids, only 70 somas were reconstructed. Thus, 52 neurons (39% of the total sample) were qualitatively categorized, and this could have led to erroneous categorizations.

In summary, we have no clear explanation for the difference in the proportions of stellates and pyramids in our samples vs. those from the Nassi and Callaway study. However, it is important to note that we have a much larger and specific sample of neurons in our study, which I believe constitutes a more accurate characterization of the circuitry between V1 L4B neurons and thick and thin stripes in V2.

We next investigated the size of cells projecting to thick and thin stripes as we sought to compare them to one another, and to those found in the Nassi and Callaway study. In this previous study, the authors found that the L4B neurons projecting to area MT were significantly larger (i.e., soma perimeter, area, and dendritic length) than the L4B neurons projecting to V2 overall. We first wanted to determine if cell size could be a differentiating factor between neurons projecting to thick vs. thin stripes. Different sizes of cells may be correlated with receptive field size and the amount of M-type information that is integrated by these neurons, and therefore it was of

interest to characterize the size of neurons projecting to each stripe. It could be hypothesized that neurons projecting to thin stripes would be smaller than those projecting to thick stripes, as spatial resolution and subsequently high spatial frequency (i.e., high information content) are thought to be more important components within the ventral visual pathway (thin stripes-to-V4) rather than the dorsal visual pathway (thick stripes-to-MT). We were also interested in investigating whether the large cells found in the Nassi and Callaway study project exclusively to MT, as the dendrites of only eight neurons projecting to V2 were reconstructed in their study.

Our some size data (perimeter, area) showed that both stellates and pyramids projecting to thick stripes were smaller than those projecting to thin stipes. However, there were no differences in dendritic length for stellates or pyramids projecting to either stripe. We then compared our samples of neurons to those reported by Nassi and Callaway and found that the pyramids we sampled projecting to thick stripes were significantly smaller than those going to V2 overall, but pyramids projecting to thin stripes were not different. Additionally, our sample of stellates projecting to thin stripes were significantly larger than those identified as projecting to V2 by Nassi and Callaway, but stellates projecting to thick stripes were not different. These results continued to suggest that there are different sizes of neurons projecting to V2. A review of the raw data from our sample revealed that there was a wide range of dendritic lengths for pyramidal and stellate

neurons projecting to both stripes. Thus, we conducted a hierarchical cluster analysis to see if it would unbiasedly group neurons of different sizes together. Our results, which are summarized in Figure 2.9, show that there are multiple groups of neurons projecting to thick and thin stripes: medium and large pyramids and stellates project to thick and thin stripes, and small pyramids and small and giant stellates only project to thick stripes. I believe the results from the hierarchical cluster analysis shed light onto the different and somewhat confusing findings comparing neurons within our sample and between our samples and those from Nassi and Callaway. The cluster analysis results reveal that there are multiple sizes of groups of neurons projecting to thick (four groups) and thin (three groups) stripes. The Nassi and Callaway study appears to have selectively reconstructed the dendrites of our medium group of stellates, and our large group of pyramids. The functional implication of different sizes of neurons projecting to each stripe is not immediately clear. However, data from the retina may provide clues. As touched on briefly in Chapter 1 of this dissertation, in the retina, it has been shown that the dendritic field size of amacrine cells is correlated with their receptive field size; cells with larger dendritic fields monitor larger areas of visual space. The different sizes of cells we report here projecting from L4B to thick and thin stripes in V2 may follow this same organizational property, and may thus integrate differing amounts, and perhaps different types, of magnocellular information. Smaller neurons monitoring small areas of

visual space may respond to relatively higher spatial frequencies, and may thus contribute a higher resolution component into each visual stream. Larger neurons may respond to relatively lower spatial frequencies and higher temporal frequencies, contributing more of a 'moving object' detection component to each visual stream. It is also important to point out that we discovered two giant spiny stellate neurons that project to thick stripes. The average dendritic length of these two cells, which were reconstructed from two different cases, was slightly larger than the average dendritic length for the L4B stellates projecting to MT in the Nassi and Callaway study. Thus, giant spiny stellate neurons do not exclusively project to MT, and therefore these giant cells are not necessarily indicative of a L4B-MT circuit, as was previously suggested. However, we only found two of these giant cells out of our entire 59 neuron sample. Thus, these giant stellates projecting to V2 thick stripes are rare. These giant cells projecting to V2 could also project simultaneously to MT, as a small proportion (4%) of these cells have previously been identified (Sincich and Horton, 2003).

Overall, I believe our data support one of the primary findings of the Nassi and Callaway paper, which is that the L4B neurons projecting to MT are generally much larger than those projecting to V2. However, our data refine the understanding of the circuits between L4B and V2 and show that thick and thin stripes receive significantly more M-type input than previously thought, and this input is relayed by multiple sizes of L4B neurons.

2.5 References

Albertini AA, Ruigrok RW, Blondel D (2011) Rabies virus transcription and replication. Advanc Virus Res 79:1-22.

Anderson JR, Jones BW, Yang JH, Shaw MV, Watt CB, Koshevoy P, Mastronarde D, Tasdizen T, Marc RE (2009) A computational framework for ultrastructural mapping of neural circuitry. PLoS Biol 7: e1000074.

Briggs F, Kiley CW, Callaway EM, Usrey WM (2016) Morphological substrates for parallel streams of corticogeniculate feedback originating in both V1 and V2 of the macaque monkey. Neuron 90:388-399.

Callaway EM, Wiser AK (1996) Contributions of individual layer 2–5 spiny neurons to local circuits in macaque primary visual cortex. Vis Neurosci 13:907-922.

DeYoe EA, Van Essen DC (1985) Segregation of efferent connections and receptive field properties in visual area V2 of the macaque. Nature 317:58-61.

Federer F, Ichida JM, Jeffs J, Schiessl I, McLoughlin N, Angelucci A (2009) Four projection streams from primate V1 to the cytochrome oxidase stripes of V2. J Neurosci 29:15455-15471.

Federer F, Williams D, Ichida JM, Merlin S, Angelucci A (2013) Two projection streams from macaque V1 to the pale cytochrome oxidase stripes of V2. J Neurosci 33:11530-11539.

Livingstone MS, Hubel DH (1987) Connections between layer 4B of area 17 and the thick cytochrome oxidase stripes of area 18 in the squirrel monkey. J Neurosci 7:3371-3377.

Lund JS (1973) Organization of neurons in the visual cortex, area 17, of the monkey (Macaca mulatta). J Comp Neurol 147:455-495.

Nassi JJ, Callaway EM (2007) Specialized circuits from primary visual cortex to V2 and area MT. Neuron 55:799-808.

Nassi JJ, Callaway EM (2009) Parallel processing strategies of the primate visual system. Nat Rev Neurosci 10:360-372.

Shipp S, Zeki S (1984) Segregation of pathways leading from area V2 to areas V4 and V5 of macaque monkey visual cortex. Nature 315:322-325.

Shipp S, Zeki S (1989) The organization of connections between areas V5 and V1 in macaque monkey visual cortex. Eur J Neurosci 1:309-332.

Shipp S, Zeki S (2002) The functional organization of area V2, I: specialization across stripes and layers. Vis Neurosci 19:187-210.

Sincich LC, Horton JC (2002) Divided by cytochrome oxidase: a map of the projections from V1 to V2 in macaques. Science 295:1734-1737.

Sincich LC, Horton JC (2003) Independent projection streams from macaque striate cortex to the second visual area and middle temporal area. J Neurosci 23:5684-5692.

Sincich LC, Horton JC (2005) Input to V2 thin stripes arises from V1 cytochrome oxidase patches. J Neurosci 25:10087-10093.

Sincich LC, Jocson CM, Horton JC (2010) V1 interpatch projections to V2 thick stripes and pale stripes. J Neurosci 30:6963-6974.

Wickersham IR, Finke S, Conzelmann KK, Callaway EM (2007) Retrograde neuronal tracing with a deletion-mutant rabies virus. Nat Meth 4:47-49.

Yabuta NH, Sawatari A, Callaway EM (2001) Two functional channels from primary visual cortex to dorsal visual cortical areas. Science 292:297-300.

CHAPTER 3

DIFFERENT CLASSES OF L4B NEURONS PROJECTING TO V2 THICK STRIPES DEFINED BY THEIR AXONAL BRANCHING PATTERNS WITHIN V1

3.1 Introduction

Neurons in L4B of V1 send direct projections to a number of different cortical areas, including V2, V3, and MT (Maunsell and Van Essen, 1983; Burkhalter et al., 1986; Ungerleider and Desimone, 1986; Livingstone and Hubel, 1987; Shipp and Zeki, 1989; Sincich and Horton 2002; Federer et al., 2009; Federer et al., 2013). These projection neurons also have extensive axonal branching within V1, thus contributing input to local circuitry.

Previous reconstructions of local axons of L4B neurons show that these cells primarily and consistently target L2/3, L4B, and L5 in V1 (Callaway and Wiser, 1996) (Figure 3.1). Outside of this study, data describing the V1 axonal branching patterns of L4B neurons are sparse, with only one study showing that there may be L4B neurons that do not project to L2/3, but do

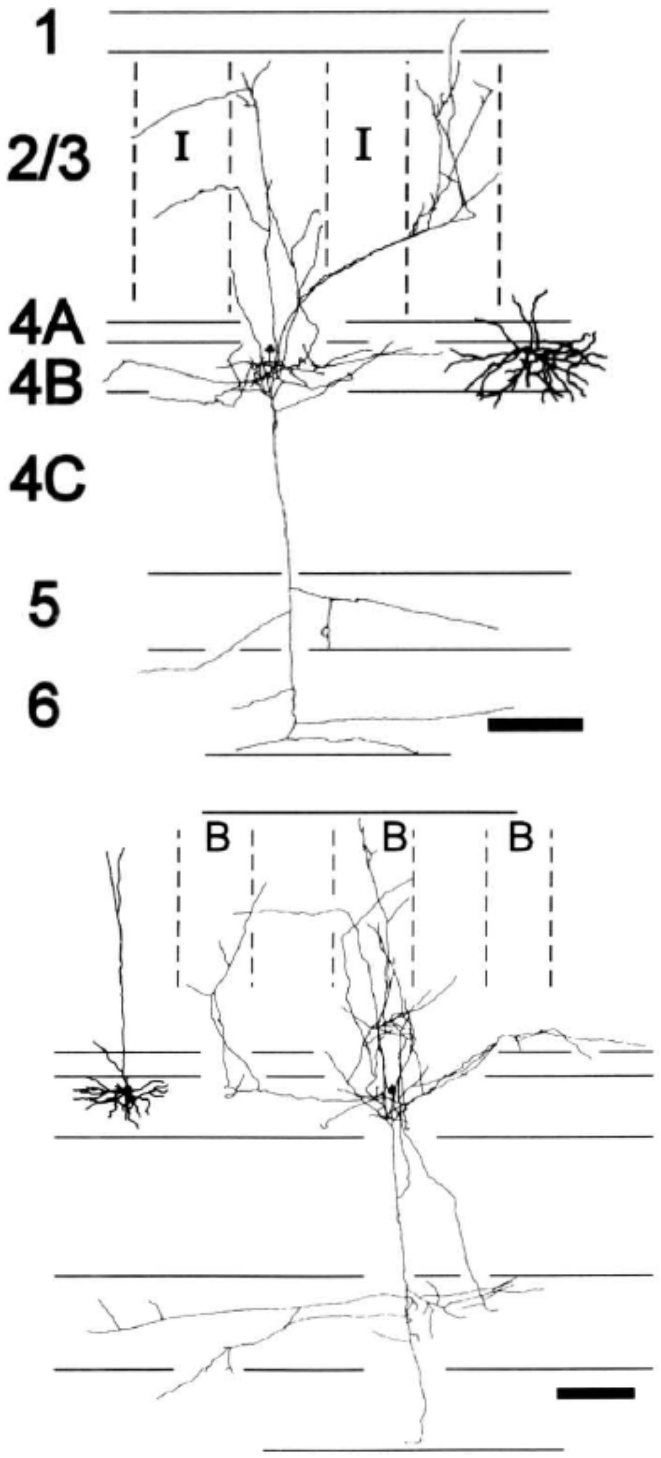

Figure 3.1: Canonical axon branching motif of L4B neurons from Callaway and Wiser (1996). Both pyramidal (top) and spiny stellate neurons in L4B mainly target L2/3, L4B and L5 with their axons. Additionally, axons target the blobs in L2/3, but are nonspecific to blobs or interblobs in layers 4B and 5.

project to L4B and L6 (Lund and Boothe, 1975). Both of these studies have limitations. The Callaway and Wiser (1996) study was performed in 400um slices of cortex. This preparation does not allow for full reconstruction of a cell's axons, nor can extrastriate projection targets be identified. The cells in this study were relatively few ($n = 15$), and were randomly filled intracellularly with biocitin, which could also lead to an unintended bias in the set of cells sampled due to their agreeableness with this labeling technique (e.g., large somas?). The Lund and Boothe (1975) study was performed on 90 um thick sections of tissue, again limiting the ability to fully reconstruct a neuron's axon, and not allowing for identification of the projection target (if any). Additionally, neurons in this study were labelled using Golgi technique, which may result in incomplete filling of axons, especially fine processes (Lund, 1973), and difficulty establishing clear laminar boundaries.

More important than the limitations of these previous studies is that nothing is known about local V1 circuitry as it relates to a neuron's extrastriate projection target. The multiple projection targets of L4B cells raises the question of whether cells projecting to each target are all from one, or multiple, populations of L4B neurons. As discussed in Chapter 2, existing data suggest that a L4B neuron's projection target may be inferred by looking at morphological characteristics of the cells. Sincich and Horton (2003) found that neurons with small somas project to V2, while neurons with large somas

project to MT. Correspondingly, Nassi and Callaway (2007) found that neurons projecting to MT have much greater soma size and dendritic length than those going to V2. However, neither of these studies investigated the morphological characteristics of the axons of these cells, nor was the V2 stripe (thick, thin, pale) to which these cells projected identified. As discussed in the introduction to this dissertation, the V2 stripes are heterogeneous in both structure and function. Thus, studies involving V2 without knowledge of the stripe type investigated are incomplete, and potentially inaccurate. After analyzing the soma size and dendritic length of neurons in L4B that project to thick stripes (Chapter 2), we then studied the local axonal branching patterns of these neurons in V1 to assess whether they recapitulated previously described canonical motifs. Here we present, for the first time, local V1 circuitry data for V1, L4B cells projecting specifically to V2 thick stripes.

3.2 Materials and Methods

In order to reveal neurons in L4B of V1 that project to thick stripes in area V2, we used visual stimuli to drive, and intrinsic signal optical imaging (OI) to locate, V2 thick stripe domains in-vivo. We then placed injections of a modified version of the retrogradely traveling rabies virus (rabies-GFP) into the putative thick stripes. Labeled cells in L4B of V1 were subsequently identified and reconstructed across serial tissue sections in order to examine

their morphological characteristics. The reconstruction process for axons was nearly identical to dendrites as described in section 2.2. The one exception being that axons were reconstructed more often using a 63x oil immersion objective.

3.2.1 Animals

The animals used and injection methodology are described in section 2.2.1

3.2.1.1 Surgical and Tracer Injection Procedures

Surgical and tracer injection procedures are identical to section 2.2.1.1

3.2.2 Optical Imaging

Optical imaging methods used are described in section 2.2.2

3.2.3 Histology

Histological processing of tissue is described in section 2.2.3

3.2.4 Data Analysis

3.2.4.1 Identification, Selection, and Reconstruction of L4B Cells

For case MK327, which was cut in the tangential plane, stereotypical CO staining revealed L2/3 blobs, L4A honeycomb, followed by CO pale L4B

and CO dark L4C. CO stained sections were aligned to adjacent sections to reveal the location of L4B cells. In one section, where L4B cell location was unambiguous, we fully reconstructed all cells (n = 11). While this was likely not exhaustive of all L4B cells in the sample, there were few potential L4B cells beyond those reconstructed.

Case MK339 was cut in the para-sagittal plane and identification of L4B cells was straightforward; the dark thin strip of CO representing L4A was clear, as was dark stained L4C, and cells in the intervening pale L4B were selected for reconstruction (see Figure 2.2). The axons of all L4Bcells (n = 10) were attempted to be reconstructed, but due to intermittent dark CO staining in this case, only one cell could confidently be considered completely reconstructed; this cell was at the most posterior edge of the label field and the surrounding sections did not contain excessively dark CO. Of the other nine cells, we were able to partially reconstruct the axons of six of these neurons. Due to their incompleteness, we were not able to sufficiently quantify the amount of axon they dedicated to each layer. However, after axonal classes were established, we were able to place these cells into Class 1 (see Results) as it was clear that they all had significant axonal branching in L2/3. These cells could not be further subdivided into Class 1a or Class 1b cells, but our impression is that they were predominantly Class 1a.

For case MK340, identical fluorescent and brightfield images were imported into Neurolucida software (MicroBrightField, Williston, VT), layers

were identified and drawn using the fluorescent image, then overlaid onto the DAB reacted tissue revealing the location of L4B cells (see Figure 2.2). For this case, there was dense labeling toward the anterior portion of the label field, making it impossible to reconstruct axons. Thus, the reconstructed axons ($n = 5$) were from somas located in the posterior, sparsely labeled portion of the label field.

All cells were digitally reconstructed using Neurolucida software on a Zeiss Axioskop 2 microscope with 40x and 63x objectives under brightfield illumination using a Qimaging color CCD camera. The axon of each neuron was initially identified as a small caliber, spine de-void, process exiting the bottom of the cell (Figure 3.2). The extensive branching and subsequent projection into white matter confirmed the identity of the process as an axon. The majority of cell axons were reconstructed well into white matter, and a few were followed all the way back to the V2 injection site. In order to reconstruct cells across multiple serial sections, the section outline and radial blood vessels were used for coarse alignment across sections. For fine scale alignment, local blood vessels and multiple exit points of processes exiting one section of tissue were marked, and subsequently aligned to their corresponding continuations in the next section. This process of using global and very local fiducial points made highly accurate and complete reconstruction of axons possible. In addition to axon reconstruction, boutons were plotted for neurons in case MK327. Boutons were identified as punctate

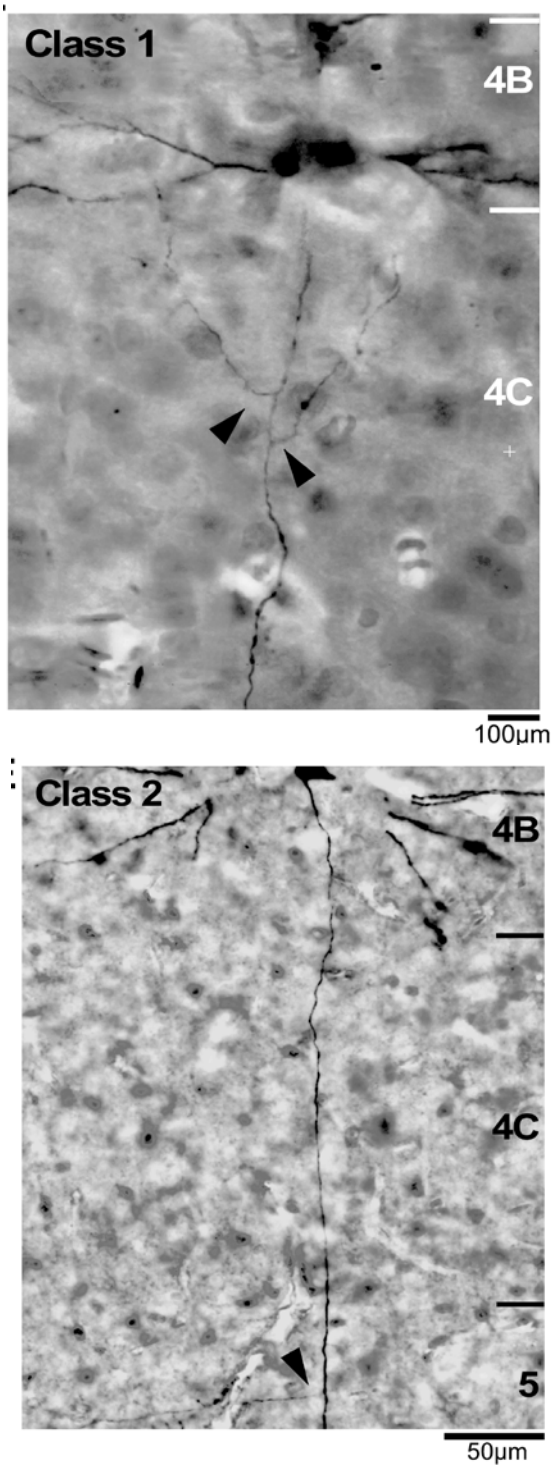

Figure 3.2: Images of Class 1 (top) and Class 2 (bottom) L4B neurons. Arrowheads denote the axon branches off the primary descending axon in L4C, and subsequently project up to L2/3 (top). For the class 2 neuron, note that there is no axonal branching in or around L4C, but only in L5 (arrowhead)

relieved from, yet attached to, the axon (bouton-termineaux), or large swellings along the axon that were greater in diameter than the thickest proximal portion of axon (bouton-en-passant). The overwhelming majority of boutons were of the termineaux variety, and due to the possible ambiguity associated with marked en-passant boutons, all boutons were analyzed together. For analysis of the quantity of axon in each layer, the total length of axon devoted to each layer in each section was calculated in Neurolucida, and subsequently aggregated across all sections in Excel. Axonal length calculations only included branches off of the primary descending axon, and were collected from unscaled tracings and were not corrected for tissue shrinkage. Because every third section was reacted for CO, exact layer delineations could not be made on each section; however, we believe the error associated with this limitation is minor and does not impact the overall conclusions of this study. In order to analyze soma and bouton position relative to CO compartments, we aligned the nearest CO section containing clear blobs to each section containing label using radial blood vessels. Local blood vessels nearest to the label were used as primary alignments points. For tissue sections containing a large area of label, we parsed label fields into segments in order to attain more precise local alignment. For CO compartments, we primarily used one section of tissue in which L3 showed clear blobs over the entire ROI. For soma and bouton alignment to CO compartments, images were scaled in Neurolucida, and warped (IR tweak,

NCRtoolset, SCI Institute at the University of Utah) if necessary (see Anderson et al., 2009; Federer et al., 2013). For boutons in the upper layers, we generally performed minimal scaling or warping, but for boutons in the lower layers, greater adjustments were needed due to differential shrinkage across tissue sections. Our results unambiguously show boutons in the lower layers consistently outside blobs, in agreement with our data across the other layers. For this reason, we feel the alignment of the lower sections with boutons, to the upper sections with blobs, is accurate.

3.2.4.2 Clustering and Statistical Analyses

Hierarchical clustering analysis was used to classify neurons based on the amount of axonal branching in layers 2/3, 4A, 4B, 4C, 5, and 6. Although layers 4A and 4C generally contain axons passing through to other layers, and layer 6 is generally not a primary target, all layers were used in the case that this un-biased analysis would classify cells based on different criteria than our qualitative impressions. The hierarchical clustering analysis plots the position of each cell in N-dimensional space based on the number of metrics used to describe the cell, which in this study is axon distribution across six different layers. The distance between cells in this space was calculated using squared Euclidian distance and linkages between cells were created using Wards method, similar to Briggs et al. (2016). All analyses were performed in SPSS. Significance testing was performed using one-way

ANOVA with post-hoc Bonferroni tests, and all tests were conducted after different classes of cells were identified by the cluster analysis.

3.3 Results

Axons in V1 from 23 L4B cells were reconstructed (14 stellates, 61%; 9 pyramids, 29%). Seventeen cells (11 stellates (65%); 6 pyramids (35%)) were completely reconstructed and the amount of axon each cell dedicated to each layer was quantified. In agreement with Callaway and Wiser, we find that the primary targets of most thick stripe projecting L4B cells are supragranular layers 2/3 and 4B, with additional projections to infragranular L5. Layers 4A and 4C were not primary targets of these cells, but did contain passing axons. Rare projections to L6 are discussed further below. Qualitative evaluation of the data suggested that there are at least two unique local branching motifs for these cells. Class 1 cells recapitulate the branching motif described by Callaway and Wiser (1996) with primary projections to L2/3, L4B, and L5. However, Class 2 cells predominantly target L5, with little ($n = 2$) or no ($n = 4$) branching in L4B; all Class 2 cells have no branching in L2/3 (Figures 3.2 and 3.3).

We used hierarchical clustering analysis (Cauli et al., 2000; Briggs et al., 2016), to acquire a quantitative and unbiased assessment of axonal branching patterns across V1 layers in order to probe our qualitative impressions. This analysis yielded two primary clusters of cells and

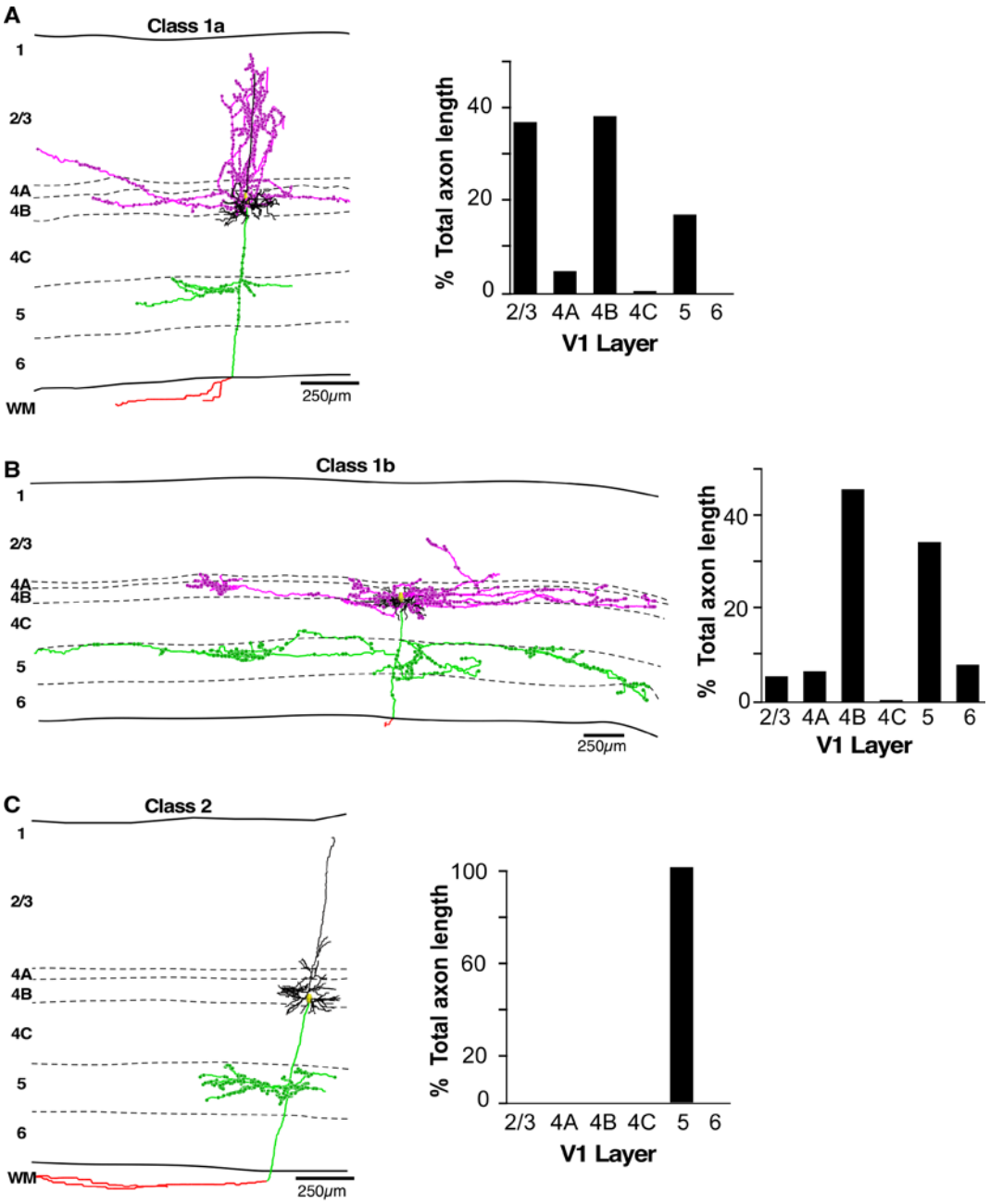

Figure 3.3: Reconstruction and quantification of the local axon of L4B neurons projecting to V2 Thick stripes. **A,** Reconstruction of a Class 1a neuron. Quantification of the amount of axon in each layer is displayed to the right. **B,** Reconstruction of a Class 1b neuron. Note the lack of branching in L2/3 compared to Class 1a neurons. **C,** Class 2 cell that only branches in L5. **Reconstruction Conventions:** black = dendrites, yellow = soma, pink = supragranular axon, green = infragranular axon, red = axon in white matter. V1 Layers are displayed on left.

supported our initial assessment of the data (Figure 3.4). Class 1 neurons (n = 15; 40% pyramidal, 60% stellate) have an average of 18% of their axon in L2/3, 50% in L4B, and 15% in L5. Class 2 neurons (n = 6, 50% pyramidal, 50% stellate) have an average of 6% of their axon in L4B and 91% in L5 (Figures 3.4 and 3.5).

Additionally, the cluster analysis revealed that Class 1 cells can be split into subgroups, confirming our inclinations, and supporting previously unrecognized differences in axon branching patterns from the literature. Class 1a cells (60% pyramids, 40% stellates) are those described previously and have an average of 37% of their axon in L2/3, 42% in L4B, and 12% in L5. Class 1b cells (100% stellates) have an average of 3% of their axon in L2/3, 56% in L4B, and 17% in L5 (Figure 3.4). Interestingly, Class 1b cells resemble the neuron in Callaway and Wiser's (1996) figure 6a, which shows a neuron that has a clear dominance of axonal branching in L4B, and little branching in L2/3. Our qualitative impression of Class 1b L2/3 axons is that they terminate in L3B or L3A. Interestingly, our Class 1b cells do differ from the cell in Callaway and Wiser's figure 6a in that they clearly target L5. Class 1b cells are differentiated from Class 1a cells due to their significant lack of axonal branching in L2/3 ($p < 0.001$) (Figure 3.4). Class 2 cells are differentiated from Class 1 and 3 cells because they have significantly more axon dedicated to L5 ($p < 0.001$), and dedicate significantly less axon to L4B ($p < 0.01$) (Figure 3.4). Again, Class 2 cells have no axonal branching in L2/3

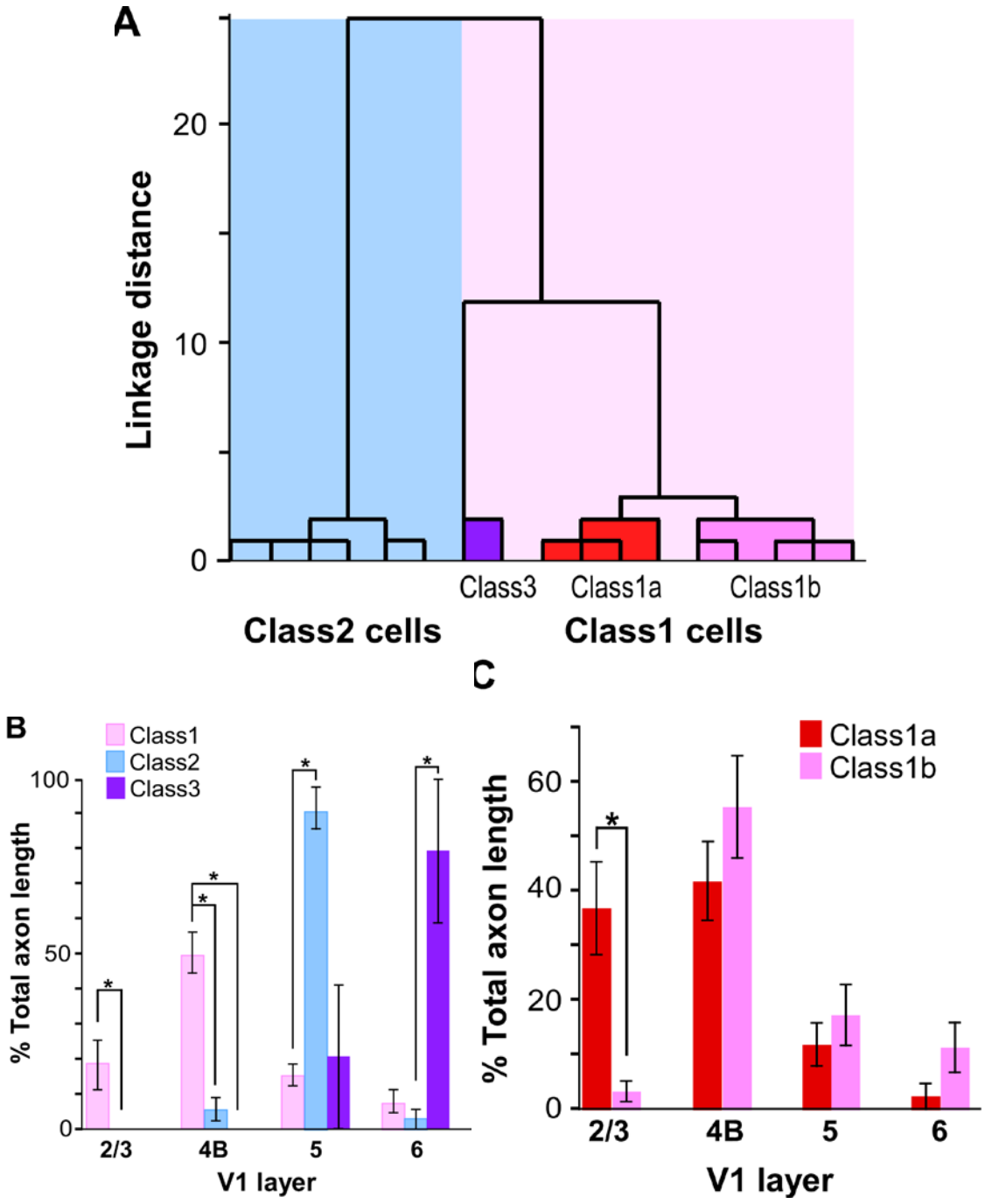

Figure 3.4: Different classes of L4B neurons derived from clustering analysis of the quantity of axon dedicate to each layer in V1. A, Cluster analysis revealing two primary groups (Class 1, Class 2) as well as subgroups (Class 1a, 1b, 3). **B**, Comparison of the amount of axon in each layer for Class 1, 2, and 3 neurons. **C**, Comparison of the amount of axon in each layer for Class 1a and 1b neurons.

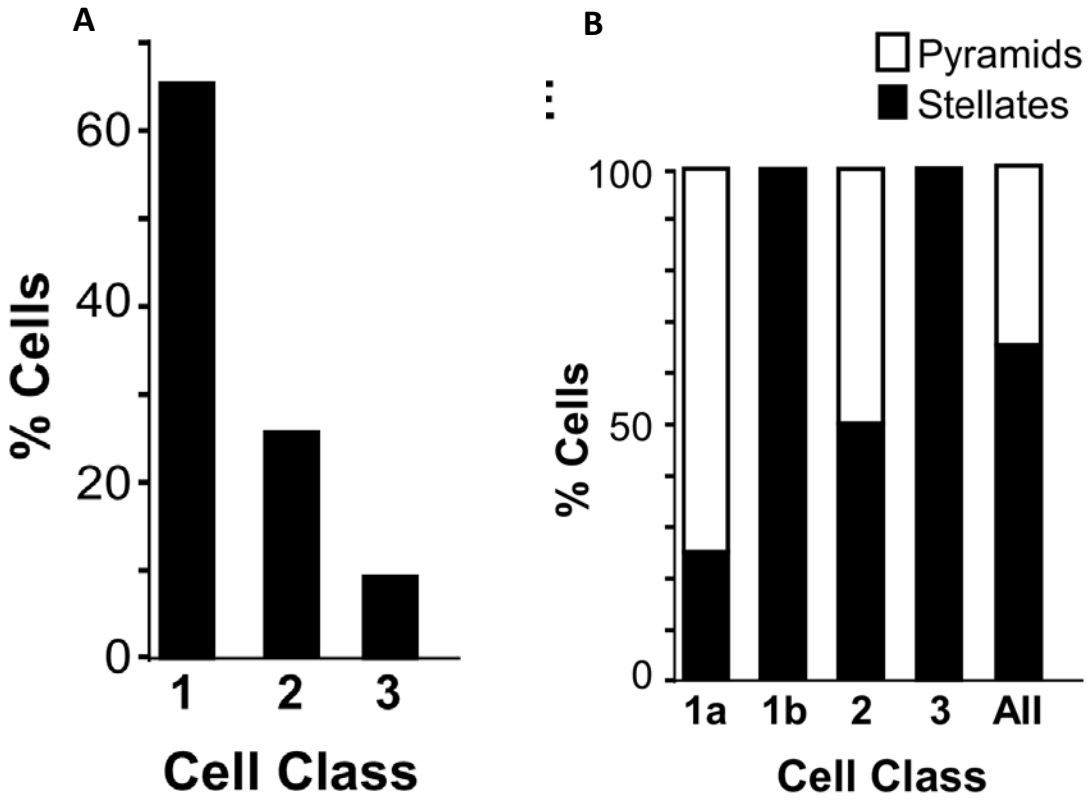

Figure 3.5: Proportions and cell composition of the different classes of L4B neurons. **A,** The majority of cells reconstructed replicated the canonical L2/3, L4B, L5 branching motif from Wiser and Callaway (1996) and are designated as Class 1 cells. Class 2 and 3 cells represent a minority of the cells found, suggesting that their sparseness is why they have not been previously identified. **B,** The proportion of spiny stellates and pyramids that comprise each cell class. Class 1a cells were mostly pyramids, while Class 1b and Class 3 neurons were all stellates. Class 2 cells were pyramids and stellates.

(see Figure 3.3). An additional subclass was identified using the cluster analysis and could be considered Class 1c or Class 3 cells (Figure 3.4). These cells have predominant branching in L6, but also have branching in L5; they have no branching in L4B or L2/3. Our initial qualitative assessment placed these neurons in Class 2, but because Class 2 cells have very little L6 branching, and because Class 1 cells have slightly more L6 branching, the cluster analysis may have reported these cells as a subgroup of the Class 1 cluster. Class 3 cells may have also been categorized as of subgroup of Class 1 cells due to the relatively smaller amount of L5 branching, which Class 1 and 3 neurons share when compared to Class 2 cells. We believe these neurons may be an entirely different class of cells, and refer to them as Class 3 cells. These cells bear resemblance to those described by Lund and Boothe (1975). Because of our small sample of the these cells ($n = 2$), the fact that the cluster analysis does not place them in their own distinct cluster, and due the theoretical difficulties with including them in Class 1, we chose to pursue a more limited characterization of these cells, except in the case of statistical analyses where it was more rigorous to utilize the data rather than remove it (e.g., one-way ANOVA).

3.4 Discussion

In this study, we examined the axons of L4B neurons that project to thick stripes in V2. We specifically looked at the amount of axon these

neurons dedicated to each layer within V1 and found that not all cells replicate the canonical branching pattern that has previously been described. We find evidence for at least two main classes of neurons. Class 1 cells are those which have been described previously and devote substantial amounts of axon to L2/3, L4B, and L5. Class 2 cells are distinguished from Class 1 cells by their lack of branching in L2/3, and significantly more branching in L5. Class 1 cells can also be broken down into subclasses; Class 1a neurons resemble those previously described as Class 1 cells, but Class 1b neurons are distinguished from Class 1a cells by significantly less branching in L2/3. Interestingly, all Class 1b cells were also spiny stellates. Finally, a subcluster of two neurons was found in the Class 1 cluster and we have chosen to call this group Class 3 cells, as they do not share the primary features of Class 1 cells. Unlike Class 1 cells, Class 3 cells have no branching in either L2/3 or L4B. Class 3 cells branch in L5 and L6. These neurons were likely not included within the Class 2 neuron cluster because no Class 2 neurons have L6 branching. Our Class 3 neurons do bear some resemblance to the neurons previously described by Lund (1973), with the exception that Class 3 cells do not have any branching in L4B.

Our replication of the axon branching motif described by Callaway and Wiser (1996) as well as its numerical superiority in our sample (~65%), substantiates that, within V1, this is likely the primary information distribution pattern for most L4B cells. However, the existence of Class 1b

cells, which have little (L3B?) or no branching in L2/3, and dominant branching in L4B, suggests a different function for these neurons. These neurons appear to be most interested in distributing information within L4B and L5 over relatively long distance (~1.5 mm on average). The distance at which Class 1b neurons can project may indicate that they are involved in some form of stereopsis, as axons can travel across more than one ocular dominance column.

Class 2 neurons were approximately 25% of our sample of neurons. According to El-Shamayleh et al. (2013), only ~8% of V1 cells in the supragranular layers project to V2. If we assume 10% of L4B neurons project to V2, and 75% of those neurons project the thick stripes, then 7.5% of L4B neurons would project to V2 thick stripes. Our Class 2 cells (25%) would thus represent ~2% (0.25*7.5) of the cells projecting from L4B to thick stripes in V2. Thus, Class 2 neurons are rare, and that is likely why they were missed in previous studies (e.g., Callaway and Wiser, 1996). The role of Class 2 neurons is to distribute information almost exclusively to L5. It is known that there are neurons in L5 that project subcortically to the superior colliculus, which is involved in orienting the eyes to different targets in the visual scene (Lund et al., 1975; Lia and Olavarria, 1996). We speculate that Class 2 neurons may be performing a unique computation in L4B and passing it to L5 in order for it to be relayed down to the superior colliculus. Class 2 cells were either pyramids or stellates, suggesting further that there

may be two unique L4B computations being passed to L5, and possibly, subsequently, down to the superior colliculus. Neurons in L4B have been suggested to be tuned for disparity (Livingstone and Hubel, 1988). The computations of Class 2 cells may assist the superior colliculus in performing orienting tasks, perhaps adding a depth component to the orienting instructions.

Because Class 1 cells have strong input to the supragranular layers 4B and 2/3, and because Class 2 cells primarily target infragranular cells, we think it is plausible that these two classes of cells contribute to two circuits within V1 that are independent of one another. The canonical L4B circuit previously described by Wiser and Callaway (1996) involves L4B neurons passing a computation to supragranular layers which is integrated in these layers and then, ostensibly, passed to other cortical areas (e.g., V2, V3, MT). Class 2 cells may be embedded in a circuit which exists in order to pass information to the superior colliculus via L5 neurons. Canonical cortical wiring diagrams in V1 suggest information flows into V1 at L4C, then up to L2/3, and down to L5. From L5, information can be relayed back up to L2/3, or down to subcortical structures. However, it has recently been shown in rat barrel cortex that infragranular neurons in layers 5 and 6 can function independent of input from the supragranular layers, suggesting the supragranular and infragranular layers can function as independent circuits. We suspect that Class 1 neurons may primarily be involved in a

supragranular circuit which passes information to extrastriate cortices, while the Class 2 neurons may primarily be involved in an infragranular circuit which passes information subcortically. This then also suggests that each cell class is also passing a unique computation to V2 thick stripes, which would constitute at least two more pathways from L4B, V1 to V2 thick stripes.

3.5 References

Anderson JR, Jones BW, Yang JH, Shaw MV, Watt CB, Koshevoy P, Mastronarde D, Tasdizen T, Marc RE (2009) A computational framework for ultrastructural mapping of neural circuitry. PLoS Biol 7: e1000074.

Briggs F, Kiley CW, Callaway EM, Usrey WM (2016) Morphological substrates for parallel streams of corticogeniculate feedback originating in both V1 and V2 of the macaque monkey. Neuron 90:388-399.

Burkhalter A, Felleman DJ, Newsome WT, Van Essen DC (1986) Anatomical and physiological asymmetries related to visual areas V3 and VP in macaque extrastriate cortex. Vision Res 26:63-80.

Callaway EM, Wiser AK (1996) Contributions of individual layer 2–5 spiny neurons to local circuits in macaque primary visual cortex. Vis Neurosci 13:907-922.

Cauli B, Porter JT, Tsuzuki K, Lambolez B, Rossier J, Quenet B, Audinat E (2000) Classification of fusiform neocortical interneurons based on unsupervised clustering. Proc Natl Acad Sci USA 97:6144-6149.

El-Shamayleh Y, Kumbhani RD, Dhruv NT, Movshon JA (2013) Visual response properties of V1 neurons projecting to V2 in macaque. J Neurosci 33:16594-16605.

Federer F, Ichida JM, Jeffs J, Schiessl I, McLoughlin N, Angelucci A (2009) Four projection streams from primate V1 to the cytochrome oxidase stripes of V2. J Neurosci 29:15455-15471.

Lia B, Olavarria JF (1996) The distribution of corticotectal projection neurons correlates with the interblob compartment in macaque striate cortex. Vis Neurosci 13:461-466.

Livingstone MS, Hubel DH (1987) Connections between layer 4B of area 17 and the thick cytochrome oxidase stripes of area 18 in the squirrel monkey. J Neurosci 7:3371-3377.

Lund JS (1973) Organization of neurons in the visual cortex, area 17, of the monkey (Macaca mulatta). J Comp Neurol 147:455-495.

Lund JS, Boothe RG (1975) Interlaminar connections and pyramidal neuron organisation in the visual cortex, area 17, of the macaque monkey. J Comp Neurol 159:305-334.

Maunsell JH, van Essen DC (1983) The connections of the middle temporal visual area (MT) and their relationship to a cortical hierarchy in the macaque monkey. J Neurosci 3:2563-2586.

Shipp S, Zeki S (1989) The organization of connections between areas V5 and V1 in macaque monkey visual cortex. Eur J Neurosci 1:309-332.

Sincich LC, Horton JC (2002) Divided by cytochrome oxidase: a map of the projections from V1 to V2 in macaques. Science 295:1734-1737.

Sincich LC, Horton JC (2003) Independent projection streams from macaque striate cortex to the second visual area and middle temporal area. J Neurosci 23:5684-5692.

Ungerleider LG, Haxby JV (1994) 'What' and 'where' in the human brain. Curr Opin Neurobiol 4:157-165.

CHAPTER 4

UNIQUE INTRA-V1 CIRCUITRY FOR L4B NEURONS PROJECTING TO V2 THICK STRIPES

4.1 Introduction

CO staining in L2/3 of V1 reveals intermittent dark patches (blobs), and non-dark 'interblob' regions (Horton and Hubel, 1981) (see Figure 1.6). It has consistently been shown that neurons in L2/3 blobs, and beneath blobs in L4B, project almost exclusively to V2 thin stripes, while neurons in and under interblobs project primarily to pale and thick stripes. This anatomical organization demonstrates that, on a broad level, there is circuit, or stream, specificity between V1 and V2 CO domains (Livingstone and Hubel, 1984; Sincich and Horton 2002; Sincich and Horton 2005; Federer et al., 2009; Sincich and Horton, 2010; Federer et al., 2013).

Receptive field property specificity of neurons in blobs and interblobs has proven to be difficult to pin down. It was initially thought that neurons in blobs responded to color stimulus, while neurons in interblobs were tuned to respond to orientation (Livingston and Hubel, 1988). However, it has since

been shown in various studies that color, orientation, and direction selectivity are distributed across both CO compartments (e.g., Lennie et al., 1990; Edwards et al., 1994; Leventhal et al., 1995). Having a clear understanding of the input into blob and interblob areas would enable the generation of better hypothesis regarding neuron receptive field properties, and would aid in understanding the differing results from physiological studies in blobs and interblobs. Understanding the specificity of V1 cells' response properties, and their anatomical locations, would then help us to better understand the kinds of information circuits are transmitting between the V1 and V2 CO compartments.

The local/interlaminar circuitry of V1 has been studied extensively (Lund, 1973; Lund and Boothe, 1975; Blasdel et al., 1985; Fitzpatrick et al., 1985; Valverde, 1985; Lund et al., 1988; Lund et al., 1991; Yoshioka et al., 1994). In particular, Lachica et al. (1992) show that blobs receive direct L4B input, and that interblobs do not. Callaway and Wiser (1996) confirm this finding by showing individual axons of neurons in L4B exclusively targeting blobs. Yabutta and Callaway (2001) have since demonstrated that L4B is dominated by magnocellular input that comes directly from L4Cα, a layer that receives direct LGN magnocellular input. Together, these studies elucidate a mechanism through which CO blobs receive a form of magnocellular input, while interblobs appear to be devoid of this input. However, Nealy and Maunsell (1994) showed that L2/3 interblob neurons can

be activated by visual stimulus even after parvocellular LGN activity is blocked, suggesting a significant magnocellular component reaches the interblobs. Additionally, L2/3 interblob neurons show magnocellular-like response properties, such as direction of motion tuning (Leventhal et al., 1995), and low spatial frequency preferences (Edwards et al., 1995). Although there is evidence for the possibility some kind of magnocellular input reaching interblobs from neurons positioned in the middle of L4C (Yabuta and Callaway, 1998a), it is unclear what kind of information these cells transmit. Thus, our current understanding of laminar circuitry does not show a clear pathway for magnocellular input to the interblobs, yet physiological data suggest interblobs receive some form of M input.

Finally, Yabuta and Callaway (1998b) also note that there appears to be border zones at the transition between blobs and interblobs in L2/3, and that cells located in these areas appear to be biased towards sending projections to other 'border' areas (i.e., like-to-like connectivity, see Livingstone and Hubel., 1983; Bosking et al., 1997). Further evidence for a blob-border zone comes from data showing that there are neurons in L4C that appear to distribute information to the area between blobs and interblobs in L2/3 (Yabuta and Callaway, 1998a). Interestingly, Federer et al. (2009) have also found a bias for cells projecting to thick stripes to be located in this border zone in both layers 2/3 and 4B, while pale stripe projecting cells are biased toward interblob regions. However, Sincich and

Horton (2010) find that cells projecting to thick and pale stripes are equally distributed across the interblobs, and that there is no bias for cells to be located near blob borders. Neurons in a blob-border zone could be functionally unique, due to the location of their dendrites within blobs and interblobs, enabling them to integrate both blob and interblob information. The existence of a unique blob-border zone in V1 remains uncertain, with good anatomical evidence supporting its existence, but also some evidence doubting the possibility. No electrophysiological studies specifically testing neurons in the border region vs. the blob or interblob region have been performed. If a blob-border zone does exist in V1, there would be important implications for the physiological properties of these cells, and the transmission of that information to specific areas in V2.

In this study, our goal was to locate and characterize neurons contributing information to a specific circuit between V1 and V2. We chose to pursue the identification of neurons in L4B of V1 that project to V2 thick stripes. Further rationale for this choice is discussed in Chapters 1 and 2. Understanding how these cells form circuits in V1 will help us to understand what kind of information is sent specifically to V2 thick stripes. In order to find the L4B cells, we placed retrograde travelling G-deleted rabies virus injections into V2 thick stripes. Subsequently, we found that the local V1 axons of L4B neurons target interblobs in L2/3 of V1, and avoid the blob column in layers 4B and 5. We also find evidence for a blob-border zone, with

cells residing in this zone sending axons to other blob-border zones, while cells in interblobs send axons to other interblob zones. Our findings show that there are at least two independent circuits emanating from L4B; one circuit, previously described, transmits L4B information to blobs, while our data show an additional L4B circuit that transmits some form of magnocellular information to the interblobs. Importantly, the circuit we have identified may be functionally specific to the V2 thick stripe projection target, demonstrating that the local circuitry of a L4B cell may differ from other L4B cells due to the projection target. Additionally, like-to-like network forming blob-border cells may also constitute yet another unique L4B circuit.

4.2 Materials and Methods

In order to reveal neurons in L4B of V1 that project to thick stripes in area V2, we used visual stimuli to drive, and intrinsic signal optical imaging (OI) to locate, thick stripe domains in-vivo. We then placed injections of a modified version of the retrogradely traveling rabies virus into thick stripes (Nassi and Callaway, 2007; Wikersham et al., 2007; Briggs et al., 2016). Labeled cells in V1 L4B were subsequently identified and reconstructed in order to examine their morphological characteristics.

4.2.1 Animals

One adult male macaque monkey was used in this study. All experimental procedures were in accordance with protocols approved by the University of Utah Institutional Animal Care and Use Committee. The animal was injected with rabies-EGFP (SADΔG-EGFP) in a single hemisphere of the brain. The injections was targeted at the exposed portion of V2, on the posterior portion of the dorsal lip of the lunate sulcus (e.g. Federer et al., 2013). The injection was delivered via a glass micropipette (~35-45 μm tip diameter) and picospritzer applied pressure. For this case (MK327), injections of CTGg, CTB555, and CTB647 were placed in V2 approximately 3 mm from the rabies injection, and an additional injection of rabies was placed contralaterally in V2.

4.2.1.1 Surgical and Tracer Injection Procedures

Surgical procedures were performed as described in section 2.2.2.1. For optical imaging, anesthesia was maintained with sufentanil citrate (5-10 μg/kg/h) and animals were paralyzed with vercromium bromide (0.3 mg/kg/h). One of our primary goals for these experiments was to obtain sparse labelling of cells in V1 in order to facilitate complete reconstruction of axonal processes. Thus, our rabies injection was very small (~500 nl); the injection was placed ~ 1 mm from the cortical surface. The animal was kept under anesthesia for the entirety of the experiment and euthanized with sodium

pentobarbital (150 mg/kg; i.v.) - 4.5 days after injection. The animal was perfused with 4% paraformaldehyde for 15 min.

4.2.2 Optical Imaging

Optical imaging methods use are described in section 2.2.2.

4.2.3 Histology

For this case, the cortex was flattened gently above the imaged region. V1 and V2 were separated from the rest of the brain by cutting through the bottom of the lunate sulcus. The V1/V2 block was postfixed in 4% PFA between glass slides for 1-2 h, sunk in 30% sucrose for cryoprotection, and frozen-sectioned tangentially at 40 μm. Every third section was reacted free floating for CO. Every section was immunostained for GFP using the anti-GFP rabbit polyclonal antibody, the biotinylated goat anti-rabbit secondary antibody, and an ABC avidin-peroxidase kit revealed with a diaminobenzidine (DAB) reaction enhanced with nickel and cobalt to create a black reaction product (Nassi and Callaway, 2007). Injections sites were identified by the labelling of a small field of glial cells located around the pipette track. To localize injections, an aggregate of all injection sites was created in Photoshop (Adobe Systems Inc.) and aligned using radial blood vessels to a composite image of CO stripes (as in Federer et al., 2009, 2013; see Figure 2.2).

4.2.4 Data Analysis

4.2.4.1 Identification, Selection, and Reconstruction of L4B Cells

This case (MK327) was cut in the tangential plane and stereotypical CO staining revealed L2/3 blobs, L4A honeycomb, followed by CO pale L4B and CO dark L4C. CO stained sections were aligned to adjacent sections to reveal the location of L4B cells. In one section, where L4B cell location was unambiguous, we fully reconstructed all cells ($n = 11$). While this was likely not exhaustive of all L4B cells in the sample, there were few potential L4B cells beyond those reconstructed.

All cells were digitally reconstructed using Neurolucida software on a Zeiss Axioskop 2 microscope with 40x and 63x objectives under brightfield illumination using a Qimaging color CCD camera. The axon of each neuron was initially identified as a small caliber, spine de-void, process exiting the bottom of the cell (e.g., Figure 3.2). The extensive branching and subsequent projection into white matter confirmed the identity of the process as an axon. The majority of cell axons were reconstructed well into white matter, and a few were followed all the way back to the V2 injection site. In order to reconstruct cells across multiple serial sections, the section outline and radial blood vessels were used for coarse alignment across sections. For fine scale alignment, local blood vessels and multiple exit points of processes exiting one section of tissue were marked, and subsequently aligned to their corresponding continuations in the next section. This process of using global

and very local fiducial points made highly accurate and complete reconstruction of axons possible. In addition to axon reconstruction, boutons were also plotted. Boutons were identified as punctation relieved from, yet attached to, the axon (bouton-termineaux), or large swellings along the axon that were greater in diameter than the thickest proximal portion of axon (bouton-en-passant). The overwhelming majority of boutons were of the termineaux variety, and due to the possible ambiguity associated with marked en-passant boutons, all boutons were analyzed together. Because every third section was reacted for CO, exact layer delineations could not be made on each section; however, we believe the error associated with this limitation is minor and does not impact the overall conclusions of this study. In order to analyze soma and bouton position relative to CO compartments, we aligned the nearest CO section containing clear blobs to each section containing label using radial blood vessels. Local blood vessels nearest to the label were used as primary alignments points. For tissue sections containing a large area of label, we parsed label fields into segments in order to attain more precise local alignment. For CO compartments, we primarily used one section of tissue in which L3 showed clear blobs over the entire ROI. For soma and bouton alignment to CO compartments, images were scaled in Neurolucida, and warped (IR tweak, NCRtoolset, SCI Institute at the University of Utah) if necessary (see Anderson et al., 2009; Federer et al., 2013). For boutons in the upper layers, we generally performed minimal

scaling or warping, but for boutons in the lower layers, greater adjustments were needed due to differential shrinkage across tissue sections. Our results unambiguously show boutons in the lower layers consistently outside blobs, in agreement with our data across the other layers. For this reason, we feel the alignment of the lower sections with boutons, to the upper sections with blobs, is accurate.

4.2.4.2 Image Processing

CO blobs and interblobs were obtained using methods previously reported by Federer et al. (2009). Digitized images of CO stained tissue were processed using low-pass, equalization, and exponential filters (Image-Pro Plus, Media Cybernetics Inc. Silverspring, MD). The darkest 33% of pixels in the image created the border of the blobs, the darkest pixels represented blob centers, and the lightest pixels represented interblob centers. All image processed CO compartment segmentation was visually inspected and found to be accurate.

4.2.4.3 Blob-border Analysis

Blob borders, blob centers, and interblob centers were drawn in Neurolucida. Tracings were exported and analyzed in Matlab (MathWorks, Natick, MA) using custom scripts. For all soma or bouton markers inside a blob-border, the distance of each was measured to the closest blob center and

closest blob border. The distance of a soma or bouton from the blob border was divided by the total distance between the blob-center and blob-border to give a Blob-Border-Index value. Index values ranged from -1 to 0, with -1 representing a soma at the blob center, and 0 representing a soma at the blob border. For somas or boutons outside of blob-borders, the Index was computed using the distance between the blob-border and the interblob center. Index values ranged from 1 to 0, with 1 representing a soma at the interblob center, and 0 representing a soma at the blob border. Histogram bins spanning -0.4 to 0.4 were used to define the blob-border-region. Our characterization of the blob-border-region was primarily driven by our observation of the data. We consistently saw distribution peaks in the 0.0 – 0.4 bin range (border), or the 0.6 - 1.0 range. While there were rarely peaks in the 0.0 to -0.4 bins, we chose this range in order to keep the blob-border region symmetrical on either side of the blob border.

4.2.4.4 Clustering and Statistical Analyses

The clustering method used is described in section 3.2.4.2.

4.3 Results

4.3.1 Soma Location Relative to CO Compartments

In order to determine the location of somas relative to the edge of a blob, we developed an index measuring system. Somas outside a blob were

measured to the blob border and to the interblob center; somas inside a blob were measured to the blob border and blob center. Values of 1.0 indicate cells in the center of an interblob, values of 0.0 indicate a cell positioned on a blob border, and values of -1.0 indicate cells in the center of a blob. We used values from 0.0 - -0.4, and 0.0 - 0.4 to indicate the blob border region. Sincich and Horton (2005) report that blobs occupy ~33% of the cortical area in V1, and thus our CO compartment categorization creates a similar proportion of cortex devoted to blobs. Using this quantitative index metric, after a rabies injection into a V2 thick stripe, we find 18% of cells in blobs, 45% in blob borders, and 36% in interblobs (n = 11, Figure 4.1). With the addition of qualitatively categorized cells, from another case, we find 18% of cells in blobs, 47% in blob borders, and 35% in interblobs (n = 17). This distribution of somas across CO compartments is consistent with Sincich and Horton (2005, 2010) and Federer et al. (2009) who show small amounts of cells in blobs going to thick stripes, and Federer et al. (2009) who found a blob-border location bias for cells projecting to thick stripes.

We find no consistent relationship between cell class (described in Chapter 3) and soma CO position. Class 1a cells are found in border and interblob zones, but not blobs. Class 1b cells are found in blobs and border zones, but not interblobs. Class 2 cells are found in all three CO compartments (Figure 4.1). Given our sample size, we do not think this necessarily represents a thorough sampling of the CO location of cells in each

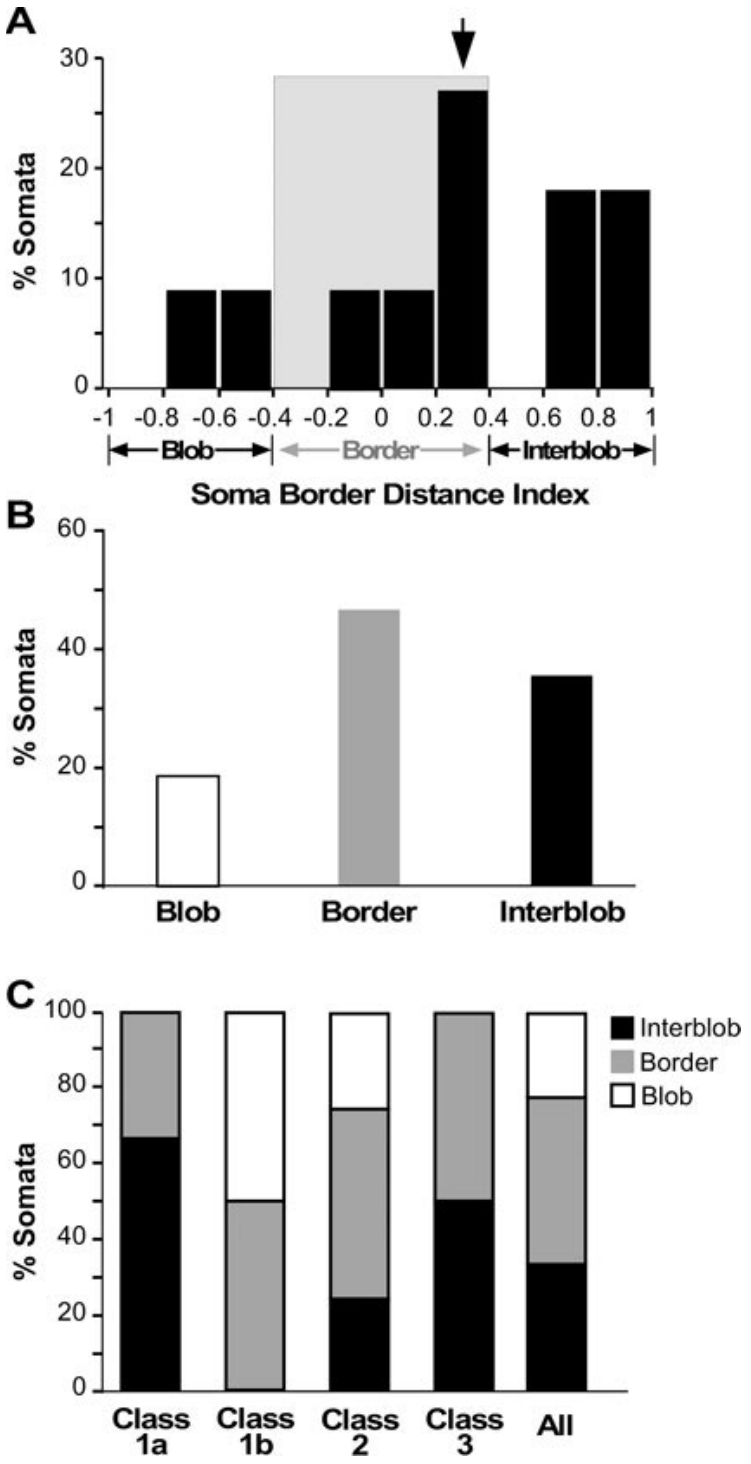

Figure 4.1: Position of L4B somas relative to CO compartments. **A,** Distribution of somas across the blob-border index. Arrow head is median for all somas ($n = 11$). **B.** Percent of somas in each CO compartment category. **C.** Distribution of somas over each CO compartment by axon class defined in Chapter 3.

class.

4.3.2 Bouton and Axon Location Relative to CO Compartments

Boutons were plotted along with axon reconstructions (as reported in Chapter 3). We quantified the distance boutons were from blob borders using the index method described above for somas. Figures 4.2-4.4 show examples of axons and boutons aligned to CO stained tissue for each neuron class and across the primary target layers (2/3, 4B, 5). Using multiple metrics, we find that the location of boutons across all layers, and cell classes, is predominantly outside of blobs (Figure 4.5, Table 4.1). We quantified the average amount of axon (20%) and boutons (18%) contained within blobs, as well as the distance each bouton was from the nearest blob center, and found boutons to be consistently outside the blob border (Table 4.1); these metrics support our index analysis findings (Figures 4.2-4.4) and clearly show that axons of L4B cells projecting to V2 thick stripes avoid blob columns. Upon examination of the distributions of bouton distances from blob-borders, we observed a tendency for there to be multiple peaks within a distribution; some cells had the majority of their boutons in interblobs, while other cells showed a bias for the blob-border region. We plotted the index distance of boutons from the blob-border as a function of the distance their somas are from blob borders (Figure 4.6), and found a positive relationship between

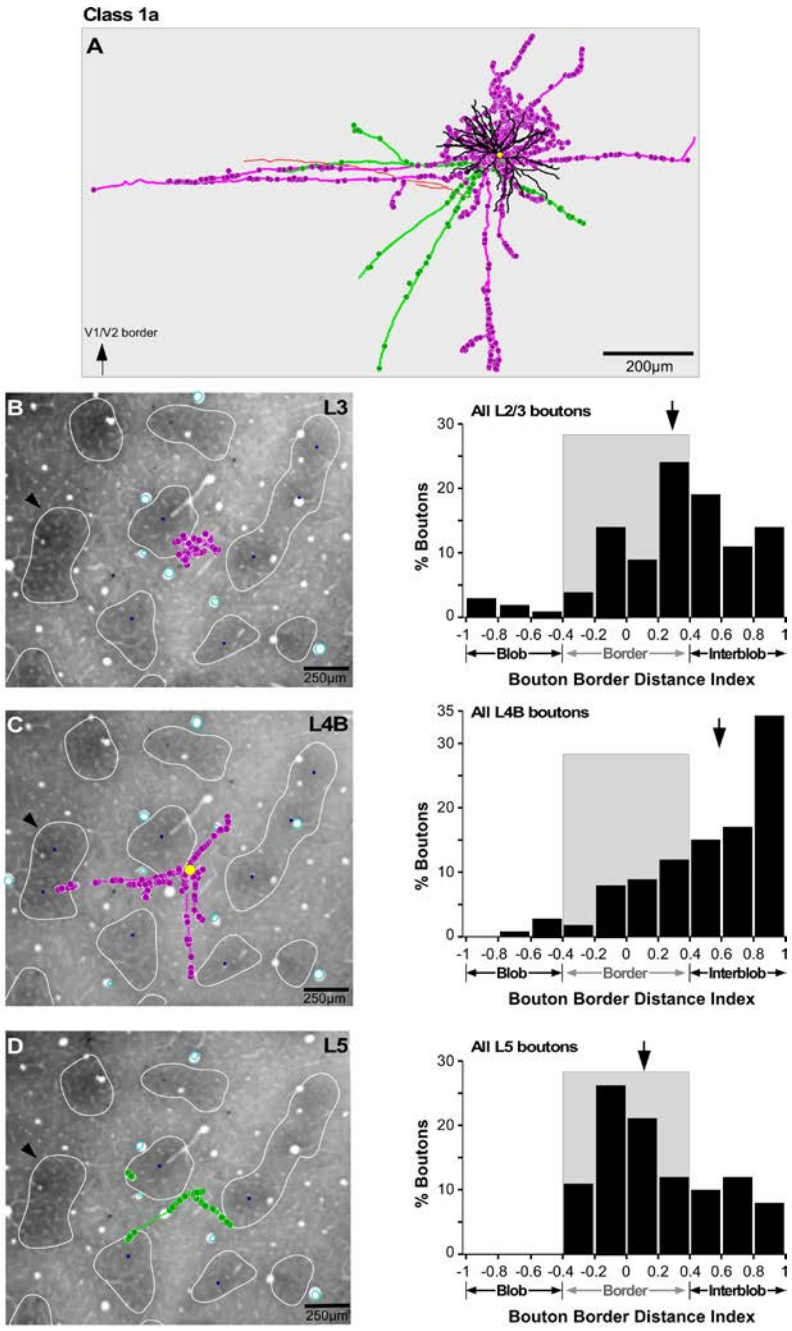

Figure 4.2: Distribution of boutons, Class 1a cell. **A**, reconstruction of a Class 1a neuron (Chapter 3), top/tangential view. **B**, Position of boutons relative to CO blobs in L2/3 (left) and quantification of boutons on blob-border index (right). **C,** Same as B, boutons are in L4B. **D,** Same as B and C, boutons are in L5. **Conventions**: Pink= supragranular, green = infragranular, red = white matter, black = dendrites, yellow = soma, white contours = blobs, dark blue markers = blob centers, light blue contours = blood vessels used for alignment

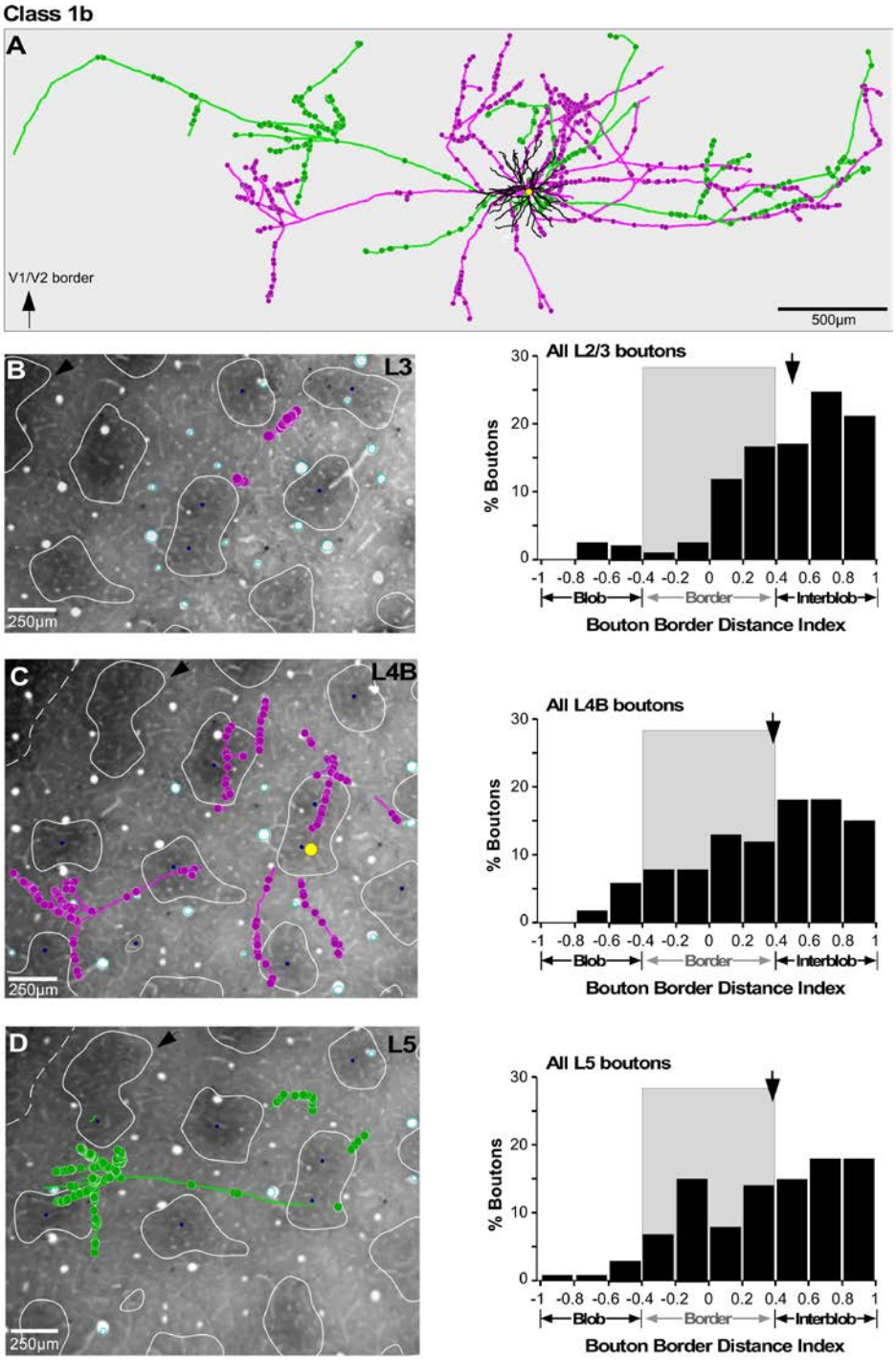

Figure 4.3: Distribution of boutons for Class 1b cell. A, 3D reconstruction of a Class 1b neuron (Chapter 3), top/tangential view. **B**, Position of boutons relative to CO blobs in L2/3 (left) and quantification of boutons on blob-border index (right). **C,** Same as B, but boutons are in L4B. **D.** Same as B and C, but boutons are in L5. **Conventions**: as in Figure 4.2

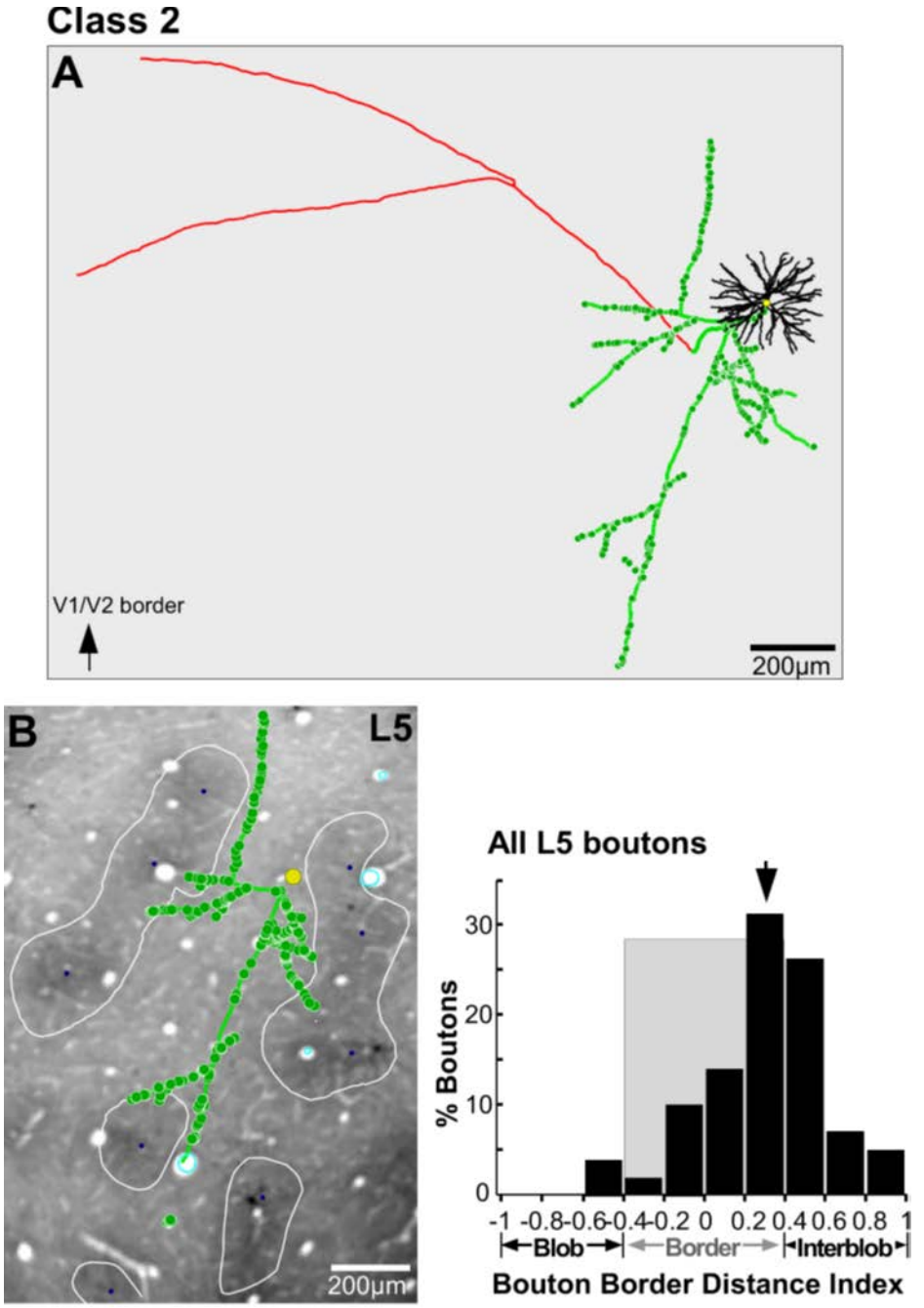

Figure 4.4: Qualitative and quantitative distribution of boutons for a Class 2 cell. A, 3D reconstruction of a Class 2 neuron (Chapter 3), top/tangential view. **B**, Position of boutons relative to CO blobs in L5 (left) and quantification of boutons on blob-border index (right).

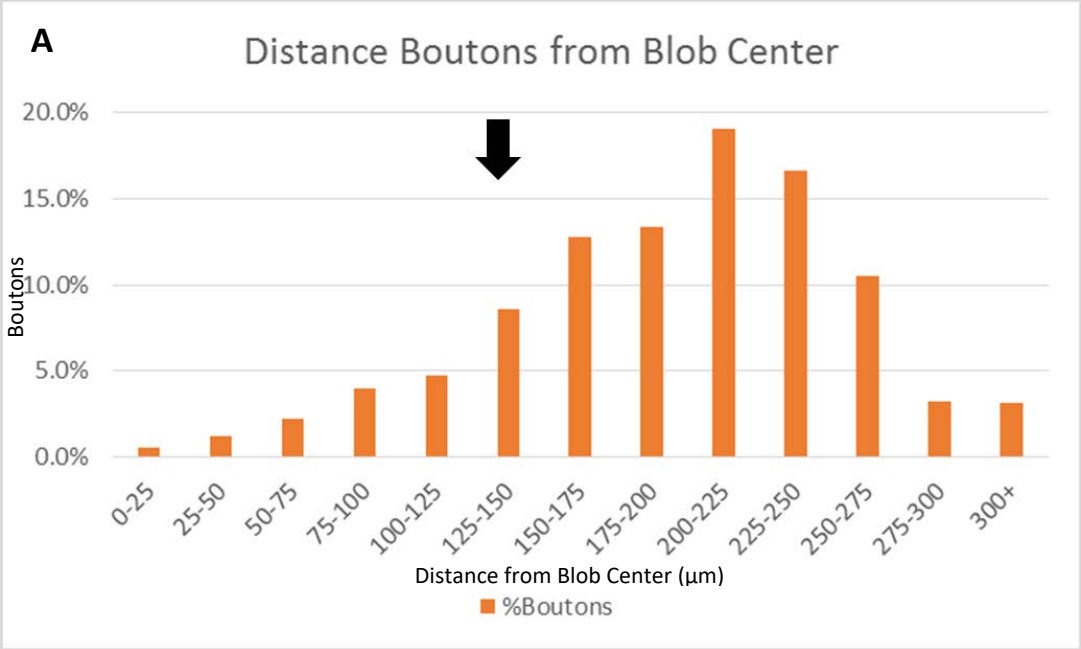

Figure 4.5: Axon and Boutons in Blobs. Distribution of boutons when measured from the center of the nearest blob. Arrow represents the median blob radius (~146 µm). The majority of boutons are outside of blobs using this alternative measuring metric.

Table 4.1: Quantification of the amount of axon and boutons present inside a blob when the blob is defined as the darkest 33% of pixels.

Average % Axon Blobs	20%
Median % Axon Blobs	19%
Range % Axon in Blob	0 - 43%

Average % of Boutons in Blobs	18%
Median % of Boutons in Blobs	21%
Range of Bouton % in Blobs	0 - 38%

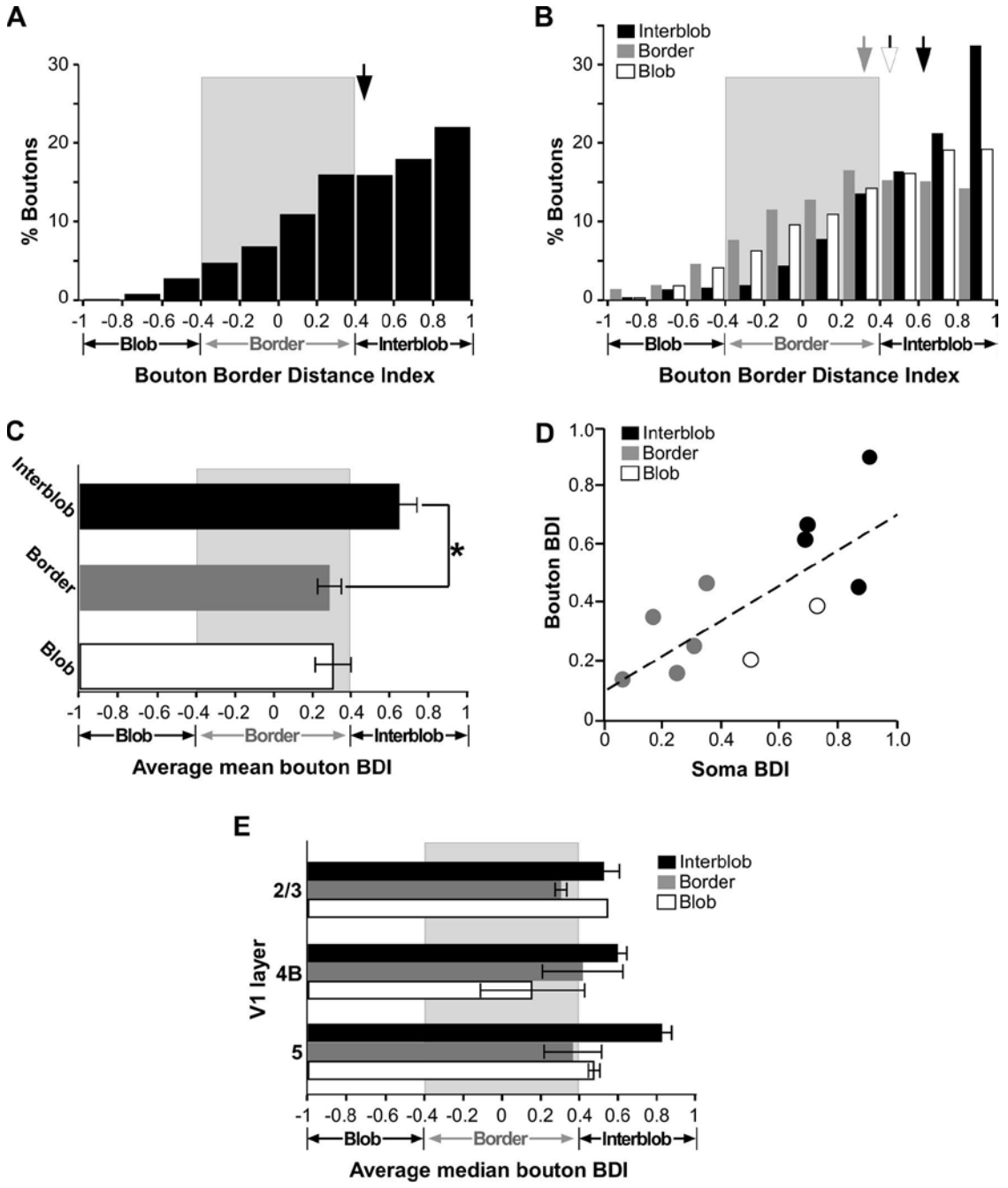

Figure 4.6: Comparison of boutons using the blob-border index. **A,** Distribution of all boutons from all cells. Arrow represents median of all values. **B,** Distribution of all boutons grouped into parent soma CO position. Arrows represent median values according to each CO compartment. **C,** Comparison of the average border index value of all boutons for parent somas in each CO category. Kruskal-walis test with Bonferroni correction, $p < 0.05$. **D,** Plot of boutons and parent soma position relative to CO compartments. **E,** Comparison of the average median border index value for each cell across each layer.

the two ($r = 0.762$; $p < 0.006$; pearson correlation). The distribution of boutons categorized by soma CO position clearly shows a bias for cells near the blob-border to also have boutons near the blob-border; cells in the interblobs have boutons in the interblobs (Figure. 4.6). The average distance of boutons from the blob border for neurons at the blob border is significantly different from the boutons from cells in the interblobs ($p < 0.001$).

Cells in our sample have different quantities of boutons, and can have differing proportions of boutons in each layer, as described previously. Thus, in order to calculate a value that equally weights boutons across each layer, and each cell in its CO category, we used the median bouton distance across each layer to get an average median bouton distance for each cell; the average of all cells in each CO category was then calculated. The result of this analysis supports our previous findings and shows that the average median distance boutons are from the blob-border for cells in the blob-border is significantly different from cells in the interblobs ($p = 0.03$) (Figure 4.6). These results support a like-to-like connectivity pattern, which is an important organizational feature of cortical circuitry (Livingstone and Hubel, 1984; Weliky et al., 1995; Bosking et al., 1997). Interestingly, although only two cells were quantitatively analyzed that reside in blobs, both cells clearly avoid blobs with their axons and boutons, violating a like-like-connectivity pattern. However, these two cells are consistent with the interblob targeting pattern of all other cells, and this motif appears to be a result of the V2 thick

stripe projection target. Callaway and Wiser noted a similar pattern: all of their L4B cells projected to blobs, irrespective of the location of their soma relative to CO compartments.

4.4 Discussion

In this study, we sought to determine the location of neurons and their axonal projections relative to V1 CO blobs and interblobs. Using a retrograde traveling rabies-GFP virus and intrinsic signal optical imaging, we identified and characterized a unique sample of cells: L4B neurons that project to V2 thick stripes. It has previously been shown that all L4B neurons send axonal projections specifically to blobs in L2/3, and are unbiased in L4B and L5; however, the extrastriate target of these neurons was not identified. Our sample of L4B neurons did not send axonal projections to L2/3 blobs; on the contrary, the axons and boutons of all sampled cells avoided CO blobs, and the column below in L4B and L5. Thus, we have identified a new circuit involving L4B neurons which distribute information to interblobs and not to blobs. Thus far, the distinguishing feature for this circuit is that all cells project to thick stripes in V2. Our data therefore suggest that the local circuitry that a projection neuron may be involved in is contingent upon the neuron's projection target.

The specific functional implications of L4B neurons projecting to the interblobs is unclear. However, we do know that L4B neurons are strongly

driven by L4Cα neurons, which receive magnocellular input from the LGN. Thus, this circuit relays M-type input to the interblobs. Additionally, about half our sample of neurons in this study were pyramids, which have been shown to be driven by L4Cα and L4Cß neurons, making these L4B neurons at least M+P integrating cells. The functional implication of the distribution of M+P information to interblobs is also unclear. Understanding the specific response properties of L4B pyramids and stellates would be enlightening due to the fact that cells in this layer play an important role in the intracortical circuitry of V1, as well as the functions of thick, thin, and pale stripes in V2, and areas MT and V3.

Interestingly, our data also support previous data showing the blob column-to-thin-stripe and interblob column-to-thick stripe streams are independent from one another. All of our cells project axons to interblob regions in V1, across all layers, and avoid blobs. Importantly, our neurons also project to thick stripes. Thus, our data suggest that the L4B neurons involved in the interblob-to-thick stripe stream do not talk to neurons in the blob-thin stripe stream. A future area of study would be to determine if L4B neurons projecting to thin stripes maintain this CO stream specificity, and if this is also the case for neurons in L2/3 blobs and interblobs, further elucidating whether and were information may be mixed or remain segregated between these two streams.

4.5 References

Anderson JR, Jones BW, Yang JH, Shaw MV, Watt CB, Koshevoy P, Mastronarde D, Tasdizen T, Marc RE (2009) A computational framework for ultrastructural mapping of neural circuitry. PLoS Biol 7: e1000074.

Blasdel GG, Lund JS, Fitzpatrick D (1985) Intrinsic connections of macaque striate cortex: axonal projections of cells outside lamina 4C. J Neurosci 5:3350-3369.

Bosking WH, Zhang Y, Schofield B, Fitzpatrick D (1997) Orientation selectivity and the arrangement of horizontal connections in tree shrew striate cortex. J Neurosci 17:2112-2127.

Briggs F, Kiley CW, Callaway EM, Usrey WM (2016) Morphological substrates for parallel streams of corticogeniculate feedback originating in both V1 and V2 of the macaque monkey. Neuron 90:388-399.

Callaway EM, Wiser AK (1996) Contributions of individual layer 2–5 spiny neurons to local circuits in macaque primary visual cortex. Vis Neurosci 13:907-922.

Edwards DP, Purpura KP, Kaplan E (1995) Contrast sensitivity and spatial frequency response of primate cortical neurons in and around the cytochrome oxidase blobs. Vision Res 35:1501-1523.

Federer F, Ichida JM, Jeffs J, Schiessl I, McLoughlin N, Angelucci A (2009) Four projection streams from primate V1 to the cytochrome oxidase stripes of V2. J Neurosci 29:15455-15471.

Federer F, Williams D, Ichida JM, Merlin S, Angelucci A (2013) Two projection streams from macaque V1 to the pale cytochrome oxidase stripes of V2. J Neurosci 33:11530-11539.

Fitzpatrick D, Lund JS, Blasdel GG (1985) Intrinsic connections of macaque striate cortex: afferent and efferent connections of lamina 4C. J Neurosci 5:3329-3349.

Horton JC, Hubel DH (1981) Regular patchy distribution of cytochrome oxidase staining in primary visual cortex of macaque monkey. Nature 292:762-764.

Lachica EA, Beck PD, Casagrande VA (1992). Parallel pathways in macaque monkey striate cortex: anatomically defined columns in layer III. Proc Natl Acad Sci USA 89:3566-3570.

Leventhal AG, Thompson KG, Liu D, Zhou Y, Ault SJ (1995) Concomitant sensitivity to orientation, direction, and color of cells in layers 2, 3, and 4 of monkey striate cortex. J Neurosci 15:1808-1818.

Livingstone MS, Hubel DH (1983) Specificity of cortico-cortical connections in monkey visual system. Nature 304:531-534.

Livingstone MS, Hubel DH (1984) Anatomy and physiology of a color system in the primate visual cortex. J Neurosci 4:309-356.

Livingstone M, Hubel D (1988) Segregation of form, color, movement, and depth: anatomy, physiology, and perception. Science 240:740-749.

Lennie P, Krauskopf J, Sclar G (1990) Chromatic mechanisms in striate cortex of macaque. J Neurosci 10:649-669.

Lund JS (1973) Organization of neurons in the visual cortex, area 17, of the monkey (Macaca mulatta). J Comp Neurol 147:455-495.

Lund JS, Boothe RG (1975) Interlaminar connections and pyramidal neuron organisation in the visual cortex, area 17, of the macaque monkey. J Comp Neurol 159:305-334.

Lund JS (1988) Anatomical organization of macaque monkey striate visual cortex. Annu Rev Neurosci 11:253-288.

Lund JS, Yoshioka T (1991) Local circuit neurons of macaque monkey striate cortex: III. neurons of laminae 4B, 4A, and 3B. J Comp Neurol 311:234-258.

Nassi JJ, Callaway EM (2007) Specialized circuits from primary visual cortex to V2 and area MT. Neuron 55:799-808.

Nealey TA, Maunsell JH (1994) Magnocellular and parvocellular contributions to the responses of neurons in macaque striate cortex. J Neurosci 14:2069-2079.

Sincich LC, Horton JC (2002) Divided by cytochrome oxidase: a map of the projections from V1 to V2 in macaques. Science 295:1734-1737.

Sincich LC, Horton JC (2005) Input to V2 thin stripes arises from V1 cytochrome oxidase patches. J Neurosci 25:10087-10093.

Sincich LC, Jocson CM, Horton JC (2010) V1 interpatch projections to V2 thick stripes and pale stripes. J Neurosci 30:6963-6974.

Valverde F (1985). The organizing principles of the primary visual cortex in the monkey. Cereb Cortex 3:207-257.

Weliky M, Kandler K, Fitzpatrick D, Katz LC (1995) Patterns of excitation and inhibition evoked by horizontal connections in visual cortex share a common relationship to orientation columns. Neuron 15:541-552.

Wickersham IR, Finke S, Conzelmann KK, Callaway EM (2007) Retrograde neuronal tracing with a deletion-mutant rabies virus. Nat Methods 4:47-49.

Yabuta NH, Callaway EM (1998a) Functional streams and local connections of layer 4C neurons in primary visual cortex of the macaque monkey. J Neurosci 18:9489-9499.

Yabuta NH, Callaway EM (1998b) Cytochrome-oxidase blobs and intrinsic horizontal connections of layer 2/3 pyramidal neurons in primate V1. Vis Neurosci 15:1007-1027.

Yabuta NH, Sawatari A, Callaway EM (2001) Two functional channels from primary visual cortex to dorsal visual cortical areas. Science 292:297-300.

Yoshioka T, Levitt JB, Lund JS (1994) Independence and merger of thalamocortical channels within macaque monkey primary visual cortex: anatomy of interlaminar projections. Vis Neurosci 11:467-489.

CHAPTER 5

CONCLUSION

The visual system is comprised of enormously complex networks of specialized cells. We currently do not have a sound understanding of how visual system circuits are built. Understanding how visual system circuits are built will provide a foundation from which to probe the computations these circuits are performing, and subsequently, how these circuits are instantiating our visual perception of the world.

In this dissertation, we sought to better understand the circuitry between area V1 and area V2. We specifically investigated the connectivity between L4B in V1 and the thick and thin stripes in V2, all of which have unique structural and functional organization. We chose to investigate these specific areas of the visual system because they present the opportunity to answer basic questions regarding the wiring between these areas.

The first question we posed is: What is the contribution of spiny stellate and pyramidal cells in L4B of V1 to the thick and thin stripes in V2? Answering this question provides insight into the kind of information flowing through these pathways. Spiny stellate neurons in L4B are known to

primarily receive magnocellular (M-type) information from the LGN via L4Cα. M-type information is useful for detection of motion and locating objects in visual space (i.e., high sensitivity to contrast and high spatial frequencies), and is thus thought to be the primary component of dorsal visual stream function. Pyramidal neurons in L4B are known to receive M-type information at their basal dendrites in L4B, but also parvocellular, or P-type, information at their apical dendrite, which extends out of L4B and perhaps all the way into L1. P-type information is useful for the detection of visual scene details, which can be cobbled together in order to create the surface features of objects (e.g., color, texture), as well as continuity within an object, and segregation between objects, all of which are important for detecting and recognizing objects in the visual scene. P-type information is thought to be the primary component of ventral visual stream function. However, it is also clear that there are components of P- and M-type information in both the ventral and dorsal visual streams, as ablation of either the M or P neurons in the LGN results in deficits in both dorsal and ventral pathways. Neurons in V2 thin stripes have been shown to project to area V4, a component of the ventral visual pathway, while neurons in V2 thick stripes have been shown to project to area MT, a component of the dorsal visual pathway. By understanding spiny stellate (M-type) and pyramidal (M+P-type) input from L4B to each V2 stripe, we can begin to unravel and understand how M and P information is routed into the dorsal

and ventral visual pathways.

In Chapter 2 of this manuscript, we show that, for a V2 thick stripe, ~55% of its L4B input comes from spiny stellates, and ~45% comes from pyramidal cells. For thin stripes, ~40% of L4B input is from stellates, and ~60% is from pyramids. While not quite significantly different from each other, our results suggest that thick stripes receive a greater contribution of M-type input from L4B, and that about half of L4B input to thick stripes is M-type, while about ~60% of input to thin stripes is M+P-type information. These findings are in contrast to that which has been previously reported. One groundbreaking study by Nassi and Callaway (2007) reported that ~80% of input to V2 from L4B was comprised of pyramidal neurons, and only 20% was from stellates. In this study, this result was in stark contrast to the input from L4B to MT, where it was found that ~80% was stellate, and ~20% was pyramidal. Additionally, this study found an unexpected differentiation between the neurons in L4B that project to MT and V2. The authors found that the neurons projecting to MT, whether pyramids or stellates, were almost twice the size of the neurons projecting to V2. The primary conclusions drawn from this study were that, 1) Area MT receives dominant M-type information, while area V2 receives dominant M+P-type information, and 2) The neurons embedded in the L4B-MT pathway were significantly larger than the neurons projecting to V2, and thus L4B neuron size is a differentiating component of the circuits from L4B to V2 and MT. In the

latter half of Chapter 2, we report that we find evidence for at least five different groups of V2 projecting L4B neurons when categorized by cell size (i.e., soma perimeter, soma area, dendritic length). We report that there are medium and large pyramids and stellates in L4B projecting to both thick and thin stripes. Importantly, we also find that there are small and giant stellates which project to thick stripes. The functional meaning of having different sizes of neurons projecting from L4B to different target areas is unclear, but, as briefly discussed in the introduction to this manuscript, neurons in the retina may provide clues. Amacrine cells in the retina were initially segregated into groups (e.g., narrow field, medium field, wide field) according to their dendritic length (measured by radius from soma). Subsequently, it has been found that dendritic length is not the only distinguishing element between amacrine cells, as neurotransmitters (e.g., glycine, acetylcholine, GABA), response properties (e.g., on-center, off-center), and laminar location (e.g., sub-lamina within the inner nuclear layer) of these neurons has also been found to differ. I suspect that the different sizes of neurons projecting to V2 and MT are indicative of additional underlying differences between these cells that have yet to be elucidated. Our data provide impetus for further investigation of the categories, or types, or neurons that exist in L4B, some of which are likely embedded into different circuits. It is also important to point out that the giant cells we identified projecting to V2 thick stripes are very similar in size to the cells projecting to MT in the Nassi and Callaway study.

We can therefore conclude that giant neurons, which were found to be two times the size of V2 neurons in the Nassi and Callaway study, do not exclusively project to area MT, and do not necessarily differentiate the circuits between L4B and MT and L4B and V2. The rabies virus we used to identify and subsequently reconstruct L4B neurons projecting to thick and thin stripes does have limitations in its use. An important limitation to using the rabies virus is that it randomly infects neurons with axon terminals at the site of injection; all neurons projecting to the area of injection are not labelled. Therefore, it is always a possibility that different types of neurons are not identified in a sample, and this was the case in the V2 cells reconstructed in the Nassi and Callaway study. Giant stellates, but thus far not giant pyramids, project to V2 thick stripes as well as MT. These cells may be those previously identified that project simultaneously to both MT and V2 (Sincich and Horton, 2003; Federer et al., 2009), and may constitute yet another category of L4B projection neurons.

In Chapters 3 and 4 of this manuscript, we investigated the axons (and their boutons) of a subset of our L4B neurons found projecting to thick stripes. We reconstructed the entire axonal arbor of these neurons and asked one main question: Where do these cells distribute information to within V1? We approached this question structurally in Chapter 3, (i.e., to which layers do the axons project to?), and functionally in Chapter 4 (i.e., do the axons of these neurons target CO blobs, interblobs, or both?). Previous research

shows a canonical axonal branching motif for all L4B neurons; neurons target L2/3 blobs, L4B, and L5 and primarily avoid L1, L4A, L4C, and L6 (Callaway and Wiser, 1996). However, a major limitation to this, and other studies, is that the extrastriate projection target of the identified L4B neurons was unknown. Because L4B neurons can project to multiple areas in V2 (thick, thin, pale stripes), and areas MT and V3, it remains very unclear if a single branching pattern, and thus circuit, of V1 interlaminar connectivity is sufficient to describe neurons projecting to different anatomical and functional domains within the visual system. In Chapter 3, we identified at least two major classes of neurons categorized by the amount of axon distributed across V1 layers. Class 1 neurons recapitulated the canonical L2/3, L4B, L5 branching pattern, with the caveat that Class 1b neurons distributed significantly less axon to L2/3, and therefore may constitute a distinct functional class themselves. Class 2 neurons have no projections to L2/3, minor projections in L4B, and dominantly target L5. While Class 1 cells target supra and infragranular layers, Class 2 cells dominantly target infragranular layers. We speculate that these two classes of neurons may in turn be the substrates for two different circuits within V1. Class 1 neurons may participate in an interlaminar V1 circuit which is purposed for distribution of information to extrastriate cortex (e.g., V2, V3, MT). Class 2 neurons may participate in an infragranular circuit which distributes information to subcortical structures (e.g., superior colliculus) via L5

neurons. In Chapter 4, we investigated the location of axon and boutons relative to CO blobs and interblobs across all layers and all classes. We found that all neurons sampled (n = 11) avoided blobs in L2/3, and the blob column below. This finding is in direct contrast to the Callaway and Wiser (1996) study which showed all L4B neurons projecting to blobs. The primary distinguishing factor between our data and that from the Callaway and Wiser data is that in our study, we know for certain that our cells project to V2 thick stripes, while the projection target of the L4B neurons in the Callaway and Wiser study was unknown. Our results strongly suggest that the V1 interlaminar circuitry a neuron is involved in can differ as a function of projection target. Thus, to understand the circuitry of a neuron, the projection target should be known, as it may dictate involvement in different local circuits. The specific functional outcome of L4B neurons projecting to interblobs is unknown, but, because L4B neurons are dominated by M-type input, we have now shown a mechanism through which L2/3 interblobs and the columns below can receive M-type information.

Overall, we are unfortunately unable to unify all of our data into a complete, or even cohesive, functional wiring diagram for L4B neurons projecting to V2 thick and thin stripes. In order to do so, much larger quantities of data would be needed. For example, it would be useful to know if Class 1 neurons were predominately small, medium, or large pyramids that lived primarily in interblobs, or, if Class 2 neurons were predominantly

small, medium, large, or giant stellates that predominantly lived at blob borders. While there are some trends in the data for some kind of grand organizational scheme (e.g., Class 1a neurons are mainly medium and large pyramids that live in interblobs or on the blob border; Class1B and Class 3 neurons are all stellates, can live anywhere, and are all sizes; Class 2 cells are primarily large pyramids and stellates that live everywhere), we simply lack the magnitude (and likely variety) of data necessary to understand the larger organizational framework these neurons are embedded in (Figure 5.1). However, our data do make the following points more clear about L4B neurons projecting to V2: 1) Both thick and thin stripes get considerably more M-type input from L4B than previously thought. 2) The sizes of neurons projecting to V2 vary considerably and warrant further investigation. 3) All L4B neurons do not distribute information homogeneously throughout V1, some neurons do not talk to L2/3, and all thick stripe neurons investigated do not talk to blobs.

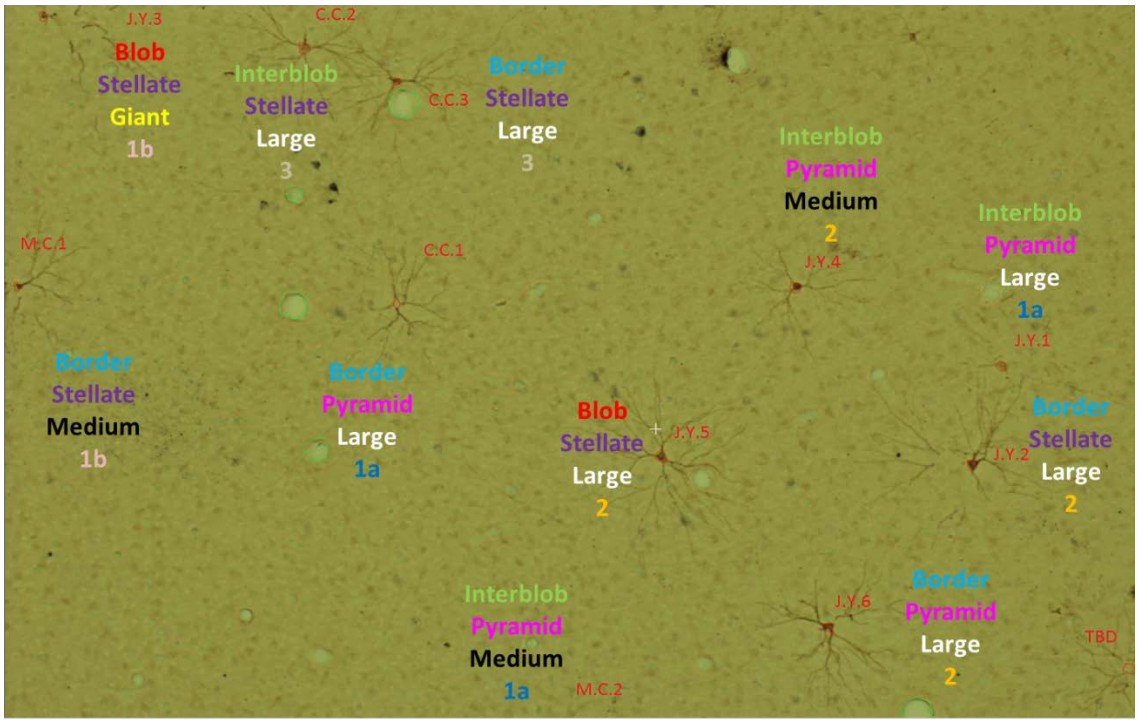

Figure 5.1: Summary of L4B neuron characterization data. Cell class as defined by axonal branching pattern is indicated for each neuron numerically (Class 1a, 1b, 2, 3). Cell type (stellate, pyramids) and cell size (small, medium, large, giant) are noted. Soma location relative to CO compartments is also noted (blob, blob-border, interblob). No clear systematic relationships are found, which is likely due to the overall small sample size.

5.1 References

Callaway EM, Wiser AK (1996) Contributions of individual layer 2–5 spiny neurons to local circuits in macaque primary visual cortex. Vis Neurosci 13:907-922.

Federer F, Ichida JM, Jeffs J, Schiessl I, McLoughlin N, Angelucci A (2009) Four projection streams from primate V1 to the cytochrome oxidase stripes of V2. J Neurosci 29:15455-15471.

Nassi JJ, Callaway EM (2007) Specialized circuits from primary visual cortex to V2 and area MT. Neuron 55:799-808.

Nassi JJ, Callaway EM (2009) Parallel processing strategies of the primate visual system. Nat Rev Neurosci 10:360-372.

Sincich LC, Horton JC (2003) Independent projection streams from macaque striate cortex to the second visual area and middle temporal area. J Neurosci 23:5684-5692.